UNIVERSITA' DEGLI STUDI DI MILANO

PhD Course in Veterinary and Animal Science
Class XXXI

THE BONE TISSUE:
MULTIDISCIPLINARY CHARACTERIZATION
IN EXPERIMENTAL ANIMALS
AND SKELETAL DEVELOPMENT IN DOGS

Candidate: Maria Elena Andreis

Supervisor: Professor Silvia C. Modina
Co-supervisor: Professor Mauro Di Giancamillo
PhD course coordinator: Professor Fulvio Gandolfi

2017-2018

Abstract

Animals are considered sentient beings by law and the notion of animal welfare, both physical and psychological, is well-established ("Five Freedoms"). As a result, regulation on animal testing puts researchers through highly regulated and restrained protocols (to reduce the number of animals included in *in vivo* experiments and replace them with alternative procedures whenever possible. This project revolves around the study of the bone tissue in different species, grounding on the idea of cadaver "recycle" applied to bone-related research. The bone, in fact, is particularly easy to study in cadavers since it suffers the early consequences of post-mortal decay to a lesser extent compared to other tissues.

The bone is a highly specialized connective tissue characterized by a mineralized extracellular matrix, specifically designed for structural, mechanical and metabolic functions. Despite general shared features, interspecific differences exist in bone microscopic organisation, which have not yet been completely elucidated. Because of its peculiarities, a comprehensive evaluation of the bone includes several different techniques, such as histology, densitometry and biomechanics. Histologic techniques are particularly common, especially when it is necessary to evaluate tissue biocompatibility and integration in animal models of bone healing and regeneration. However, due to highly mineralized nature of its matrix, several problems arise during bone processing, especially during decalcification (the removal of mineral from the bone while preserving all the essential microscopic elements and tissue antigenicity), a process that is yet far from being standardized, but is necessary to prepare paraffin-embedded specimens.

The first two aims of this project were the definition of species-specific and site-specific guidelines for bone specimens' decalcification and the characterization of swine and ovine bone tissue with a multidisciplinary approach.

Basic protocols for trabecular bone decalcification in different species with different solutions were provided, showing that excellent morphologic results can be achieved with solution containing strong acids in rodents, sheep and pig. As a general rule, hydrochloric acid solution proved to be too aggressive, as previously reported. On the other hand, the combined use of hydrochloric acid and formic acid proved to be a very good compromise, shortening experimental time and preserving morphology. Finally, a combination of citric acid formic acid provided excellent morphology, but at the expenses of decalcification time. Collagen I was preserved in swine, canine and ovine samples that proved to have good/excellent morphology, while it wasn't preserved in rats or mice, despite their excellent morphology. A multidisciplinary approach to the study of the bone in pigs and sheep was developed, evaluating several different parameters with different techniques on the same samples, also providing standard reference parameters about swine and ovine bone histology, densitometry and biomechanics, to be compared with future research results, to deepen the knowledge on the bone tissue and facilitate biomedical research on animal models.

The histogenesis of bone can be divided in two modalities: endochondral and intramembranous, which share a common sequence of events. Bone growth starts during the fetal stage, and then continues after birth

together with the growth of the entire individual. Special structures, called cartilage canals, are involved in the process of endochondral ossification, with nutrients supply to the growing cartilage and waste products elimination being their primary functions. Cartilage canals have been described in several species, but little information is known about them in dogs. The development of a newborn into an adult implies dramatic changes in both body size and shape. The dog, in particular, exhibits the highest intraspecific differences in body shape and size among mammals, and this might be reflected by different growth patterns. This is especially true when the skull is considered, as it is the most variable body part among different breeds. Little information is known about skull development in dogs in relation to their adult craniometric category (brachycephalic, mesaticephalic, dolychocephalic). Due to the extreme plasticity of young bones, moreover, skeletal development could potentially be influenced by the presence of orthopaedic diseases, which could modify the normal shape and size of the future adult bones.

The last three aims of this project were the study of endochondral ossification in long bones, with particular emphasis on the role role of cartilage canals; the study of the effects of pathology (quadriceps contracture) on hindlimb development; and the study of skull development and its compared features in brachycephalic, mesaticephalic and dolychocephalic breeds.

New insights on cartilage canals in small-sized dogs were provided, which confirmed their involvement in bone extracellular matrix production in dogs, as in other species, laying the basis for more extensive studies on the delicate mechanism of the formation of ossification centres and the regulation of ossification. The abnormalities induced by quadriceps contracture on hind limb skeletal development, mainly consisted of volume reduction and abnormal shape of several centres, were described in a litter of Dobermann. These alterations that should be carefully considered when evaluating puppies affected by the disease to plan a therapy. Finally, novel contribution in canine craniometry and skull development were provided, documenting morphometric differences among dolichocephalic, mesaticephalic and brachycephalic purebred puppies in the early neonatal period through a radiographic and anatomic study.

Cadavers invariably proved to be an invaluable source of research material, providing a valid alternative to *in vivo* experiments and contributing to the reduction of the use of experimental animals.

Abstract

Gli animali sono considerati esseri senzienti per legge e la nozione di benessere animale, sia fisico che psicologico, è ben consolidata ("Cinque libertà"). Di conseguenza, la regolamentazione sulla sperimentazione sugli animali obbliga i ricercatori a protocolli altamente regolamentati nel tentativo di ridurre il numero di animali inclusi negli esperimenti *in vivo* e sostituirli con procedure alternative, quando possibile. Questo progetto ruota attorno allo studio del tessuto osseo in diverse specie, basandosi sull'idea del "riciclo" dei cadaveri applicato alla ricerca sul tessuto osseo. L'osso, infatti, è un tessuto particolarmente facile da studiare nei cadaveri poiché subisce le conseguenze del decadimento post-mortale in misura minore rispetto ad altri tessuti.

L'osso è un tessuto connettivo altamente specializzato caratterizzato da una matrice extracellulare mineralizzata, specificamente progettato per funzioni strutturali, meccaniche e metaboliche. Nonostante molte caratteristiche generali condivise, tuttavia, esistono differenze interspecifiche nell'organizzazione microscopica del tessuto osseo, che non sono state completamente chiarite.

Per via delle sue peculiarità, una valutazione completa dell'osso include obbligatoriamente diverse tecniche, per esempio tecniche istologiche, densitometriche e l'istologia, biomeccaniche. Le tecniche istologiche, in particolare, sono assai diffuse, soprattutto per la valutazione della biocompatibilità e dell'osteointegrazione nell'ambito della medicina rigenerativa. Inoltre, a causa della natura altamente mineralizzata della sua matrice, il processamento del tessuto osseo presenta molteplici problematiche, in particolare per quanto riguarda la decalcificazione (ovvero la rimozione dei minerali dal tessuto osseo, preservando le sue caratteristiche microscopiche di base e l'antigenicità tissutale), un processo che è ancora lontano dall'essere standardizzato, ma che risulta indispensabile al fine dell'inclusione dei campioni di osso in paraffina.

I primi due obiettivi di questo progetto sono la definizione di linee guida specifiche per la decalcificazione dell'osso, in base alla specie animale, al tipo di tessuto e al sito di prelievo, e la caratterizzazione del tessuto osseo suino e ovino tramite un approccio multidisciplinare.

Sono stati definiti protocolli di base per la decalcificazione dell'osso trabecolare in diverse specie (suino, ovino, cane, ratto, topo) con diverse soluzioni: risultati morfologici eccellenti risultati sono stati raggiunti con l'utilizzo di una soluzione contenente acidi forti nei roditori, negli ovini e nei suini. In generale, l'acido cloridrico come unico componente di una soluzione decalcificante si è dimostrato troppo aggressivo. L'uso di una soluzione a base di acido cloridrico e acido formico, invece, si è dimostrato un ottimo compromesso, accorciando i tempi di decalcificazione e preservando contemporaneamente la morfologia tissutale. Infine, l'utilizzo di una soluzione a base di acido formico e acido citrico ha consentito di ottenere una morfologia tissutale eccellente, a spese tuttavia delle tempistiche di decalcificazione. L'antigenicità tissutale (collagene I) è risultata conservata nei campioni di suino, pecora e cane caratterizzati da una buona/eccellente morfologia; così non è stato, invece, per i campioni di topo e ratto, nonostante risultati morfologici eccellenti. Non è chiaro, tuttavia, se questo risultato possa essere legato all'utilizzo di tecniche di smascheramento eccessivamente aggressive. È stato sviluppato un approccio multidisciplinare allo studio dell'osso di suino e ovino, valutando diversi parametri con diverse tecniche sugli stessi campioni in modo da

garantire uno studio completo ed approfondito di tutte le caratteristiche ossee fondamentali nell'ambito della ricerca. Sono stati così inoltre definiti numerosi parametri di riferimento istologici, densitometrici e biomeccanici sul tessuto osseo di queste specie, al fine di approfondire le conoscenze sul tessuto osseo e fornire un piccolo contributo alla ricerca biomedica applicata che prevede l'utilizzo di modelli animali.

L'istogenesi dell'osso può essere suddivisa in due modalità: endocondrale e intramembranosa, che condividono una sequenza comune di eventi. Nel processo di ossificazione endocondrale sono coinvolte speciali strutture definite canali cartilaginei, le cui principali funzioni sono l'apporto di nutrienti alla cartilagine in crescita e l'eliminazione degli scarti cellulari. Lo sviluppo scheletrico inizia durante la vita fetale, per continuare poi nella vita postnatale in modo coordinato con la crescita dell'intero individuo. I canali cartilaginei sono stati descritti e studiati in diverse specie; tuttavia, non sono disponibili molte informazioni riguardo alle loro caratteristiche nella specie canina. Lo sviluppo di un neonato ad adulto implica cambiamenti radicali nelle dimensioni e nella forma del corpo. Il cane, in particolare, si caratterizza per enormi differenze intraspecifiche nella forma e nelle dimensioni corporee. Questa peculiarità potrebbe tradursi in diversi pattern di accrescimento e sviluppo scheletrico, in particolare se si considera lo sviluppo del cranio, che rappresenta la parte del corpo più variabile tra le diverse razze canine; non molto, tuttavia, si conosce attualmente dello sviluppo del cranio nel cane in relazione alla categoria craniometrica dell'adulta (brachicefalo, mesaticefalo, dolicocefalico). A causa dell'estrema plasticità dell'osso nei cuccioli, infine, lo sviluppo scheletrico è potenzialmente influenzato dalla presenza di malattie ortopediche, che potrebbero modificarne la normale forma e le dimensioni, risultando in deformità scheletriche.

Gli ultimi tre obiettivi di questo progetto sono stati lo studio dell'ossificazione endocondrale nelle ossa lunghe, con particolare riferimento al ruolo dei canali cartilaginei; lo studio degli effetti della contrattura del quadricipite sullo sviluppo degli arti posteriori; e lo studio dello sviluppo del cranio e le sue caratteristiche nei neonati di razze brachicefale, mesaticefale e dolicocefale.

I risultati ottenuti sui canali cartilaginei nei cani di piccola taglia hanno confermato il loro coinvolgimento nella produzione di matrice extracellulare, come in altre specie, ponendo le basi per studi più approfonditi sul delicato meccanismo di sviluppo dei centri di ossificazione e della regolazione dell'ossificazione endocondrale. Sono state descritte le anomalie indotte dalla contrattura del quadricipite sullo sviluppo scheletrico degli arti posteriori in una cucciolata di Dobermann, principalmente rappresentate dalla riduzione del volume e da anomalie di forma di numerosi centri di ossificazione. Queste alterazioni dovrebbero essere attentamente considerate quando si valutano cuccioli colpiti da questa malattia, nel tentativo di pianificare una corretta terapia. Infine, sono state documentate differenti intraspecifiche tra gli indici craniometrici di neonati appartenenti a razze brachicefale, mesaticefale e dolicocefale attraverso uno studio radiografico e anatomico.

Il cadavere si è dimostrato una eccellente fonte di materiale per la ricerca, contribuendo alla riduzione dell'uso di animali in qualità di alternativa agli esperimenti *in vivo*.

TABLE OF CONTENTS

1. GENERAL INTRODUCTION

The use of cadavers in Veterinary Medicine is very common, with teaching and research being the major purposes. It allows to spare experimental animals and perfectly embraces the current Italian law on the subject (D.lgs 26/14). Animals are considered sentient beings by law (Trattato di Lisbona, 2009) and the notion of animal welfare, both physical and psychological, is well-established ("Five Freedoms"). Therefore, the idea of using living animals for exclusively human purposes is more and more debated. As a result, regulation on animal testing has become rather restrictive as compared to the past, and puts researchers through highly regulated and restrained protocols in order to reduce the number of animals included in *in vivo* experiments and replace them with alternative procedures (such as cell, tissue and organ cultures, simulators and others) whenever possible.

This project revolves around the study of the bone tissue in different species, grounding on the idea of cadaver "recycle" applied to bone-related research. The bone, in fact, is particularly easy to study in cadavers since it suffers the early consequences of post-mortal decay to a lesser extent compared to other tissues and is not significantly altered by preservation techniques like freezing; however, proper preservation of bone samples is essential in order to avoid artifacts and obtain reliable experimental results.

The bone tissue

The bone is a highly specialized connective tissue, specifically designed for structural, mechanical and metabolic functions. It is composed of 60-70% mineral, 10-20% collagen and 9-20% water (Park, 1987); small quantities of other organic components (e.g. proteins, lipids, polysaccharides) are also present (Gunderson et al., 1991). It is extremely active from a metabolic point of view, and its functions are: support, protection of soft tissues, movement, mineral and fat storage and hematopoiesis.

Microscopic organisation

Based on its microscopic organization, mammalian bone tissue is classified as cortical or trabecular. Cortical bone forms the diaphysis of long bones and the outer layer of short and flat bones. It is organized in functional units called osteons (Haversian systems), formed by lamellae circumferentially arranged around a longitudinal vascular channel (Haversian canal), connected to the other canals, the periosteum and the endosteum by means of transverse/oblique canals (Volkmann's canals). Moreover, several uninterrupted layers of lamellae are to be found immediately underneath the periosteum and on the internal surface adjacent to the endosteum of the shaft (circumferential lamellae). Finally, interstitial lamellae fill the gaps between Haversian systems (Webster, 1988). Despite these shared features, however, high interspecific difference exists in its microscopic organisation (Table 1) Primary vascular plexiform bone is predominant in non-human large mammals, mixed with areas of dense Haversian tissue and avascular bone (Martiniakova et al., 2006; Martiniakova et al., 2006; Hillier and Bell, 2007); in these species,

circumferential lamellae at the endosteal and periosteal surfaces appear as narrow rings (Martiniakova, 2006). The cortical bone of dogs and cats mainly consists of dense Haversian tissue; periosteal and endosteal circumferential lamellae are well developed and often interrupted by scattered Haversian osteons (Hillier and Bell, 2007). In rodents, primary longitudinal bone tissue is prevalent, with rare scattered osteons which are more frequent at the endosteal surface (Hillier and Bell, 2007); circumferential systems are poorly developed (Hillier and Bell, 2007).

	Similar to human			Different from human		
	Anatomy	Physiology	Others	Anatomy	Physiology	Others
Mouse				- lack of Haversian canals	- regeneration and remodeling	
Rat	- microarchitecture			- lack of Haversian canals - periosteal vascularization - trabecular density	- regeneration and remodeling	- composition
Rabbit			- bone mineral density	- microarchitecture - structural pattern - periosteal vascularization	- regeneration and remodeling	
Dog	- microarchitecture	- regeneration and remodeling*	- composition	- presence of primary and plexiform bone	- remodeling*	
Cat						
Sheep	- trabecular density	- regeneration and remodeling	- composition	- presence of plexiform bone - Haversian canals distribution - trabecular density	- regeneration and remodeling	
Goat		- regeneration and remodeling		- Haversian canals distribution	- remodeling	
Pig	- microarchitecture - trabecular organization	- regeneration and remodeling	- composition	- trabecular density		

Tab. 1 – Differences and similarities between human and animal bone.

Trabecular bone, on the other hand, forms the inner core of short and flat bones, as well as the metaphysis and epiphysis of long bones. It consists of a network of anastomosing trabeculae, containing bone marrow within their pores. Parallel sheets of lamellae form angular segments called trabecular packets, the functional analogous of osteons (Webster, 1988). Because of its porous microscopic organisation, trabecular bone shows lower resistance as compared to cortical bone; however, it contributes to bone rigidity providing support and load distribution and preventing elastic instability in long bones. Moreover, it is constantly involved in mineral homeostasis. No relevant inter-specific difference exists in the lamellar organisation of

trabecular bone, except for their hierarchical organisation, thickness and spatial arrangement (van Griensven, 2015).

Bone biomechanics

Mostly due to its hierarchical organisation, bone is a rigid and anisotropic material, specifically designed to resist flexion, compression and torsion forces and absorb impulsive forces. Its mechanical properties, which reflect its composition (organic and inorganic components), organisation and function, are often used in pre-clinical and clinical studies to quantitatively determine its quality (Bailey and Vashishth, 2018). They are critical for the assessment of its load-bearing capacity and functionality, which is affected by aging, disease and pharmacological intervention (Osterhoff et al., 2016; Donnelly, 2011). Basic comprehensive descriptors of bone biomechanical properties are the Elastic modulus (E), which describes the relationship between the deformation that follows the application of a force to a bone, and the Ultimate Strength (US), which is the maximum strength a bone can handle before it fractures. The rigidity and resistance of cortical bone are higher for loadings along its longitudinal axis when compared to loadings in the circumferential or radial direction: this is reflected by its efficiency in resisting to the uniaxial loadings that develop longitudinally during normal locomotion (Park, 1987). It is characterized by toughness at low strain rates, but it behaves like a brittle material at high rates (Park, 1987). In fact, under uniaxial traction or compression it initially exhibits a linear elastic behaviour, followed by a breaking at relatively a low deformation force (Turner et al., 1999). During traction, it is more fragile if loaded transversally when compared to longitudinal load, while no difference is noted during compression (Ascenzi and Bonucci, 1967; Currey, 1998; Reilly et al., 1974). Trabecular bone, on the other hand, is highly adaptable to loading conditions (Hébert et al., 2012; Ford et al., 1991; Goff et al., 2012; Odgaard, 1997; Bruyère et al., 1999). Its complex microstructure (rods and plates in different proportion) is different throughout the body, producing different mechanical properties at different sites (Ohman et al., 2007)). As a general rule, trabeculae tend to align with the major loading direction, being also dependent on joint movements and muscle action (Fiala, 1993). It exhibits three behavioural regimens: a small strain linear-elastic response, which ends when the cell walls of low-density bone collapse, a plateau, which continues until opposite cell walls touch, causing a steep increase in stress (Hayes and Carter, 1976; Pugh et al, 1973; Stone et al., 1983; Gibson 1985; Wu et al., 2014). Moreover, because of its involvement in several pathological conditions (e.g. osteoporosis), several attempts to predict its biomechanical behaviour have been made (Ford et al., 1991; Potdevin et al., 2012; Bobby and Ramakrishnan, 2008; Majumdar, 1998, Faulkner et al., 1991; Adachi et al., 2001; Depalle et al., 2012; Wang et al., 2012; Parr et al., 2013).

Bone tissue characterisation

When approaching a comprehensive evaluation of the bone (in normal, pathological and experimental conditions), none of its basic features such as morphology, composition, mineral density and biomechanics can be left behind without the risk of precluding the reliability of the obtained results. The bone is a very complex and metabolically active tissue, and each of its properties and function can be optimally tested with

a specific method; to date, no single technique exists that allows to provide information simultaneously all the basic characteristics of bone quality.

Dual-energy X-rays absorptiometry

The use of dual-energy absorptiometry to measure bone mineral content and density is widespread in humans and has been adapted to animals because of the need to examine bone and body composition in longitudinal studies (Grier et al. 1996). It allows rapid, precise, non-invasive and relatively inexpensive measurements of bone mass or density at almost any skeletasl site, and is mostly used in humans to determine vertebral and femoral fracture risk (Grier et al., 1996). In fact, although it has been proven that microarchitecture can be accounted for the majority of bone biomechanical behaviour (Parfitt, 1992; Kleerekoper et al., 1985; Parfitt et al., 1983; Jensen et al., 1990), BMD contributes significantly to the mechanical properties of bone (Wu et al., 2014). In pigs and sheep, examinations were performed to determine normal bone density in normal conditions both on live animals and *ex vivo* (Turner et al. 1995; Pouilles et al., 1999), for the evaluation of the effects of different types of diets on the bone tissue (Skiba et al. 2016), for the non-invasive evaluation of carcasses' composition (Bernau et al., 2015; Soladoye et al., 2016) and for the quantitative analysis of bone healing and regeneration in normal and pathological conditions (den Boer et al., 1999; Floerkemeier et al., 2010; Heiss et al., 2017).

Histology

Histological analysis is an essential step for the microscopic evaluation of the bone, as it allows to ascertain its morphology and composition. Descriptive histology is used to provide a general evaluation of the tissue, including morphology, structure and arrangements of cells, matrix and possibly implants and tissue/implant interface. Mineral components can be removed from bone specimens (decalcification), or the bone can be evaluated undecalcified.

The routine staining for bone cellular detail is Hematoxylin and Eosin. Moreover, special staining can be applied depending on the experimental question. For example, von Kossa is used demonstrate mineralization in bone, Safranin O' detects the presence of proteoglycans and Trichrome stainings allow the visualisation of collagen fibres. Moreover, *in vivo* labelling techniques (e.g. tetracycline labelling) can be used to evaluate the mineralization front during bone growth and remodelling (Milch et al, 1958). Finally, the localisation of bone specific antigens (e.g. different types of collagen, glycoproteins, proteoglycans) cane be semiquantitatively evaluated with immunofluorescence. Bone evaluation without previous decalcification is also common, as it shows both the mineralised and cellular components of bone, which provides vital information on bone turnover or bone formation and resorption (Goldschlager et al., 2010). However, performing undecalcified bone histology is challenging and requires variations in technique from those used in standard paraffin embedded histology (e.g. special embedding and sectioning procedures) (Goldschlager et al., 2010). Together with descriptive histology, bone histomorphometry can be used to quantitatively analyse parameters of interest such as lengths, distances between points, areas and number of components. Parameters describing the three-dimensional organisation of bone can be deduced based on two-dimensional microscopic images (Dalle Carbonare et al., 2005). Common and useful applications of

two-dimensional histomorphometry are the analysis of structural changes in trabecular bone and the patological changes in degenerative disease (e.g. osteoarthrosis) (Kang et al., 1998).

Micro-computed tomography

Although the possibility to deduce the three-dimensional organization of trabecular bone from two-dimensional histologic sections is possible through histomorphometric analysis, the most reliable method to assess trabecular bone microscopic structure is micro-computed tomography (µCT) (Müller et al., 1998; Hildebrand, et al., 1999; Chappard et al., 2005). Microarchitectural parameters which have a fundamental role in bone quality (Fazzalari et al., 1998; Hernandez and Keaveny, 2006) are rapidly measured in a more direct fashion with micro-CT than they are in histomorphometry. This allows a significant improvement of the tools available for studying and understanding the mechanical function on the bone, especially trabecular bone, providing for a wealth of possibilities and unbiased determination of it architectural properties (Odgaard, 1997). Basic micro-CT parameters include bone volume/tissue volume ratio (the proportion of bone tissue in a sample); trabecular indices such as trabecular number per mm, trabecular thickness and trabecular separation; connectivity (the three-dimensional organisation of the trabeculae); structural model index (the proportion of plate-like and rod-like tissue) and degree of anisotropy. Micro-CT analysis is invaluable not only from a descriptive point of view, but also because through different types of mathematical models (e.g. finite element analysis) the biomechanical properties of the bone can be inferred (Parr et al., 2012; Faulkner et al., 1991; Depalle et al., 2012).

Biomechanical testing

Several different mechanical analyses exist to examine bone's mechanical competence and fracture risk, which selectively allow to test different parameters of clinical relevance and interest, providing different types of information, and they can be grouped as follows: whole bone testing, mesoscale cortical and cancellous bone testing, microscale testing and nanoscale testing (Bailey and Vashishth, 2018) (Fig. 1). Whole bone testing is typically performed in axial, bending or torsional loading modes (Hernandez and Keaveny, 2006; Cole and van der Muelen, 2011). Bending tests are especially useful when trying to assess the mechanical properties of long bones, while compression tests are usually aimed to determine vertebral mechanical properties (Turner and Burr, 1993; Goodyear and Aspden, 2012). The characteristics of the bone which are more relevant for whole bone testing and influence the results are geometry and composition (Bailey and Vashishth, 2018).
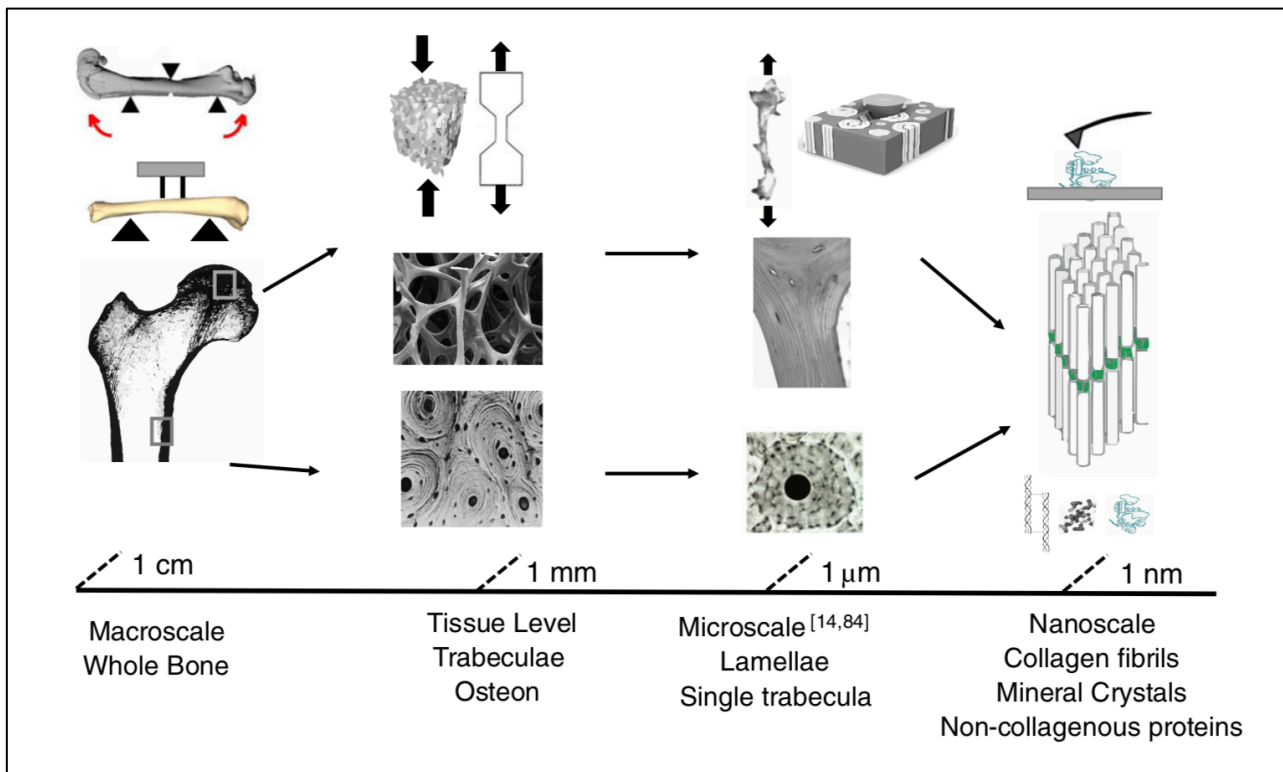
Fig. 1 - Schematic of bone structural hierarchy with the commonly used mechanical characterisation technique at each length scale (from Bailey and Vashishth, 2018).

Bone properties at the mesoscale are evaluated through the mechanical analysis of regularly shaped specimens of cortical and trabecular bone, which are typically loaded to failure in compression, tension, torsion or bending (Bailey and Vashishth, 2018). Being independent of whole bone geometry, these tests are aimed to test the contribution of bone microarchitecture, porosity and density (Bailey and Vashishth, 2018). Microindentation can be used to test bone at the microscale, analysing the biomechanical behaviour of osteons and individual trabeculae (Hunt and Donnelly, 2016). Mechanical outcome of this type of test are basically hardness and elastic modulus (Nyman et al., 2016). Alternative approaches include bending of single trabeculae and osteons (Tang et al., 2007, 2009; Ascenzi et al., 2007). Collagen fibres infiltrated with hydroxyapatite crystals are tested when analysing the bone at the nanoscale (Rho et al., 1998; Burket et al., 2013) through nanoindentation, scratch tests and other in-situ tests. For nanoindentation, a force-displacement curve is evaluated, providing mechanical outcomes of hardness and indentation modulus. Scratch test is used to evaluate in situ toughness and fracture toughness (Islam et al., 2012), and is able to detect changes in bone matrix fracture resistance due, for example, to water removal (Wang et al. 2016). Tension, compression and bending in situ allow to study in real time specific deformation and failure mechanisms that can only be inferred in traditional tests (Zimmermann et al. 2014).

Bone processing

Because of the peculiar composition of its matrix, characterized by a high mineral content in a densely packed network of collagenous and non-collagenous materials, several problems arise during bone processing (Liu et al., 2017), which is considered very challenging. In particular decalcification, the technique that removes mineral from the bone while preserving all the essential microscopic elements and tissue antigenicity (Gül et al., 2014), is a frustrating step. It is a very complicated and delicate step, to the point that special equipment (e.g. polymer resins, special microtome blades, special pre-staining and staining techniques) has been created in order to be able to process undecalcified bone. The most used decalcification methods are: immersion in acid of calcium chelators' solutions (Kiviranta, 1980; Guibas et al., 2014; Mattuella et al., 2007; Yamamoto-Fukud, 2000; Liu et al., 2017; Neves et al., 2011; Yoshioka et al., 2002; Gupta et al., 2014; Morse, 1945), sonication (Reineke et al., 2006; Hatta et al., 2013) and microwave (Kok and Boone, 1992; Imaizumi et al., 2013; Sangeetha et al., 2013; Katoh, 2016; Pitol et al., 2007); agitation and/or heat are reported as enhancing factors (Schajaowicz and Cabrini, 1955; Verdenius and Alma, 1958; Pitol et al., 2007; Kapila et al., 2015). Immersion in decalcifying solution is probably the most available methods in laboratory routine. However, despite the existence of several processing techniques, few accepted protocols and guidelines are available.

Animal models in bone-related research

Despite the promising results of alternative procedures, in many cases animal models are still irreplaceable. In fact, cell or tissue cultures alone cannot recreate the complex *in vivo* situation and the efficacy and safety of almost every therapy has to be preliminarily tested on appropriate animal models. An animal model is "a living organism with an inherited, naturally acquired, or induced pathological process that in one or more respects closely resembles the same phenomenon occurring in man" (Wessler, 2976), to be used in medical research in order to obtain results that can be extrapolated to human medicine. As far as bone-related research is concerned, animal models are essential for economical, ethical and regulatory reasons. Preclinical studies are often less expensive compared with large-scale clinical trials; cell and tissue cultures results cannot always be extrapolated to the living organism and never allow a complete biological evaluation; European animal testing regulation (European Medicines Agency guidelines), finally, often requires targeted preclinical *in vivo* evaluations (Stravropoulos et al., 2000). A huge number of animal bone models exist, in order to meet specific experimental requirements in all bone research fields: maxillo-facial and orthopaedic surgery (with research being done on mice, rats, rabbits, dogs, sheep, goats and pigs) (Fyda et al., 1995; Kuroda, 1995; Pearce et al., 2007; Por et al., 2008; Icekson et al., 2009; Bornstein et al., 2009; Horner et al., 2010; Gomes and Fernandes, 2011; Reifenrath et al., 2014; Liu et al., 2014; Cray et al., 2014; Bigham-Sadegh and Oryan, 2015; Stavropoulos et al., 2015; Semyari et al., 2015; Van Griensven, 2015)

dentistry (with research mostly being done on rats, rabbits, dogs, pigs and non-human primates) (Pearce et al., 2007; Bhardway and Bhardway, 2012; Katsamakis et al., 2013; Liu et al., 2014; Bigham-Sadegh and Oryan, 2015; Starvropoulos et al., 2015); metabolic, neoplastic (Yu et al., 2009) and degenerative diseases such as osteoporosis (with research being done mainly on mice and rats) (Lelovas et al. 2008; Ochi and Takeda, 2011), and others. Such great bone models assortment reflects the great differences occurring in bone composition and structure in different species and anatomic sites (Aerssens et al., 1998; Barbier et al., 1999; Nunamaker, 1998; Schnapper et al., 2002; Kastl et al., 2002; Boutroy et al., 2005; Martiniakova et al., 2006; Martiniakova et al., 2006; Van der Linden et al., 2006; Por et al., 2008; Lorinson et al., 2008; Diederichs et al., 2009; Donnelly et al., 2010; Bagi et al., 2011; Barak e t al., 2013; Shipov et al., 2013). As a consequence, different animal models turn out to be more or less useful depending on the experimental question, showing similarities and differences with several human physiological and pathological conditions (Aerssens et al., 1998; Nunamaker, 1998; Pearce et al., 2007; Bagi et al., 2011; Katsamakis et al., 2013; Reinfenrath et al., 2014; Bigham-Sadegh and Oryan, 2015; Teng et al., 1997; Ventura et al., 2014). In addition, bone tissue is highly dynamic and metabolically active, and exhibits substantial intra-specific changes based both on the tissue and the animal age. In fact, its composition and microarchitecture change as it ages and as the animal ages (Eckstein et al., 2007; Furst et al., 2008; Lochmuller et al., 2008; Gourion-Arisquaud et al., 2009; Donnelly et al., 2010; Turunen et al., 2013; Vaccaro et al., 2012; Uchida et al. 2012), adapting to the mechanical loading environment according to Wolff's law. Just as many differences exist in several skeletal diseases physiopathology and bone healing processes (Nunamaker, 1998; Barker and Wright, 2014; Katsamakis et al., 2013; Reinfenrath et al., 2014; Bigham-Sadegh and Oryan, 2015; Teng et al., 1997; Ventura et al., 2014) (which are bone-specific and trace embryological development), and they must be taken into account during experimental design. This is particularly true if bone remodeling and regeneration preclinical studies are to be carried out: selecting an animal of unspecified "skeletal age" (usually juvenile *vs* adult) can mislead the researchers when interpreting test results. Based on these observations, a detailed knowledge of all the different models of bone normal morphology is undeniable. The ultimate goal of bone research, whether it's about traumatology, orthopedics, oncology, degenerative diseases or more, is achieving a functionally efficient clinical outcome. As a consequence, species-specific bone features must be preserved after therapeutic interventions, which must aim to species-specific *restitutio ad integrum*. Despite the great number of studies on the subject, selecting an appropriate animal model is still complicated (Reinfenrath et al., 2014; Bigham-Sadegh and Oryan, 2015), and often grounds on convenience (cost, ease of handling and care, size, acceptability to society) rather than coherence. Notwithstanding that no single pre-clinical *in vivo* model is ideal, the lack of conclusive data about the normal bone features in animal of different species and age is still a relevant obstacle that often prevents researchers to achieve reliable outcomes and forces them to waste valuable resources.

The first aim of the project is to bridge the gaps in normal bone features and support the researchers who operate in the field by:

a) the definition of species-specific and site-specific guidelines for bone specimens' decalcification

b) the characterization of swine and ovine bone tissue with a multidisciplinary approach (histology, densitometry, microCT and biomechanical testing)

Skeletal development

The development of a newborn into an adult implies dramatic changes in body size and shape, which happen via continuous body growth and progressive maturation of the musculoskeletal and nervous systems (Helmsmuller et al, 2013). Bone growth and maturation start during the fetal stage, and then continue after birth together with the whole growth and maturation of the entire individual.

Osteogenesis

In the histogenesis of bone, the first tissue that is formed is an immature type of bone known as primary or woven bone, characterised by randomly oriented collagen fibres and low-mineralized matrix. It is a temporary tissue, which is replaced by secondary or lamellar bone or disappears to form the bone marrow cavity. In contrast, secondary bone is characterised by regularly arranged collagen fibres, higher matrix mineralisation and a higher number of osteocytes. The replacement of primary bone by secondary bone occurs via two modalities of osteogenesis (endochondral and intramembranous ossification), which share a common sequence of events: differentiation of osteoblasts, which deposit matrix that is after mineralized, formation of woven trabeculae which are then removed to form the bone marrow cavity, replaced by secondary trabeculae or converted into primary cortical bone. When this process takes place within primitive connective tissue), it is called intramembranous ossification; when it occurs in pre-existing calcified cartilage, it is called endochondral ossification (Webster, 1988).

Intramembranous ossification typically occurs in regions of reduced/absent loadbearing, such as skull flat bones (e.g. frontal and parietal bones) (Hyttel, 2010). The primitive event of intramembranous ossification, which completes within foetal life, is mesenchymal cells' grouping to form osteoblasts, together with neoangiogenesis. (Percival and Richtmeier, 2013). Osteoblasts depose a dense osteoid-rich intercellular matrix, where they are eventually entrapped as osteocytes. Mineral is then deposed on the osteoid matrix, and an irregular net of primitive nonlamellar bone trabeculae is formed, which are finally replaced by mature lamellar bone (Noden, 1983; Noden, 1991; Hall and Miyake, 1992; Dunlop and Hall, 1995; Jiang et al., 2002; Helms and Schneider, 2003).

Endochondral ossification typically occurs in loadbearing regions, such as long bones. It develops within a cartilage model, which influences the shape, size and orientation of the future bone (Webster, 1988). The primitive event of endochondral ossification is proliferation and hypertrophy of the cell that occupy the central diaphysis, which arrange in columns; these cells undergo gradual regression due to the reduction and mineralization of extracellular matrix. Perichondrium-derived blood vessels and mesenchymal cells then invade the diaphyseal region, and form the diaphyseal (primary) ossification centre, which gradually expands at its periphery while cavitating at its internal side, to form primitive marrow cavities. Entrapped mesenchymal cells differentiate into osteoblasts, which are responsible for osteoid deposition within the

primitive bone trabeculae. While growing in diameter thanks to perichondral apposition, the diaphyseal ossification centres gradually develop in length in the direction of the epiphyseal (secondary) ossification centres, which invariably appear after birth. Basic events for the development of epiphyseal ossification centres mostly retrace the steps described for the diaphyseal ossification centres; their concentrical growth continues in the direction of the diaphyseal ossification centre at one side, and the future articular surface at the other side (Erlebacher et al., 1995; Olsen et al., 2000; Karsenty and Wagner, 2002; Kronenberg, 2003).

Cartilage canals

Cartilage canals are perichondrium-derived tube-shaped formations containing a central arteriole which branches out into an anastomosing network of capillaries. They house lymphatics (Wilsman and Van Sickle, 1972), unmyelinated nerve fibers (Wilsman and Van Sickle, 1972; Stockwell, 1971; Hedberg et al., 1995) and mesenchymal stem cells, embedded within a loose extracellular matrix (Blumer et al., 2008). Cartilage canals have been described in several species, including birds and mammals (Burkus et al., 1993; Shapiro, 1998; Ytrehus et al., 2004; Blumer et al., 2005; Blumer et al., 2006; Blumer et al., 2007; Olstad et al., 2007; Olstad et al., 2009; Olstad et al., 2013; Toth et al., 2013; Nissi et al., 2014; Hellings et al., 2015; Hendrickson et al., 2015; Kinsley et al., 2015; Nissi et al. 2015). Little detailed information are reported about dogs (Wilsman e Van Sickle, 1970; Wilsman and Van Sikle, 1971), mostly it is in relation to the development of orthopaedic diseases (Guthrie et al., 1992; Wolschrijn et al., 2008). However, a wide variety of CCs size and shape has been described in dogs, from short unbranched channels to long channels coursing from one side of the epiphysis to the other (Wilsman and Van Sickle, 1972), all of them tightly associated with epiphyseal ossification centres (Wilsman and Van Sickle, 1970). Their primary function is nutrients supply to the growing cartilage and waste products elimination. Other functions, still under discussion, may include a contribution to the formation and maintenance of secondary ossification centres (Blumer et al., 2005; Blumer et al., 2007; Blumer et al., 2006; Alvarez et al., 2005) and possibly the transformation of perivascular cells into matrix-producing chondrocytes as cartilage physiologically regresses, serving the cartilage growth itself (Olstad, 2007). Evidence demonstrated that defects of cartilage canal blood supply lead to disturbance of endochondral ossification, in humans as well as in other animals (Ythreus et al., 2007). The way these diseases are initiated is still debated.

Skeletal development in dogs

- Axial skeleton

The skeletal development of the skull is very complex (Fig. 2): the neurocranium forms a protective case around the brain, while the splanchnocranium forms the skeleton of the face, also sorrounding head visceral cavities. In general, the front of the head is derived from the neural crest, while the back is derived from a combination of neural crest cells and head mesoderm. The bones of the skull have three different origins: the skeleton of the face is formed through intramembranous ossification from the branchial arches and the ectomesenchymal swelling of the facial area; the flat bones of the calvarium are formed through intramemembranous ossification as well; the bones of the floor and ventral portion of the cranial vault are predominantly formed by endochondral ossification (Evans, 1993; Hyttel, 2010).

Based on the shape of their adult skull, dogs have been classified in three cathegories: brachycephalic, mesaticephalic and dolichocephalic (Evans, 1993). As a general rule, dolichocephalic dogs show a greater development of the skull longitudinal axis; brachycephalic dogs have a shorter and larger skull, and mesaticephalic dogs exhibit intermediate skull features. Most veterinarian craniometric studies have been performed on adult animals to define their morphotype (Ellenberger and Baum, 1932; Stockard, 1941; Bourdelle et Bressou, 1953; Seiferle, 1966; Brehm et al., 1985; Lignereux et al., 1991; Onar et al., 2001; Alpak et al., 2004; Gacsi et al., 2009; Schmidt et al., 2011; Koch et al., 2012); several studies have also been performed to investigate the canine skull pattern derived from the wolf from a morphometric and genetic point of view (Drake and Klingenberg, 2010; Bannasch et al., 2010; Boyko et al., 2010; Shearin et al., 2010; Schoenebeck and Ostrander, 2013).

Currently, no detailed information is currently available on growing dogs, except for two studies on German Shepherd puppies (Onar, 1999; Onar and Gunes, 2003). However, it has been postulated that in brachycephalic breeds the skull shape is generated before birth and continues its development after birth (Starck, 1962).
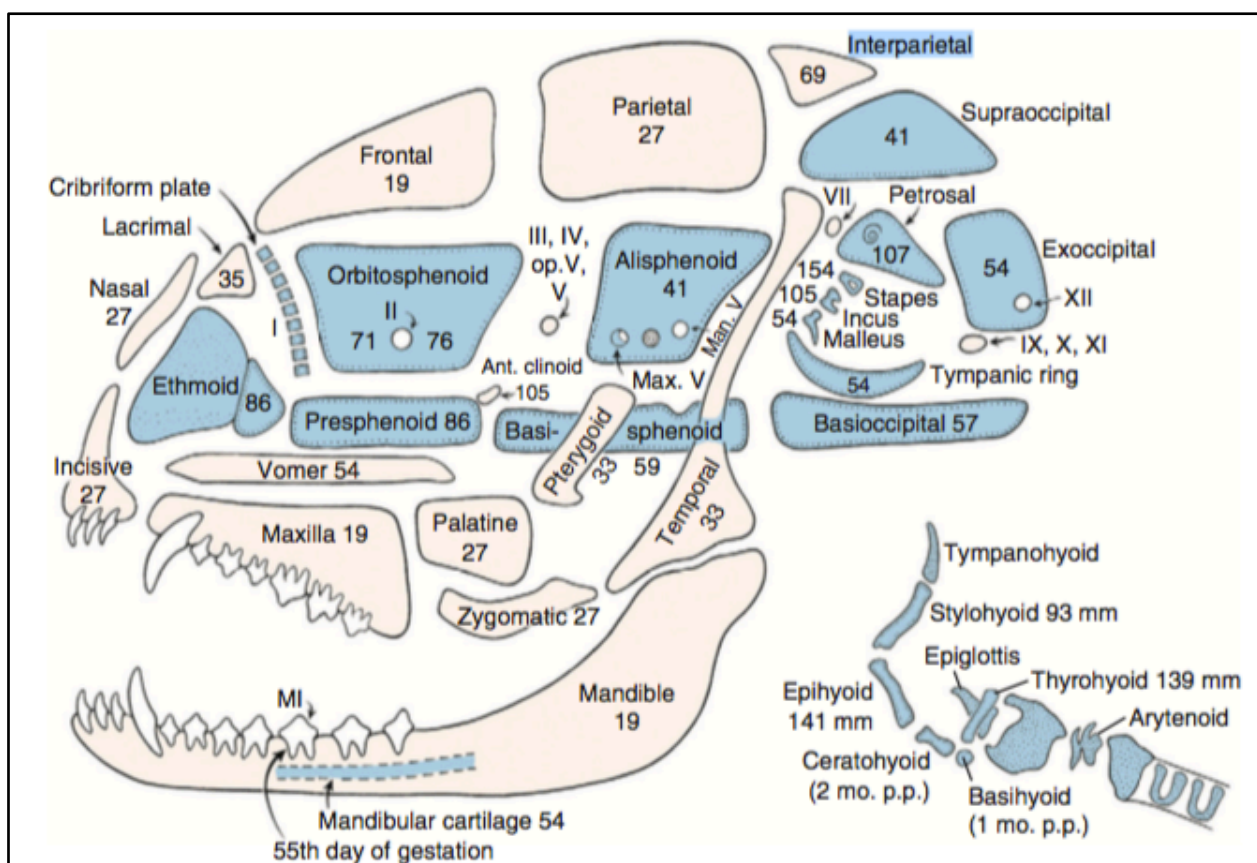

Fig. 2 – Diagrammatic dog skull showing the sequence of initial ossification. The numerals indicate the fetal size in millimetres at which time each of the bone begins to ossify. Blue bones with dotted outline are formed in cartilage (from Evans HE: Prenatal development of the dog, Ithaca, NY, 1974, 24th Gaines Veterinary Symposium).

The vertebral column is formed by perichondral and endochondral ossification. For each vertebra, with the exception of the atlas and the axis, form from 5 ossification centres (three for the vertebral body and two for

the neural arch) (Evans, 1993). The development of the body of the atlas and axis is peculiar, because part of the atlas centre fuses with the axis. In fact, the atlas is finally formed by three centres (one for the body and two for the vertebral arch), while the axis forms from seven centres (5 for the bosy and dens, two for the vertebral arch). The vertebral arches of the atlas fuse dorsally after 100 days approximately, then they fuse with the body around 110-120 days, while complete fusion of the axis occurs in the range of 220-400 days. (Watson and Evans, 1986; Watson et al., 1976; Watson 1981).

- Appendicular skeleton

In dog, as in other mammals, limbs bones develop through endochondral ossification. Limb bud growth starts towards the end of the fourth week of gestation, with a gap of 1-2 days between the morphogenesis of forelimbs and hindlimbs (Hyttel et al., 2010; Evans and De Lahunta, 2013). Diaphyseal (primary) ossification centres of long bones (develop during foetal life, while the epiphyseal (secondary) ossification centres of long bones and most of the ossification centres of the short bones formed after birth. Skeletal development then proceeds in stages until adulthood, when the closure of growth plates arrests bone growth. Some bones are entirely formed from a single ossification centre (e.g. the clavicle most of carpal/tarsal bones, the phalanx III and the sesamoid bones (Cerny and Cizinauskas, 1995; Evans and De Lahunta, 2013), (Hare, 1959; Hare, 1961); the others derive from the fusion of different centers. In particular, all carpal and tarsal bones derive from a single centre, with the exception of the accessory carpal bone and the calcaneus (two centeres) and the *intermedioradial* carpal bone (three centres), (Hare, 1959; Hare, 1961; Hare, 1959; Hare, 1961). Metacarpal/metatarsal bones and phalanges I/II are formed from a diaphyseal ossification centres which fuses with a single epiphyseal ossification centres, which is located in a distal (metacarpal/metatarsal bones) or proximal position (phalages I/II) (Hare, 1960). The scapula develops from two centers (body and and *tuber scapulae)* (Smith, 1960; Hare, 1961; Yonamine et al., 1980). In the radius, ulna and fibula three centres fuse (corpus, proximal and distal epiphysis); recently, an independent centre for the anconeal process has been described in in large and medium breeds (Van Sickle, 1966; Gustaffson et al., 1975; Olsson, 1983; Guthrie et al., 1992; Turner et al., 1998). The humerus , femur and tibia develop from five centres (Chapman, 1965; Hare, 1960; Smith and Allocock, 1960); the pelvis from seven/eight centres (Riser, 1973). Irrespective of the breed, fusion takes place with the same, definite sequence. Interestingly, the first two that fuse are traction epiphyses: accessory carpal bone, where the flexor ulnary muscle is attached, and scapular tuberosity from where the bicicips brachii arises. For the same reason, the tuber calcis also fuses very early (Sumner-Smith, 1966*)*. Therefore it is reasonable to assume that mechanical loading due to the insertion of major muscle masses could facilitate diffusion of molecules inside the hypertrophic cells of cartilage, thus accelerating ossification processes (Peinado Cortes et al., 2011). Complete skeletal maturity is reached in dogs around one year of age; however, the growth plate of the iliac crest may be still visible around two years in some individuals, or may remain open permanently (Ticer, 1975).
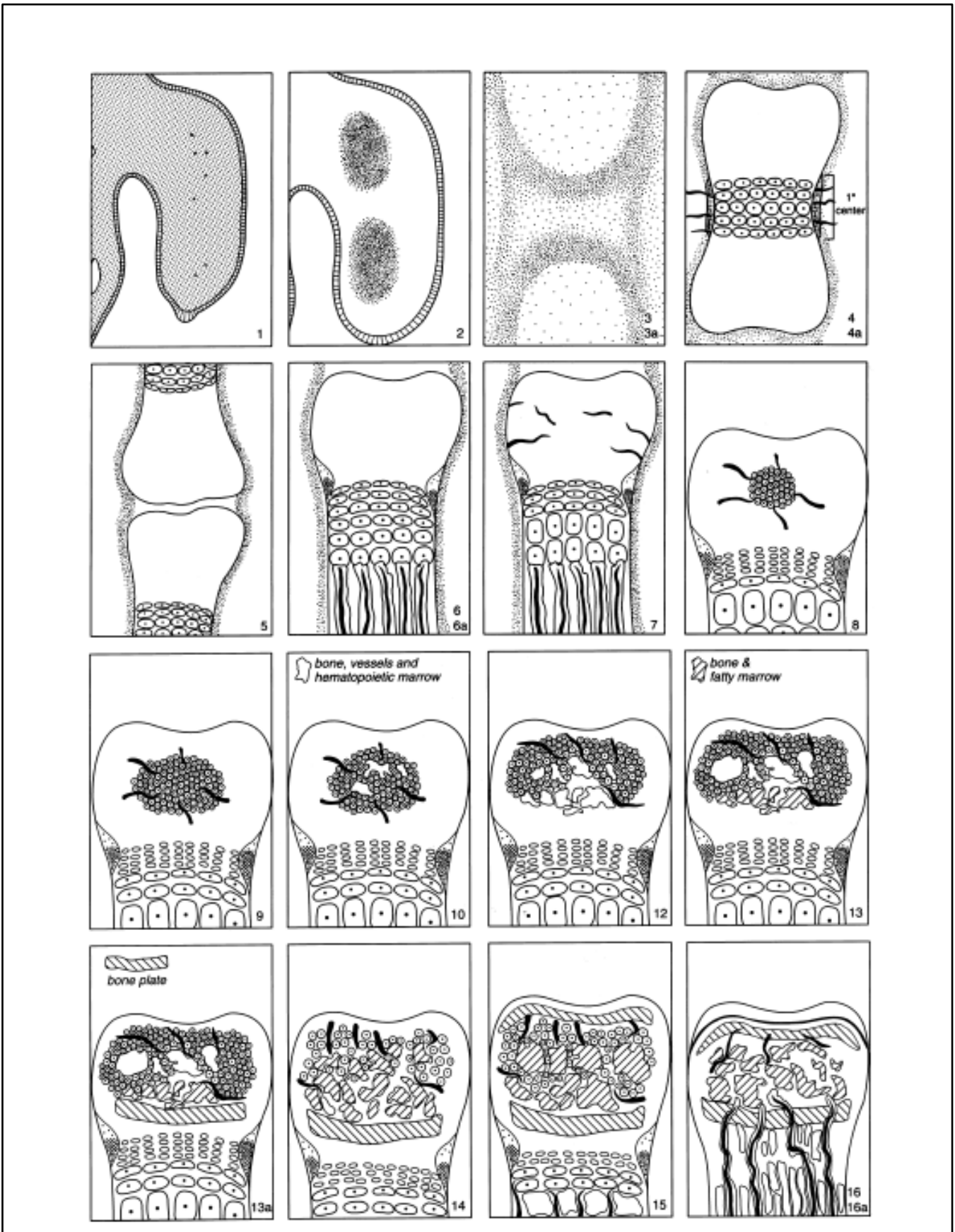
Fig. 3– The major stages in the formation and development of long bones (from Rivas and Shapiro, 2002).

In the last decades, limb development in dogs has been investigated with morphometric, radiographic and densitometric approaches. Several studies aimed to establish breed standards (Onar, 1999; Onar and Gunes, 2003; Schmidt et al., 2011), investigate abnormal skeletal development (Vanden Berg-Foels et al., 2006; Breit et al., 2004) or exclude pathological conditions (Emmerson et al., 2000; Todhunter et al., 1997; Vanden Berg-Foels et al., 2011), quantify the long bone healing (Zotti et al., 2004), assess density variation in different breeds (Markel et al., 1994), and evaluate the resistance of canine spine to traumatic lesions (Zotti et al., 2011). Most of the investigations about skeletal development, however, aimed to age determination, and therefore focused on the time of appeerence of limbs' ossification centers and the time of growth plate closure (skeletal maturity). Since puppy trafficking has become a pressing issue in Europe, in fact, veterinarians are often asked to precisely determine the age of puppies in forensic scenarios. Even if a large number of studies are available on the subject, reported are often inhomogeneous and therefore incomparable, due to small sample size, unstandardized protocols and different enrollment age. For this reason, our research group recently performed a literature review of the about the time of ossification centres' appearance and fusion, proposing a revised and simplified version of previously published table to provide user-friendly indications for both forensic veterinarians and clinicians. Mastering bones growth patterns from birth to adulthood is mandatory also to diagnose and potentially treat skeletal developmental abnormalities (Breit et al, 2004; Vanden Berg-Foels et al, 2006; Vanden Berg-Foels et al, 2011). In fact, in 1973 Riser (Riser, 1973) already reported that "a clear understanding of the normal developmental pattern is imperative as rational base for comparison in evaluating radiographic changes associated with disease and injury of the hip". Several studies focused on skeletal development abnormalities, such as hip and elbow dysplasia. Works about hip development, for example, suggest that its onset in Labrador Retrievers (Todhunter et al., 1997) (Vanden Berg-Foels et al., 2011) and German Shepherd (Madsen et al., 1991) might be related to ossification defects. Similarly, ossification abnormalities have been proposed to have a role in the pathogenesis of ununited anconeal process and coronoid disease (Janutta and Distl, 2008).

However, it must be kept in mind that this type of investigations imply repeated exposures of very young animals to invasive X-ray examination, might imply euthanasia for precise anatomic/pathologic evaluation, and require validation on a reasonably large number of animals. Radiographic examination on dead animals whose date of birth is certain may therefore represent a convincing alternative with regard to the reduction of the use of living animals for research purposes.

The second aim of this project was the study of some aspects of skeletal development in dogs, focusing on:
- skull development and its compared features in brachycephalic, mesaticephalic and dolichocephalic breeds
- the role of cartilage canals in long bones development
- the effects of pathology (quadriceps contracture) on hindlimb development

References

1. Adachi T, Tsubota K, Tomita Y, Hollister SJ. Trabecular surface remodeling simulation for cancellous boneusing microstructural voxel finite element models. J Biomech Eng. 2001 Oct;123(5):403-9.
2. Aerssens J., Boonen S., Lowet G., Dequeker J. Interspecies differences in bone composition, density, and quality: potential implications for *in vivo* bone research. Endocrinology. 1998 Feb;139(2):663-70.
3. Alpak H, Mutus R, Onar V. Correlation analysis of the skull and long bone measurements of the dog. Annals of anatomy = Anatomischer Anzeiger : official organ of the Anatomische Gesellschaft. 2004;186(4):323-30.
4. Ascenzi A, Bonucci E. The tensile properties of single osteons. Anat Rec. 1967 Aug;158(4):375-86.
5. Bagi C.M., Berryman E., Moalli M.R. Comparative bone anatomy of commonly used laboratory animals: implications for drug discovery. Comp Med. 2011 Feb;61(1):76-85.
6. Bailey S, Vashishth D. Mechanical Characterization of Bone: State of the Art in Experimental Approaches-What Types of Experiments Do People Do and How Does One Interpret the Results? Curr Osteoporos Rep. 2018 Jun 18. doi: 10.1007/s11914-018-0454-8.
7. Bannasch D, Young A, Myers J, Truve K, Dickinson P, Gregg J, et al. Localization of canine brachycephaly using an across breed mapping approach. PloS one. 2010;5(3):e9632.
8. Barbier A., Martel C., De Vernejoul M.C., Tirode F., Nys M., Mocaer G., Morieux C., Murakami H., Lacheretz F. The Visualization and evaluation of bone architecture in the rat using three-dimensional x-ray microcomputed tomography. J Bone Miner Metab. 1999;17(1):37-44.
9. Bernau M[1], Kremer PV[2], Lauterbach E[3], Tholen E[4], Petersen B[4], Pappenberger E[3], Scholz AM[3]. Evaluation of carcass composition of intact boars using linear measurements from performance testing, dissection, dual energy X-ray absorptiometry (DXA) and magnetic resonance imaging (MRI). Meat Sci. 2015 Jun;104:58-66. doi: 10.1016/j.meatsci.2015.01.011. Epub 2015 Feb 7.
10. Bhardwaj A., Bhardwaj S.V. Contribution of animal models in periodontal research. Ijavms, Vol.6, Issue 3: 150-157.
11. Bigham-Sadegh A., Oryan A. Selection of animal models for pre-clinical strategies in evaluating the fracture healing, bone graft substitutes and bone tissue regeneration and engineering. Connect Tissue Res. 2015 Jun;56(3):175-94.
12. Blumer MJ, Fritsch H, Pfaller K, Brenner E. Cartilage canals in the chicken embryo: ultrastructure and function. Anat Embryol (Berl) 2004;207(6):453-62.
13. Blumer MJ, Longato S, Fritsch H. Structure, formation and role of cartilage canals in the developing bone. Ann Anat 2008;190:305-15.
14. Blumer MJ, Longato S, Richter E, Perez MT, Konakci KZ, Fritsch H. The role of car- tilage canals in endochondral and peri- chondral bone formation: are there simi- larities between these two processes? J Anat 2005;206:359-72.
15. Blumer MJ, Longato S, Schwarzer C, Fritsch H. Bone development in the femoral epiphysis of mice: the role of car- tilage canals and the fate of resting chon- drocytes. Dev Dyn 2007;236:2077-88
16. Blumer MJ, Schwarzer C, Perez MT, Konakci KZ, Fritsch H. Identification and location of bone-forming cells within carti- lage canals on their course into the sec- ondary ossification centre. J Anat 2006;208: 695-707.
17. Bobby TC[1], Ramakrishnan S. Characterization of trabecular structure in human femur radiographic images using ridgelet transform and support vector machines. Biomed Sci Instrum. 2012;48:532-9.
18. Bornstein M.M., Heynen G., Bosshart D.D., Buser D. Effect of two bioabsorbable barrier membranes on bone regeneration of standardized defects in calvarial bone: a comparative histomorphometric study in pigs. J Periodontol. 2009 Aug;80(8):1289-99.
19. Bourdelle E, Bressou C. Anatomie regionale des animaux domestiques. Paris1953.
20. Boutroy S., Bouxsein M.L., Munoz F., Delmas P.D. *In vivo* assessment of trabecular bone microarchitecture by high-resolution peripheral quantitative computed tomography. J Clin Endocrinol Metab. 2005 Dec;90(12):6508-15.
21. Boyko AR, Quignon P, Li L, Schoenebeck JJ, Degenhardt JD, Lohmueller KE, et al. A simple genetic architecture underlies morphological variation in dogs. PLoS Biol. 2010;8(8):e1000451.

22. Brehm H, Loeffler K, Komeyli H. [Skull forms in dogs]. Anatomia, histologia, embryologia. 1985;14(4):324-31.

23. Breit, S., Kunzel, W., Seiler, S., 2004. Variation in the ossification process of the anconeal and medial coronoid processes of the canine ulna. Research in Veterinary Science 77, 9-16.

24. Bruyère Garnier K[1], Dumas R, Rumelhart C, Arlot ME. Mechanical characterization in shear of human femoral cancellous bone: torsion and shear tests. Med Eng Phys. 1999 Nov;21(9):641-9.

25. Burket JC, Brooks DJ, MacLeay JM, Baker SP, Boskey AL, van der Meulen MC. Variations in nanomechanical properties and tissue composition within trabeculae from an ovine model of osteoporosis and treatment. Bone. 2013 Jan;52(1):326-36. doi: 10.1016/j.bone.2012.10.018. Epub 2012 Oct 23.

26. Cerny, H., Cizinauskas, S., 1995. The Clavicle of Newborn Dogs. Acta Veterinaria Brno 64, 139-&.

27. Chapman, W., 1965. Appearance of ossification centers and epiphyseal closures as determined by radiographic techniques. J Am Vet Med Assoc 147, 138-141.

28. Chappard D, Retailleau-Gaborit N, Legrand E, Baslé MF, Audran M. Comparison insight bone measurements by histomorphometry and microCT. J Bone Miner Res. 2005 Jul;20(7):1177-84. Epub 2005 Feb 14.

29. Cole JH[1], van der Meulen MC. Whole bone mechanics and bone quality. Clin Orthop Relat Res. 2011 Aug;469(8):2139-49. doi: 10.1007/s11999-011-1784-3.

30. Cray J. Jr., Henderson S.E., Smith D.M., Kinsella C.R. Jr., Bykowski M., Cooper G.M., Almarza A.J., Losee J.E. Bmp-2-regenerated calvarial bone: a biomechanical appraisal in a large animal model. Ann Plast Surg. 2014 Nov;73(5):591-7.

31. Currey JD. Mechanical properties of vertebrate hard tissues.Proc Inst Mech Eng H. 1998;212(6):399-411.

32. Dalle Carbonare L, Valenti MT, Bertoldo F, Zanatta M, Zenari S, Realdi G, Lo Cascio V, Giannini S. Bone microarchitecture evaluated by histomorphometry.Micron. 2005;36(7-8):609-16. Epub 2005 Sep 6.

33. den Boer FC, Patka P, Bakker FC, Wippermann BW, van Lingen A, Vink GQ, Boshuizen K, Haarman HJ. New segmental long bone defect model in sheep: quantitative analysis of healing with dual energy x-ray absorptiometry. J Orthop Res. 1999 Sep;17(5):654-60.

34. Depalle B, Chapurlat R, Walter-Le-Berre H, Bou-Saïd B, Follet H. Finite element analysis dependence of stress evaluation for human trabecular bone. J Mech Behav Biomed Mater. 2013 Feb;18:200-12. doi: 10.1016/j.jmbbm.2012.08.012. Epub 2012 Nov 21.

35. Diederichs G., Issever A.S., Greiner S., Linke B., Korner J. Three-dimensional distribution of trabecular bone density and cortical thickness in the distal humerus. J Shoulder Elbow Surg. 2009 May-Jun;18(3):399-407.

36. Donnelly E. Methods for assessing bone quality: a review. Clin Orthop Relat Res. 2011 Aug;469(8):2128-38. doi: 10.1007/s11999-010-1702-0.

37. Donnelly E., Chen D.X., Boskey A.L., Baker S.P., Van Der Meulen M.C. Contribution of mineral to bone structural behavior and tissue mechanical properties. Calcif Tissue Int. 2010 Nov;87(5):450-60.

38. Drake AG, Klingenberg CP. Large-scale diversification of skull shape in domestic dogs: disparity and modularity. Am Nat. 2010;175(3):289-301.

39. Ellenberger W, Baum H. Handbuch der vergleichenden Anatomie der Haustiere. Berlin:

40. Emmerson, T.D., Lawes, T.J., Goodship, A.E., Rueux-Mason, C., Muir, P., 2000. Dual-energy X-ray absorptiometry measurement of bone-mineral density in the distal aspect of the limbs in racing Greyhounds. American Journal of Veterinary Research 61, 1214-1219.

41. Evans H, editor: The Skeleton. *Miller's Anatomy of the Dog,* ed 3, Philadelphia, 1993, Saunders.

42. Evans HE, De Lahunta A. Miller's Anatomy of the Dog. Fourth edition ed. St Louis (MO) USA: Saunders/Elsevir; 2013. 872 p.

43. Faulkner KG, Cann CE, Hasegawa BH. Effect of bone distribution on vertebral strength: assessment with patient-specific nonlinear finite element analysis. Radiology. 1991 Jun;179(3):669-74.

44. Fazzalari NL, Forwood MR, Smith K, Manthey BA, Herreen P. Assessment of cancellous bone quality in severe osteoarthrosis: bone mineral density, mechanics, and microdamage. Bone. 1998 Apr;22(4):381-8.

45. Fiala P[1], Hert J. Principal types of functional architecture of cancellous bone in man. Funct Dev Morphol. 1993;3(2):91-9.

46. Floerkemeier T, Wellmann M, Thorey F, Hurschler C, Witte F, Windhagen H. Comparison of bone mineral parameter measurements by dual-energy x-ray absorptiometry with bone stiffness measurements as indicators of the load-bearing capacity of regenerating bone. J Orthop Trauma. 2010 Mar;24(3):181-7. doi: 10.1097/BOT.0b013e3181bae887.

47. Ford JC, Wehrli FW. *In vivo* quantitative characterization of trabecular bone by NMR interferometry and localized proton spectroscopy. Magn Reson Med. 1991 Feb;17(2):543-51.

48. Fyda T.M., Callaghan J.J., Fulghum C.S., Seaber A.V., Myers B.S. A model of cortical window healing in the rabbit. Orthopedics. 1995 Feb;18(2):177-84.

49. Gacsi M, McGreevy P, Kara E, Miklosi A. Effects of selection for cooperation and attention in dogs. Behav Brain Funct. 2009;5:31.

50. Gibson LJ. The mechanical behaviour of cancellous bone. J Biomech. 1985;18(5):317-28.

51. Goff MG, Slyfield CR, Kummari SR, Tkachenko EV, Fischer SE, Yi YH, Jekir MG, Keaveny TM, Hernandez CJ. Three-dimensional characterization of resorption cavity size and location in human vertebral trabecular bone. Bone. 2012 Jul;51(1):28-37. doi: 10.1016/j.bone.2012.03.028. Epub 2012 Apr 3.

52. Goldschlager T, Abdelkader A, Kerr J, Boundy I, Jenkin G.

53. Gomes P.S., Fernandes M.H. Rodent models in bone-related research: the relevance of calvarial defects in the assessment of bone regeneration strategies. Lab Anim. 2011 Jan;45(1):14-24.

54. Goodyear SR, Aspden RM. Mechanical properties of bone ex vivo. Methods Mol Biol. 2012;816:555-71. doi: 10.1007/978-1-61779-415-5_35.

55. Grier SJ, Turner AS, Alvis MR. The use of dual-energy x-ray absorptiometry in animals. Invest Radiol. 1996 Jan;31(1):50-62.

56. Guibas GV, Lakis S, Gkimpas C, Manda M, Kapoukranidou D, Spandou E. Efficiency of different decalcification protocols for nasal osseous structures in a rat experimental model of allergic rhinitis, and their effects on epithelial histology: an attempt at standardization. Exp Toxicol Pathol. 2014 Dec;66(9-10):469-75. doi: 10.1016/j.etp.2014.09.001. Epub 2014 Sep 18.

57. Gül M, Bayat N, Gül S, Hüz M, Yıldız A, Otlu Al. A Comparison of Three Different Agents of Decalcification for a Histological Examination of Bone Tissues. Journal of Turgut Ozal Medical Center. 2014, Vol. 21 Issue 4, p274-279. 6p.

58. Gunderson SL, Schiavone RC, in: S. M. Lee (Ed.), International Encyclopedia of Composites, VCH Publishers, New York, 1991

59. Gupta S, Jawanda MK, Sm M, Bharti A. Qualitative histological evaluation of hard and soft tissue components of human permanent teeth using various decalcifying agents - a comparative study. J Clin Diagn Res. 2014 Sep;8(9):ZC69-72. doi: 10.7860/JCDR/2014/10195.4874. Epub 2014 Sep 20.

60. Gustaffson, P.O., Olsson, S.E., Kasstrom, H., Wennman, B., 1975. Skeletal development of greyhounds, German Shepherd dogs and their crossbreed offspring. Acta Radiologica, 81-107.

61. Guthrie, S., Plummer, J.M., Vaughan, L.C., 1992. Etiopathogenesis of Canine Elbow Osteochondrosis - a Study of Loose Fragments Removed at Arthrotomy. Research in Veterinary Science 52, 284-291.

62. Hare, W.C., 1959. Radiographic Anatomy of the Canine Pectoral Limb. Part -II. Developing Limb. J Am Vet Med Assoc 135, 305-310.

63. Hare, W.C., 1960. The age at which epyphiseal union takes places in the limb bones of the dog. Wien Tierarztl Mschr Festschrift Schreiber 9, 224-245.

64. Hare, W.C., 1961. The ages at which the centers of ossification appear roentgenographically in the limb bones of the dog. American Journal of Veterinary Research XXII, 825-835.

65. Hatta H, Tsuneyama K, Nomoto K, Hayashi S, Miwa S, Nakajima T, Nishida T, Nakanishi Y, Imura J. A simple and rapid decalcification procedure of skeletal tissues for pathology using an ultrasonic cleaner with D-mannitol and formic acid. Acta Histochem. 2014 Jun;116(5):753-7. doi: 10.1016/j.acthis.2014.01.006. Epub 2014 Feb 21.

66. Hayes WC, Carter DR. Postyield behavior of subchondral trabecular bone. J Biomed Mater Res. 1976 Jul;10(4):537-44.

67. Hébert D, Lebrun R, Marivaux L. Comparative three-dimensional structure of the trabecular bone in the talus of primates and its relationship to ankle joint loads generated during locomotion. Anat Rec (Hoboken). 2012 Dec;295(12):2069-88. doi: 10.1002/ar.22608. Epub 2012 Oct 25.

68. Hedberg A, Messner K, Persliden J, Hildebrand C. Transient local presence of nerve fibers at onset of secondary ossifica- tion in the rat knee joint. Anat Embryol (Berl) 1995;192:247-55.

69. Heiss C, Kern S, Malhan D, Böcker W, Engelhardt M, Daghma DES, Stoetzel S, Schmitt J, Ivo M, Kauschke V, Lips KS, Tushtev K, Rezwan K, El Khassawna T. A New Clinically Relevant T-Score Standard to Interpret Bone Status in a Sheep Model. Med Sci Monit Basic Res. 2017 Oct 2;23:326-335.

70. Hellings, I.R., S. Ekman, K. Hultenby, N.I. Dolvik and K. Olstad (2015). "Discontinuities in the endothelium of epiphyseal cartilage canals and relevance to joint disease in foals." J Anat doi: 10.1111/joa. 12391.

71. Hendrickson, E.H., K. Olstad, A. Nodtvedt, E. Pauwels, L. van Hoorebeke and N. I. Dolvik (2015). "Comparison of the blood supply to the articular-epiphyseal growth complex in horse vs. pony foals." Equine Vet J 47(3): 326-332.

72. Hernandez CJ, Keaveny TM. A biomechanical perspective on bone quality. Bone. 2006 Dec;39(6):1173-81. Epub 2006 Jul 28.

73. Hildebrand T, Laib A, Müller R, Dequeker J, Rüegsegger P. Direct three-dimensional morphometric analysis of human cancellous bone: microstructural data from spine, femur, iliac crest, and calcaneus. J Bone Miner Res. 1999 Jul;14(7):1167-74.

74. Hillier ML[1], Bell LS. Differentiating human bone from animal bone: a review of histological methods. J Forensic Sci. 2007 Mar;52(2):249-63.

75. Horner E.A., Kirkham J., Wood D., Curran S., Smith M., Thomson B., Yang X.B. Long bone defect models for tissue engineering applications: Criteria For Choice. Tissue Eng Part B Rev. 2010 Apr;16(2):263-71.

76. Hunt HB[1], Donnelly E[12]. Bone quality assessment techniques: geometric, compositional, and mechanical characterization from macroscale to nanoscale. Clin Rev Bone Miner Metab. 2016 Sep;14(3):133-149. doi: 10.1007/s12018-016-9222-4. Epub 2016 Aug 22.

77. Hyttel, P., Sinowatz, F., Vejlsted, M., 2010. Essentials of Domestic Animal Embryology.

78. Icekson M., Regev E., Neuman R., Margulis a. Transport distraction osteogenesis for closing full-thickness calvarial defects in sheep. Cleft Palate Craniofac J. 2009 Jul;46(4):363-7.

79. Imaizumi K, Taniguchi K, Ogawa Y. An evaluation of the effect of microwave irradiation on bone decalcification aimed to DNA extraction. Leg Med (Tokyo). 2013 Sep;15(5):272-7. doi: 10.1016/j.legalmed.2013.06.001. Epub 2013 Jul 6.

80. Islam A, Neil Dong X, Wang X. Mechanistic modeling of a nanoscratch test for determination of in situ toughness of bone. J Mech Behav Biomed Mater. 2012 Jan;5(1):156-64. doi: 10.1016/j.jmbbm.2011.08.019. Epub 2011 Sep 1.

81. Janutta V, Distl O. Review on canine elbow dysplasia: pathogenesis, diagnosis, prevalence and genetic aspects. Dtsch Tierarztl Wochenschr. 2008 May;115(5):172-81. Review.

82. Jensen KS, Mosekilde L, Mosekilde L. A model of vertebral trabecular bone architecture and its mechanical properties. Bone. 1990;11(6):417-23.

83. Kang Q, An YH, Butehorn HF, et al: Morphological and mechanical study of the effects of experimentally induced inflammatory knee arthritis on rabbit long bones. J Mater Sci Mater Med 9:463–473, 1998.

84. Kastl S., Sommer T., Klein P., Hohenberger W., Engelke K. Accuracy and precision of bone mineral density and bone mineral content in excised rat humeri using fan beam dual-energy x-ray absorptiometry. Bone. 2002 Jan;30(1):243-6.

85. Katoh K. Microwave-Assisted Tissue Preparation for Rapid Fixation, Decalcification, Antigen Retrieval, Cryosectioning, and Immunostaining. J Cell Biol. 2016;2016:7076910. Epub 2016 Oct 20.

86. Katsamakis S., Slot D.E., Van Der Sluis L.W., Van Der Weijden F. Histological responses of the periodontium to mta: a systematic review. J Clin Periodontol. 2013 Apr;40(4):334-44.

87. Kinsley M.A., S.A. Semevolos and K.F. Duesterdieck-Zellmer (2015). "Duesterdieck-Zellmer KF[1]. Wnt/β-catenin signaling of cartilage canal and osteochondral junction chondrocytes and full thickness cartilage in early equine osteochondrosis." J Orthop Res. 33(10):1433-1438.

88. Kiviranta I, Tammi M, Lappalainen R, Kuusela T, Helminen HJ. The rate of calcium extraction during EDTA decalcification from thin bone slices as assessed with atomic absorption spectrophotometry. Histochemistry. 1980;68(2):119-27.

89. Kleerekoper M, Villanueva AR, Stanciu J, Rao DS, Parfitt AM. The role of three-dimensional trabecular microstructure in the pathogenesis of vertebral compression fractures. Calcif Tissue Int. 1985 Dec;37(6):594-7.

90. Koch DA, Wiestner T, Balli A, Montavon PM, Michel E, Scharf G, et al. Proposal for a new radiological index to determine skull conformation in the dog. SAT, Schweizer Archiv fur Tierheilkunde. 2012;154(5):217-20.

91. Kok LP, Boon ME. Microwaves for declcification. In: Microwave cookbook for microscopists: art and science of visualization. Leyden: Coulomb Press; 1992 (Chapter 13).

92. Kuroda T. Bone formation and mechanical properties of the cancellous bone defect site filled with hydroxyapatite granules. Nihon Seikeigeka Gakkai Zasshi. 1995 Oct;69(10):1037-49.

93. Lelovas P.P., Xanthos T.T., Thoma S.E., Lyritis G.P., Dontas I.A. The laboratory rat as an animal model for osteoporosis research. Comp Med. 2008 Oct;58(5):424-30.

94. Lignereux Y, Regodon S, Pavaux C. Cephalic typology in dogs Typologie cephalique canine. Revue de Medecine Veterinaire. 1991;142(6):469-80.

95. Liu H, Zhu R, Liu C, Ma R, Wang L, Chen B, Li L, Niu J, Zhao D, Mo F, Fu M, Brömme D, Zhang D, Gao S. Evaluation of Decalcification Techniques for Rat Femurs Using HE and Immunohistochemical Staining. Biomed Res Int. 2017;2017:9050754. doi: 10.1155/2017/9050754. Epub 2017 Jan 26.

96. Liu H, Zhu R, Liu C, Ma R, Wang L, Chen B, Li L, Niu J, Zhao D, Mo F, Fu M, Brömme D, Zhang D, Gao S. Evaluation of Decalcification Techniques for Rat Femurs Using HE and Immunohistochemical Staining. Biomed Res Int. 2017;2017:9050754. doi: 10.1155/2017/9050754. Epub 2017 Jan 26.

97. Liu N., Lyu X., Fan H., Shi J., Hu J., Luo E. Animal models for craniofacial reconstruction by stem/stromal cells. Curr Stem Cell Res Ther. 2014 May;9(3):174-86.

98. Lorinson K., Loebcke S., Skalicky M., Grampp S., Lorinsond D. Signalment differences in bone mineral content and bone mineral density in canine appendicular bones. A Cadaveric Study. Vet Comp Orthop Traumatol. 2008;21(2):147-51.

99. Majumdar S. A review of magnetic resonance (MR) imaging of trabecular bonemicro-architecture: contribution to the prediction of biomechanical properties and fracture prevalence. Technol Health Care. 1998 Dec;6(5-6):321-7.

100. Markel MD, Sielman E, Bodganske JJ. Densitometric properties of long bones in dogs, as determined by use of dual-energy x-ray absorptiometry. Am J Vet Res. 1994 Dec;55(12):1750-6.

101. Martiniaková M, Grosskopf B, Vondráková M, Omelka R, Fabis M. Differences in femoral compact bone tissue microscopic structure between adult cows (Bos taurus) and pigs (Sus scrofa domestica). Anat Histol Embryol. 2006 Jun;35(3):167-70.

102. Martiniakova' M., Grosskopf B., Omelka R., Vondrakova' M., Bauerova' M. Differences among species in compact bone tissue microstructure of mammalian skeleton: use of a discriminant function analysis for species identification. J Forensic Sci. 2006 Nov;51(6):1235-9.

103. Mattuella LG, Bento LW, Vier-Pelisser FV, Araujo FB, Fossati ACM. Revista Odonto Ciência – Fac. Odonto/PUCRS, v. 22, n. 56, abr./jun. 2007

104. Milch RA, Rall DP, Tobie JE: Fluorescence of tetracycline antibiotics in bone. J Bone Joint Surg [Am] 40:897–910, 1958.

105. Morse A. Formic Acid-Sodium Citrate Decalcification and Butyl Alcohol Dehydration of Teeth and Bones for Sectioning in Paraffin. Journal of Dental Research Vol 24, Issue 3-4, pp. 143 – 153 First Published June 1, 1945 https://doi.org/10.1177/00220345450240030501.

106. Müller R, Van Campenhout H, Van Damme B, Van Der Perre G, Dequeker J, Hildebrand T, Rüegsegger P. Morphometric analysis of human bone biopsies: a quantitative structural comparison of histological sections and micro-computed tomography. Bone. 1998 Jul;23(1):59-66.

107. Neves, Juliana & Omar, Nádia & Aparecida Orsini Narvaes, Eliene & Gomes, Jose & Novaes, Pedro. (2011). Influence of different decalcifying agents on EGF and EGFR immunostaining. Acta histochemica. 113. 484-8. 10.1016/j.acthis.2010.04.006.

108. Nissi M.J., F. Toth, J. Zhang, S. Schmitter, M. Benson, C.S. Carlson and J.M. Ellermann (2014). "Susceptibility weighted imaging of cartilage canals in porcine epiphyseal growth cartilage ex vivo and *in vivo*." Magn Reson Med 71(6): 2197-2205.

109. Nissi M.J., F. Toth, L. Wang, C.S. Carlson and J.M. Ellermann (2015). "Improved Visualization of Cartilage Canals Using Quantitative Susceptibility Mapping." PLoS One 10(7): e0132167.

110. Nunamaker D.M. Experimental models of fracture repair. Clin Orthop Relat Res. 1998 Oct;(355 Suppl):S56-65.

111. Nyman JS, Granke M, Singleton RC, Pharr GM. Tissue-Level Mechanical Properties of Bone Contributing to Fracture Risk. Curr Osteoporos Rep. 2016 Aug;14(4):138-50. doi: 10.1007/s11914-016-0314-3. Review.

112. Ochi H., Takeda S. Animal Models For Bone And Joint Disease. The genetically-modified mice as a tool for osteoporosis research. Clin Calcium. 2011 Feb;21(2):226-32.

113. Odgaard A. Three-dimensional methods for quantification of cancellous bonearchitecture. Bone. 1997 Apr;20(4):315-28.

114. Ohman C, Baleani M, Perilli E, Dall'Ara E, Tassani S, Baruffaldi F, Viceconti M. Mechanical testing of cancellous bone from the femoral head: experimental errors due to off-axis measurements. J Biomech. 2007;40(11):2426-33. Epub 2007 Jan 25

115. Olsson, S.E., 1983. The early diagnosis of fragmented coronoid process and osteochondritis dissecans of the canine elbow joint. Journal of the American Animal Hospital Association 19, 616-626.

116. Olstad K, Ytrehus B, Ekman S, Carlson CS, Dolvik NI. Early lesions of osteochondrosis in the distal tibia of foals. J Orthop Res 2007;25:1094-105.

117. Olstad K., B. Ytrehus, S. Ekman, C.S. Carlson and N.I. Dolvik (2008). "Epiphyseal cartilage canal blood supply to the tarsus of foals and relationship to osteochondrosis." Equine Vet J 40(1): 30-39.

118. Olstad K., E.H. Hendrickson, C.S. Carlson, S. Ekman and N.I. Dolvik (2013). "Transection of vessels in epiphyseal cartilage canals leads to osteochondrosis and osteochondrosis dissecans in the femoro-patellar joint of foals; a potential model of juvenile osteochondritis dissecans." Osteoarthritis Cartilage 21(5): 730-738.

119. Onar V, Gunes H. On the variability of skull shape in German shepherd (Alsatian) puppies. Anatomical Record Part a-Discoveries in Molecular Cellular and Evolutionary Biology. 2003;272A(1):460-6.

120. Onar V, Ozcan S, Pazvant G. Skull typology of adult male Kangal dogs. Anatomia, histologia, embryologia. 2001;30(1):41-8.

121. Onar V. A morphometric study on the skull of the German shepherd dog (Alsatian). Anatomia Histologia Embryologia-Journal of Veterinary Medicine Series C-Zentralblatt Fur Veterinarmedizin Reihe C. 1999;28(4):253-6.

122. Osterhoff G, Morgan EF, Shefelbine SJ, Karim L, McNamara LM, Augat P. Bone mechanical properties and changes with osteoporosis. Injury. 2016 Jun;47 Suppl 2:S11-20. doi: 10.1016/S0020-1383(16)47003-8.

123. Parfitt AM. Compact bone and fracture risk. Calcif Tissue Int. 1992 Jan;50(1):97-8.

124. Parfitt AM. Recent developments in bone physiology. Henry Ford Hosp Med J. 1983;31(4):209-10. No abstract available.

125. Park JB, Biomaterials Science and Engineering, Plenum Press, New York, 1987.

126. Parr WC, Chamoli U, Jones A, Walsh WR, Wroe S. Finite element micro-modelling of a human ankle bone reveals the importance of the trabecular network to mechanical performance: new methods for the generation and comparison of 3D models. J Biomech. 2013 Jan 4;46(1):200-5. doi: 10.1016/j.jbiomech.2012.11.011. Epub 2012 Dec 4.

127. Pearce A.I., Richards R.G., Milz S., Schneider E., Pearce S.G. Animal models for implant biomaterial research in bone: a review. Eur Cell Mater. 2007 Mar 2;13:1-10.

128. Peinado Cortes, L.M., Vanegas Acosta, J.C., Garzon Alvarado, D.A., 2011. A mechanobiological model of epiphysis structures formation. Journal of theoretical biology 287, 13-25.

129. Pitol DL, Caetano FH, Lunardi LO. Microwave-induced fast decalcification of rat bone for electron microscopic analysis: an ultrastructural and cytochemical study. Braz Dent J. 2007;18(2):153-7.

130. Por Y.C., Barcelo' C.R., Salyer K.E., Genecov D.G., Troxel K., Gendler E., Elsalanty M.E., Opperman L.A. Bone generation in the reconstruction of a critical size calvarial defect in an experimental model. J Craniofac Surg. 2008 Mar;19(2):383-92.

131. Potdevin G[1], Malecki A, Biernath T, Bech M, Jensen TH, Feidenhans'l R, Zanette I, Weitkamp T, Kenntner J, Mohr J, Roschger P, Kerschnitzki M, Wagermaier W, Klaushofer K, Fratzl P, Pfeiffer F. X-ray vector radiography for bone micro-architecture diagnostics. Phys Med Biol. 2012 Jun 7;57(11):3451-61. doi: 10.1088/0031-9155/57/11/3451. Epub 2012 May 11.

132.   Pouilles JM¹, Collard P, Tremollieres F, Frayssinet P, Railhac JJ, Cahuzac JP, Autefage A, Ribot C. Accuracy and precision of *in vivo* bone mineral measurements in sheep using dual-energy X-ray absorptiometry. Calcif Tissue Int. 2000 Jan;66(1):70-3.

133.   Pugh JW, Rose RM, Radin EL. A structural model for the mechanical behavior of trabecular bone. J Biomech. 1973 Nov;6(6):657-70.

134.   Reifenrath J., Angrisani N., Lalk M., Besdo S. Replacement, refinement, and reduction: necessity of standardization and computational models for long bone fracture repair in animals. J Biomed Mater Res A. 2014 Aug;102(8):2884-900.

135.   Reilly DT, Burstein AH, Frankel VH. The elastic modulus for bone. J Biomech. 1974 May;7(3):271-5.

136.   Reineke T, Jenni B, Abdou MT, Frigerio S, Zubler P, Moch H, Tinguely M. Ultrasonic decalcification offers new perspectives for rapid FISH, DNA, and RT-PCR analysis in bone marrow trephines. Am J Surg Pathol. 2006 Jul;30(7):892-6.

137.   Rho JY, Kuhn-Spearing L, Zioupos P. Mechanical properties and the hierarchical structure of bone. Med Eng Phys. 1998 Mar;20(2):92-102.

138.   Riser, W.H., 1973. Growth and development of the normal canine pelvis, hip joints and femurs from birth to maturity: a radiographic study. Journal of the American Veterinary Radiology Society 14, 24-34.

139.   Riser, W.H., 1975. The dog as a model for the study of hip dysplasia Growth, form, and development of the normal and dysplastic hip joint. Veterinary pathology 12, 229-334.

140.   Rivas R¹, Shapiro F. Structural stages in the development of the long bones and epiphyses: a study in the New Zealand white rabbit. J bone Joint Surg Am. 2002 Jan;84-A(1):85-100.

141.   Sangeetha R, Uma K, Chandavarkar V. Comparison of routine decalcification methods with microwave decalcification of bone and teeth. J Oral Maxillofac Pathol. 2013 Sep;17(3):386-91. doi: 10.4103/0973-029X.125204.

142.   Schajowicz F, Cabrini RL. The effect of acids (decalcifying solutions) and enzymes on the histochemical behavior of bone and cartilage. J Histochem Cytochem. 1955 Mar;3(2):122-9.

143.   Schmidt MJ, Neumann AC, Amort KH, Failing K, Kramer M. Cephalometric measurements and determination of general skull type of Cavalier King Charles Spaniels. Veterinary radiology & ultrasound : the official journal of the American College of Veterinary Radiology and the International Veterinary Radiology Association. 2011;52(4):436-40.

144.   Schnapper A., Reumann K., Meyer W. The architecture of growing compact bone in the dog: visualization by 3d-reconstruction of histological sections. Ann Anat. 2002 May;184(3):229.

145.   Schoenebeck JJ, Ostrander EA. The genetics of canine skull shape variation. Genetics. 2013;193(2):317-25.

146.   Seiferle E. [On the topography of the brain on long and short skulls in dog breeds]. Acta anatomica. 1966;63(3):346-62.

147.   Semyari H., Rajipour M., Sabetkish S., Sabetkish N., Abbas F.M., Kajbafzadeh A.M. Evaluating the bone regeneration in calvarial defect using osteoblasts differentiated from adipose-derived mesenchymal stem cells on three different scaffolds: An Animal Study. Cell Tissue Bank. 2015 Jun 25

148.   Shearin AL, Ostrander EA. Canine morphology: hunting for genes and tracking mutations. PLoS Biol. 2010;8(3):e1000310.

149.   Skiba G, Sobol M, Raj S. Femur morphometry, densitometry, geometry and mechanical properties in young pigs fed a diet free of inorganic phosphorus and supplemented with phytase. Arch Anim Nutr. 2017 Feb;71(1):81-92. Epub 2016 Nov 14.

150.   Smith, R.N., 1960. Radiological observations on the limbs of young greyhounds. The Journal of small animal practice 1, 84-90.

151.   Smith, R.N., Allocock, J., 1960. Epiphyseal fusion in the grey-hound. The Veterinary record 72, 75-79

152.   Soladoye OP, López Campos Ó, Aalhus JL, Gariépy C, Shand P, Juárez M.Accuracy of dual energy X-ray absorptiometry (DXA) in assessing carcass composition from different pig populations. Meat Sci. 2016 Nov;121:310-316. doi: 10.1016/j.meatsci.2016.06.031. Epub 2016 Jul 1.

153. Stavropoulos A., Sculean A., Bosshardt D.D., Buser D., Klinge B. Pre-clinical *in vivo* models for the screening of bone biomaterials for oral/craniofacial indications: focus on small-animal models. Periodontol 2000. 2015 Jun;68(1):55-65.

154. Stockard CR. The genetic and endocrinic basis for differences in form and behavior. American Anatomy Memoir. 19. Philadelphia: Wistar Institute of Anatomy and Biology; 1941.

155. Stockwell RA. The ultrastructure of carti- lage canals and the surrounding cartilage in the sheep fetus. J Anat 1971;109:397- 410

156. Stone JL, Beaupre GS, Hayes WC. Multiaxial strength characteristics of trabecular bone. J Biomech. 1983;16(9):743-52.

157. Teng S., Choi I.W., Herring S.W., Rensberger J.M. Stereological analysis of bone architecture in the pig Zygomatic Arch. Anat Rec. 1997 Jun;248(2):205-13.

158. Ticer, J.W. (1975) Radiographic Technique in Small Animal Practice. Philadelphia: Saunders.

159. Todhunter, R.J., Zachos, T.A., Gilbert, R.O., Erb, H.N., Williams, A.J., Burton-Wurster, N., Lust, G., 1997. Onset of epiphyseal mineralization and growth plate closure in radiographically normal and dysplastic Labrador retrievers. J Am Vet Med Assoc 210, 1458-1462.

160. Toth, F., M.J. Nissi, J. Zhang, M. Benson, S. Schmitter, J.M. Ellermann and C.S. Carlson (2013). "Histological confirmation and biological significance of cartilage canals demonstrated using high field MRI in swine at predilection sites of osteochondrosis." J Orthop Res 31(12): 2006-2012.

161. Turner AS, Mallinckrodt CH, Alvis MR, Bryant HU. Dual-energy X-ray absorptiometry in sheep: experiences with *in vivo* and ex vivo studies. Bone. 1995 Oct;17(4 Suppl):381S-387S.

162. Turner CH[1], Burr DB. Basic biomechanical measurements of bone: a tutorial. Bone. 1993 Jul-Aug;14(4):595-608.

163. Turner, B.M., Abercromby, R.H., Innes, J., McKee, W.M., Ness, M.G., 1998. Dynamic proximal ulnar osteotomy for the treatment of ununited anconeal process in 17 dogs. Veterinary and Comparative Orthopaedics and Traumatology 11, 76-79.

164. Turunen M.J., Prantner V., Jurvelin J.S., Kroger H., Isaksson H. Composition and microarchitecture of human trabecular bone change with age and differ between anatomical locations. Bone. 2013 May;54(1):118-25.

165. Uchida K., Urabe K., Naruse K., Kozai Y., Onuma K., Mikuni-Takagaki Y., Kashima I., Ueno M., Sakai R., Itoman M., Takaso M. Differential age-related bone architecture changes between female and male str/ort mice. Exp Anim. 2012;61(1):59-66.

166. Undecalcified bone preparation for histology, histomorphometry and fluorochrome analysis.

167. Vaccaro C., Busetto R., Bernardini D., Anselmi C., Zotti A. Accuracy and precision of computer-assisted analysis of bone density via conventional and digital radiography in relation to dual-energy x-ray absorptiometry. Am J Vet Res. 2012 Mar;73(3):381-4.

168. Van Der Linden J.C., Waarsing J.H., Weinans H. The Use of micro-ct to study bone architecture dynamics noninvasively. Drug Discov Today Technol. 2006 Summer;3(2):213-9.

169. Van Griensven M. Preclinical testing of drug delivery systems to bone. Adv Drug Deliv Rev. 2015 Jul 23. Pii: S0169-409x(15)00159-3.

170. Vanden Berg-Foels, W.S., Schwager, S.J., Todhunter, R.J., Reeves, A.P., 2011. Femoral head shape differences during development may identify hips at risk of degeneration. Annals of biomedical engineering 39, 2955-2963.

171. Vanden Berg-Foels, W.S., Todhunter, R.J., Schwager, S.J., Reeves, A.P., 2006. Effect of early postnatal body weight on femoral head ossification onset and hip osteoarthritis in a canine model of developmental dysplasia of the hip. Pediatric research 60, 549-554.

172. Ventura M., Boerman O. C., De Korte C., Rijpkema M., Heerschap A., Oosterwijk E., Jansen J. A., Walboomers X. F. Preclinical imaging in bone tissue engineering. Tissue Eng Part B Rev. 2014 Dec;20(6):578-95.

173. Verdenius HH; Alma L. A quantitative study of decalcification methods in histology. J Clin Pathol. 1958 May;11(3):229-36.

174. Wang S, Park WM, Gadikota HR, Miao J, Kim YH, Wood KB, Li G. A combined numerical and experimental technique for estimation of the forces and moments in the lumbar intervertebral disc. Comput Methods Biomech Biomed Engin. 2013;16(12):1278-86. doi: 10.1080/10255842.2012.668537. Epub 2012 May 3.

175.	Watson A, Evans H, de Lahunta A: Ossification of the atlas-axis complex in the dog, *Anat Histol Embryol* 15:122-138, 1986.

176.	Watson A, Evans H: The development of the atlas-axis complex in the dog, *Anat Rec* 184:558, 1976.

177.	Webster S. S. J. The skeletal tissue; in Cell and tissue biology. Leon Weiss Editor, 1988, sixth edition, Urban and Schwarzenberg, Germany

178.	Wilsman NJ, Van Sickle DC. Cartilage canals, their morphology and distribution. Anat Rec 1972;173:79-93.

179.	Wolschrijn, C. F., E. Gruys, C. W. van der Wiel and W. A. Weijs (2008). "Cartilage canals in the medial coronoid process of young Golden Retrievers." Veterinary Journal 176(3): 333-337.

180.	Wu S, Liu X, Yeung K, Liu C, Yang X. Biomimetic porous scaffolds for bone tissue engineering. Materials Science and Engineering, 2014: R: Reports. 80. 1–36. 10.1016/j.mser.2014.04.001.

181.	Wu S, Liu X, Yeung K, Liu C, Yang X. Biomimetic porous scaffolds for bone tissue engineering. Materials Science and Engineering, 2014: R: Reports. 80. 1–36. 10.1016/j.mser.2014.04.001.

182.	Yamamoto-Fukud T, Shibata Y, Hishikawa Y, Shin M, Yamaguchi A, Kobayashi T and Koji T. Effects of various decalcification protocols on detection of DNA strand breaks by terminal dUTP nick end labelling. Histochem J 2000; 32: 697-702.

183.	Yonamine, H., Ogi, N., Ishikawa, T., Ichiki, H., 1980. Radiographic studies on skeletal growth of the pectoral limb of the beagle. Japanese Journal of Veterinary Science 42, 417-425.

184.	Yoshioka M, Yoshida Y, Inoue S, Lambrechts P, Vanherle G, Nomura Y, Okazaki M, Shintani H, Van Meerbeek B. Adhesion/decalcification mechanisms of acid interactions with human hard tissues. J Biomed Mater Res. 2002 Jan;59(1):56-62.

185.	Yu Z., Sun ., Long H., Yang T., Ma B. Establishment of reproducible osteosarcoma rat model using orthotopic implantation technique. Oncol Rep. 2009 May;21(5):1175-80.

186.	Zimmermann EA, Gludovatz B, Schaible E, Busse B, Ritchie RO. Fracture resistance of human cortical bone across multiple length-scales at physiological strain rates. Biomaterials. 2014 Jul;35(21):5472-

187.	Zotti A, Gianesella M, Gasparinetti N, Zanetti E, Cozzi B. A preliminary investigation of the relationship between the "moment of resistance" of the canine spine, and the frequency of traumatic vertebral lesions at different spinal levels. Res Vet Sci. 2011 Apr;90(2):179-84. doi: 10.1016/j.rvsc.2010.05.036. Epub 2010 Jun 17.

188.	Zotti A, Isola M, Sturaro E, Menegazzo L, Piccinini P, Bernardini D. Vertebral mineral density measured by dual-energy X-ray absorptiometry (DEXA) in a group of healthy Italian boxer dogs. J Vet Med A Physiol Pathol Clin Med. 2004 Jun;51(5):254-8.

189.	D.lgs 26/14, attuazione della direttiva 2010/63/UE sulla protezione degli animali utilizzati a fini scientifici.

190.	Trattato di Lisbona, 2009.

2. COMPARISON OF THREE ACID DECALCIFICATION SOLUTIONS FOR CANCELLOUS BONE IN FIVE ANIMAL SPECIES

M. E. Andreis[1], A. Di Giancamillo[1], S. C. Modina[1]

[1]Department of Health, Animal Science and Food Safety, Università degli Studi di Milano, Italy

Introduction

The bone tissue is among the hardest and most challenging tissue encountered at the bench by researchers. Decalcification, the technique that removes mineral from the bone while preserving all the essential microscopic elements and tissue antigenicity (Gül et al., 2014), is probably one of the most frustrating stages in bone processing. A good decalcification agent should remove rapidly and completely the calcium from the tissue, minimise cells and tissue damage and guarantee reliable results in the sequential staining and immunolocalization (Culling, 1985; Sangeetha et al., 2013). Decalcification is a very complicated and delicate step, to the point that special equipment (e.g. polymer resins, special microtome blades, special pre-staining and staining techniques) has been created in order to be able to process undecalcified bone. Such equipment, though, is quite expensive and not available to most laboratories, so decalcification followed by paraffin embedding is still widely used for bone specimens processing (Ehrlich et al., 2008; Farrell et al., 2015).

The most used decalcification methods are: immersion (Kiviranta, 1980; Guibas et al., 2014; Mattuella et al., 2007; Yamamoto-Fukud, 2000; Liu et al., 2017; Neves et al., 2011; Yoshioka et al., 2002; Gupta et al., 2014; Morse, 1945), sonication (Reineke et al., 2006; Hatta et al., 2013), microwave (Kok and Boone, 1992; Imaizumi et al., 2013; Sangeetha et al., 2013; Katoh, 2016; Pitol et al., 2007) and electrolytic; agitation and/or heat are reported as enhancing factors (Schajaowicz and Cabrini, 1955; Verdenius and Alma, 1958; Pitol et al., 2007; Kapila et al., 2015). Immersion in decalcifying solution is probably the most available methods in laboratory routine. Two large families of decalcifying agents are available: acids and calcium chelators. Acid decalcifiers are classified as strong (hydrochloric acid, nitric acid) or weak (formic acid, picric acid, acetic acid). The most used calcium chelator is ethylenediaminetetraacetic acid (EDTA), which is considered the gold standard for cellular detail and structural tissue integrity preservation (Callis and Sterchi, 1998; Emans et al., 2005; Frank et al., 1993; Pitol et al., 2007; Savi et al., 2017; Bancroft, 2002; Sanjeet and Keya, 2010; Sanjai et al., 2012; Sanjeetha et al., 2013). Strong acids are very rapid, and thus prone to over-decalcification tissue damage risk (Alers et al., 1999; Mattuella et al., 2007; Begum et al., 2010; Callis and Sterchi, 1998; Leong, 2009). Weak acids and calcium chelators are more "delicate", but need long decalcification timing (Yamamoto-Fukud, 2000) and multiple renewal. Solutions obtained by a combination

of different decalcifying agents have also been proposed (Mori et al., 1988; Castania et al., 2015; Silva et al., 2012). Determination of decalcification degree and endpoint is another tricky stage. It can be evaluated radiographically, through manipulation (bending, probing, cutting), chemical testing and radiologic analysis (Farrell et al., 2015; Savi et al., 2017; Gonzáles-Chávez et al., 2013; Guibas et al., 2014; An and Martin, 2003).

Several decalcification protocols have been described in literature, based on different components combination and concentration. Anyway, solution concentration, decalcification timing, samples dimension and type (cortical vs cancellous bone) are often unspecified, leading to potential misinterpretation and inability to choose a suitable protocol.

The aim of this study was to compare three acid solutions for the decalcification of cancellous bone in five animal species, to obtain user-friendly guidelines for everyday bone-related laboratory routine.

Methods

A total of 202 bone samples from 25 animals were included in the study: five mice, Balb/c; five rats, Sprague Dawley (both from Charles River Laboratories Italia s.r.l., Calco (LC), Italy); five dog, mixed-breed; five sheep, Bergamasca; five pigs, Landrace-Large White cross. Pig bones were collected from the slaughterhouse. Sheep, rats and mice were collected from external laboratories, after euthanasia as part of unrelated experiments. The experiments were approved by Italian Ministry of Health – Permit N. 264/2013-B (sheep); by the Mario Negri Institute for Pharmacological Research IRFMN Animal Care and Use Committee IACUC - Permit N. 363/2015-PR (rats); and by the Committee on the Ethics of Animal Experiments of the University of Milano and by Italian Ministry of Health - authorization n. 68/14 (mice). Dogs died/were euthanized because of incurable diseases; the owner consented in writing to post-mortem sampling. Canine bones were collected from animals euthanized for reasons unrelated to the study and donated by the owner to our institution for experimental purposes. Mice and rats were 6 months old; dogs were 5 to 12 years old; sheep were 3 years old; the precise age of pigs was unknown, but it was around four to seven months (weight: 70-80 kg). They were immediately refrigerated after death, and then stored at a temperature of -20°C until sampling. For large animals, samples with an approximate thickness of 1-2 mm were collected with a band saw from the femoral/tibial condyles. For mice the whole femur/tibia and for rats the whole condyles were sampled. The weight of each sample was recorded before fixation in 10% neutral buffered formalin for 48 hours; samples were then rinsed in running tap water for three hours and stored in three different decalcifying solutions (sample to solution ratio= 1g of bone to 50 ml of solution): solution A, combination of weak acid (7,5% citric acid + 25% formic acid in distilled water), solution B, strong acid (10% hydrochloric acid) and solution C, combination of strong and weak acids (1,85% hydrochloric acid, 4% formic acid in distilled water) (Tab. 1). Decalcification was performed at room temperature for all solutions, which were renewed every 3-5 days.

	Solution	Mouse (n=17)	Rat (n=16)	Dog (52)	Sheep (n=62)	Pig (n=55)
A	7,5% citric acid + 25% formic acid	n=6	n=5	n=19	n=21	n=16
B	10% hydrochloric acid	n=6	n=6	n=21	n=15	n=13
C	1,85% hydrochloric acid + 4% formic acid	n=5	n=5	n=12	n=26	n=26

Tab. 1. Sample size.

The decalcification degree of each sample was subjectively evaluated twice a day for rodents and once a day for mammals, according to the following criteria: floating, flexibility and cracking when cut with a blade. Samples were removed from the decalcifying solution when subjectively considered ready to be processed (floating, very flexible, minimum/no cracarsking at blade cutting), rinsed in running tap water for five hours. All samples were then dehydrated in a graded 50% (v/v), 70% (v/v), 95% (v/v) and 100% (v/v) ethanol series, embedded in paraffin and transversally cut into 5- μm -thick sections. The obtained sections were dewaxed and rehydrated and stained with Hematoxilin-Eosin (HE).

Three observers independently evaluated the general features of the tissue for each section, stained with EE, in 3 microscopic fields at 20 X with a Nikon Eclipse E600 microscope to spot indicators of poor/good/excessive decalcification. A subjective score (0=poor: tissue/lamellar tearing, poor HE staining, absent nuclei; 1=fair: tissue/lamellar integrity, consistent HE staining, absent scant nuclei; 2=good: tissue/lamellar integrity, consistent HE staining, presence of > 50% of osteocytes-occupied lacunae; 3=excellent: tissue/lamellar integrity, consistent HE staining, presence of 100% of osteocytes-occupied lacunae; Fig. 1). The mean value of the scores assigned to each sample by the three observers was used for statistical analysis.

Collagen I was immunolocalized in score-2 and score-3 samples to evaluate antigen preservation (sample choice was made based on the longest available decalcification time for each solution), on samples mounted on special adhesion-control slides (SuperFrost Plus, Thermo Fisher Scientific) were employed and slides were stored over night at 60°C in a thermostat to ensure a firm adhesion of the sections during the immunofluorescence protocols. Briefly, 2 sections/species, decalcified with A and C solutions were dewaxed and rehydrated and then incubated in Tris-EDTA buffer (ph 9) at 37 °C over night to allow antigen retrieval, according to product information sheet. With the same aim two sections/species, decalcified at the same manner, were submitted to MW treatment in sodium citrate buffer (ph6) at 800 W for two cycles of 5 minutes and then allowed to cool in the same buffer for 45 min at room temperature. Immunolocalization of collagen I was performed with a polyclonal anti collagen I antibody (EPR7785 ab138492 Abcam) incubated overnight at room temperature in a humid chamber. The antigen–antibody complex was detected with a TRITC-labeled donkey anti-rabbit (1:100; Vector Laboratories, Inc.) incubated for 30 min at room temperature. After incubation with secondary antibodies sections were washed and finally mounted on slides in the antifade medium Vecta Shield (Vector Laboratories, Inc) supplemented with 1 μg/ml 40,6-diamidino-2-phenylindole (DAPI). Samples were analysed on an epifluorescence microscope (Eclipse E600, Nikon) also equipped for epifluorescence and a digital camera (Nikon Digital Sight, DS-U3) and software (NIS

elements Imaging Software; Nikon).

Statistical analysis was performed with SAS statistical software (version 9.3, Cary Inc., NC). Differences in time and tissue morphology among different species and among different species with different solutions were tested with one-way ANOVA, standardizing for sample weight. Differences in tissue morphology between different solutions at different times for every species were tested with two-way ANOVA, standardizing for sample weight. Differences between means were considered significant at $P<0,05$.
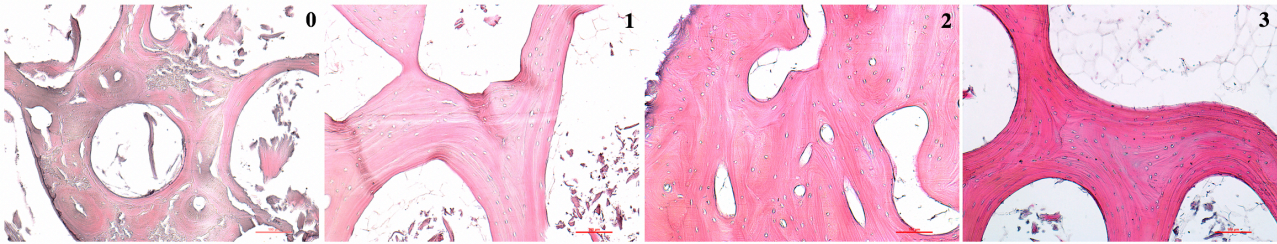

Fig. 1 - Subjective score for tissue morphology. 0=poor: tissue/lamellar tearing, poor HE staining, absent nuclei; 1=fair: tissue/lamellar integrity, consistent HE staining, absent/scant osteocytes-occupied lacunae; 2=good: tissue/lamellar integrity, consistent HE staining, presence of > 50% of osteocytes-occupied lacunae; 3=excellent: tissue/lamellar integrity, consistent HE staining, presence of 100% of osteocytes-occupied lacunae. Representative images of sheep bone samples decalcified with 1,85% hydrochloric acid, 4% formic acid.

Results

The results of the comparison of the time needed for decalcification in the different species and the obtained score are showed in Tab. 2A and 2B and depicted in Fig. 2A and 2B respectively. Overall, significantly longer time was required to decalcify canine samples; significantly higher score was obtained in mice, rats and pigs. Examples of excellent morphology in rats, mice and sheep are depicted in Fig. 3.

The results of the comparison of the time needed for decalcification and the score obtained with the different solutions for every species are showed in Tab. 3A and 3B and depicted in Fig. 4A and 4B respectively. Significantly longer time was necessary for decalcification in all species with solution A. The decalcification time among solution B and solution C was significantly different only in dogs (solution B faster than solution C). Significantly higher score was obtained with solution C in rats and pigs and with solution A in dogs and sheep. Overall, a lower score was obtained with solution B in all species, although this difference was not significant in mice.

The results of the effect of decalcification solution and time combined on tissue morphology for every species are showed in Tab. 4 and depicted in Fig. 5. Based on decalcification time, results can be divided in two groups: rodents (4A, three time frames) and mammals (4B, four time frames). In mice, significantly higher score was obtained with solution B and C in 0-4 days, and with solution A in 5-8 days. In rats, significantly higher score was obtained with solution C in 0-8 days. In dogs and sheep general lower score was achieved with significant difference only for solution A in sheep with 6-12 days. In pigs, significantly higher score was obtained with solution C with relatively short decalcification time (0-12 days); solution A gave significantly higher score with longer decalcification time (13-21 days).

33

Most microwaved sections detached from the slices, notwhistanding the overnight passage at 60°; on these samples, collagen I immunolocalization was not carried out. Preliminary results of the immunolocalization of collagen I in the samples that underwent EDTA incubation show that solution A and C preserve tissue antigenicity in pigs, sheep and dogs (Fig. 6). Best results were obtained is samples decalcified with solution A, where the distribution of collagen fibres' deposition was very clear. No signal corresponding to collagen I fibres was detected in rats and mice samples. Nuclei were only occasionally preserved in all samples. Immunofluorescence negative controls, which were performed by omitting the primary antibodies, did not show any staining under the same exposure settings.

Species	Time (days)
Mouse	5,9±1,7
Rat	8±1,8
Dog	17,7±0,9
Sheep	8,9±0,9
Pig	9,7±1

Tab. 2B - Results of the comparison of the overall score obtained in the different species. Values have been standardized for sample weight and are expressed as mean±ES.
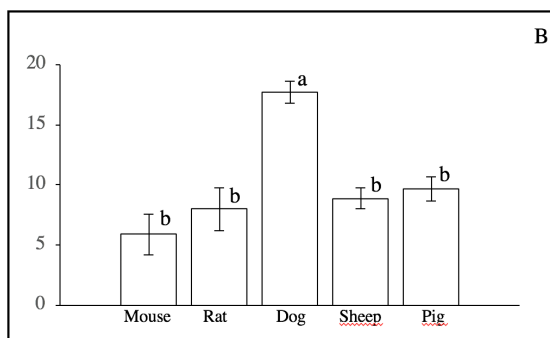

Fig. 2A – Graphical representation of the comparison of the overall time needed for decalcification in the different species. Values (days) have been standardized for sample weight and are expressed as mean±ES. Columns with different letters are significantly different (P<0,05).

Species	Score
Mouse	2,5±0,2
Rat	2,1±0,2
Dog	1,5±0,1
Sheep	1,5±0,1
Pig	2,2±0,1

Tab. 2A - Results of the comparison of the overall time needed for decalcification in the different species. Values (days) have been standardized for sample weight and are expressed as mean±ES.
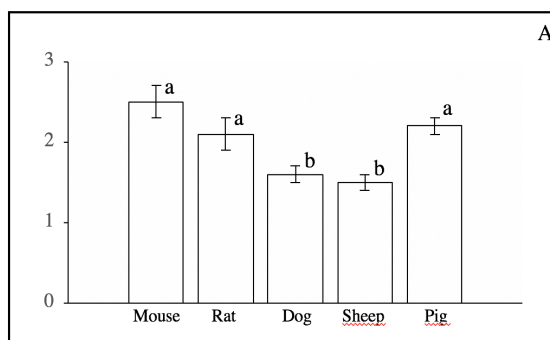

Fig. 2B – Graphical representation of the comparison of the overall score obtained in the different species. Values have been standardized for sample weight and are expressed as mean±ES. Columns with different letters are significantly different (P<0,05).

Species	Solution	Time (days)
Mouse	Solution A	12,3±2,6
	Solution B	2,5±2,5
	Solution C	3±2,8
Rat	Solution A	13,1±2,8
	Solution B	5,8±2,6
	Solution C	4,6±2,7
Dog	Solution A	32,9±1,7
	Solution B	5,3±1,5
	Solution C	18,1±2
Sheep	Solution A	13,6±1,9
	Solution B	4±2,8
	Solution C	8,6±1,8
Pig	Solution A	18,7±0,9
	Solution B	4,7±1
	Solution C	4,6±0,7

Tab. 3A – Time needed for sample decalcification in different species with different solutions. Values (days) have been standardized for sample weight and are expressed as mean±ES.

Species	Solution	Score
Mouse	Solution A	2,7±0,3
	Solution B	2,2±0,3
	Solution C	2,8±0,3
Rat	Solution A	2,2±0,4
	Solution B	1,4±0,3
	Solution C	2,7±0,4
Dog	Solution A	2,2±0,1
	Solution B	1,1±0,1
	Solution C	1,4±0,2
Sheep	Solution A	2,2±0,2
	Solution B	0,7±0,26
	Solution C	1,56±0,2
Pig	Solution A	2,4±0,1
	Solution B	1,4±0,2
	Solution C	2,9±0,1

Tab. 3B – Scores obtained in different species with different solutions. Values have been standardized for sample weight and are expressed as mean±ES.
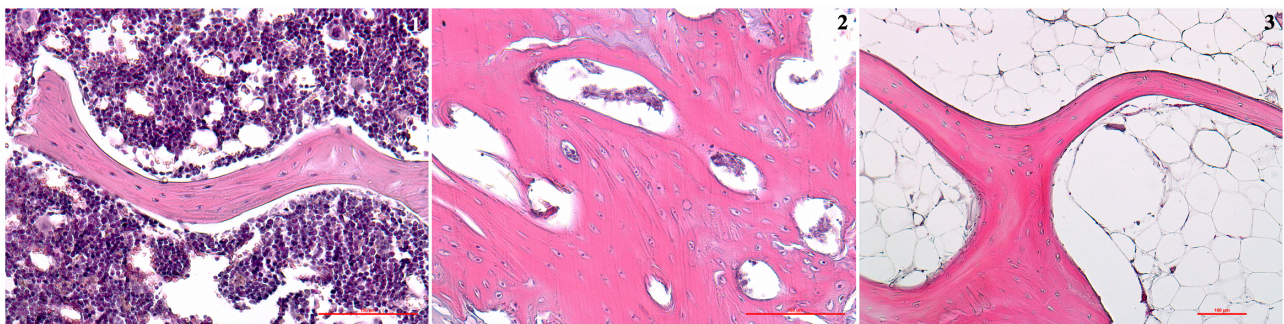

Fig. 3 - Excellent (score 3) tissue morphology was obtained with strong acid solution, especially in rodents. 1: mouse, 10% hydrochloric acid; 2: rat, 1,85% hydrochloric acid, 4% formic acid; 3: sheep, 1,85% hydrochloric acid, 4% formic acid.
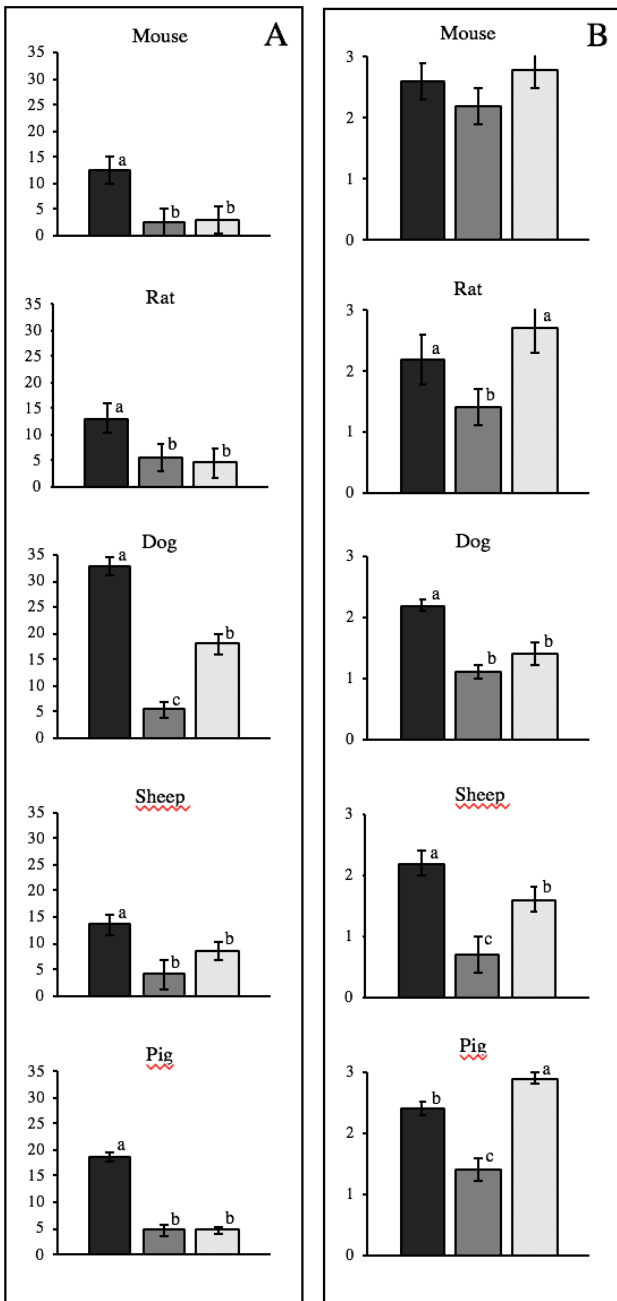
Fig. 4 – Graphical representation of the time needed for sample decalcification (A) and the score obtained (B) in the different species with different solutions. Black: solution A; dark grey: solution B; light grey: solution C. Values (A: days) have been standardized for sample weight and are expressed as mean±ES. Columns with different letters are significantly different (P<0,05).

Species	Solution	Score		
		Time 1	Time 2	Time 3
Mouse	Solution A	-	3±0,2	2,2±0,2
	Solution B	3±0,2	1,3±0,2	-
	Solution C	3±0,2	2,1±0,3	-
Rat	Solution A	2±0,5	-	2,3±0,5
	Solution B	1,8±0,3	0,5±0,5	-
	Solution C	3±0,4	3±0,7	1,3±0,9

Tab. 4A - Results of the effect of decalcification solution and time combined on tissue morphology for rodents. Time 1= 0-4 days; time 2= 5-8 days; time 3= >8 days. Values have been standardized for sample weight and are expressed as mean±ES.
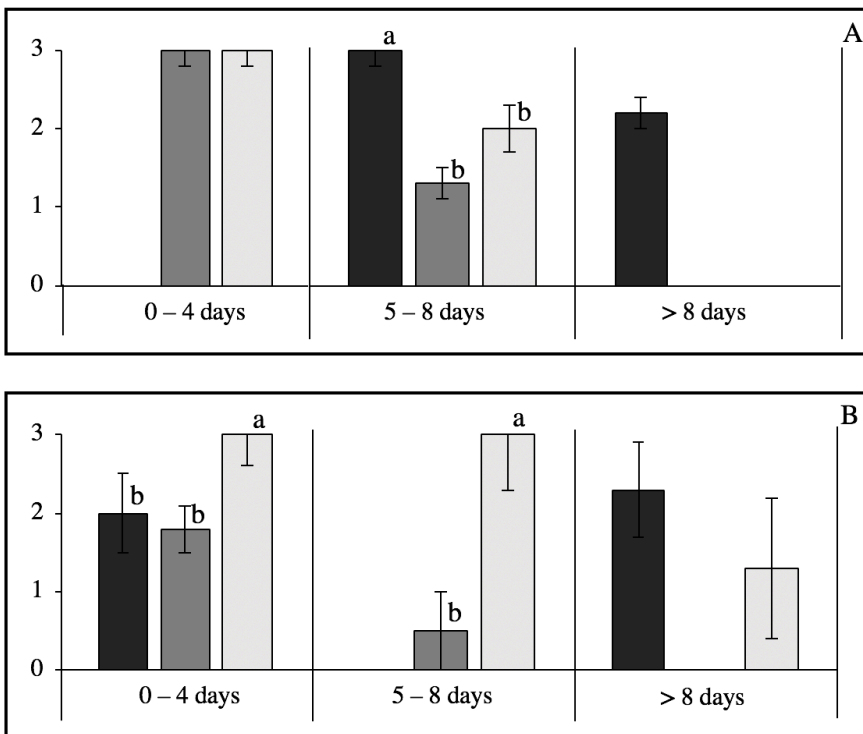

Fig. 5A – Graphical representation of the effect of decalcification solution and time combined on tissue morphology for rodents. A: mouse; B: rat. Black: solution A; dark grey: solution B; light grey: solution C. Values have been standardized for sample weight and are expressed as mean±ES. Columns with different letters are significantly different (P<0,05).

Species	Solution	Score			
		Time 1	Time 2	Time 3	Time 4
Dog	Solution A	-	2±0,3	-	2,2±0,19
	Solution B	1,1±0,2	-	-	-
	Solution C	0,7±0,4	1,4±0,3	1,7±0,3	-
Sheep	Solution A	-	2,1±0,3	-	2,2±0,2
	Solution B	1,1±0,1	-	-	-
	Solution C	0,9±0,3	1,3±0,2	1,7±0,3	-
Pig	Solution A	-	2,2±0,4	2,1±0,3	2,3±0,3
	Solution B	1,8±0,2	1±0,4	1,1±0,3	-
	Solution C	3±0,2	3±0,2	-	-

Tab. 4B - Results of the effect of decalcification solution and time combined on tissue morphology for mammals. Time 1= 0-10 days for dog, 0-5 days for sheep and pig; time 2= 11-20 days for dog, 6-12 days for sheep and pig; time 3: 21-30 days for dog, 13-21 days for sheep, 13-20 days for pig; time 4= >30 days for dog, >21 days for sheep, >20 days for pig. Values have been standardized for sample weight and are expressed as mean±ES.
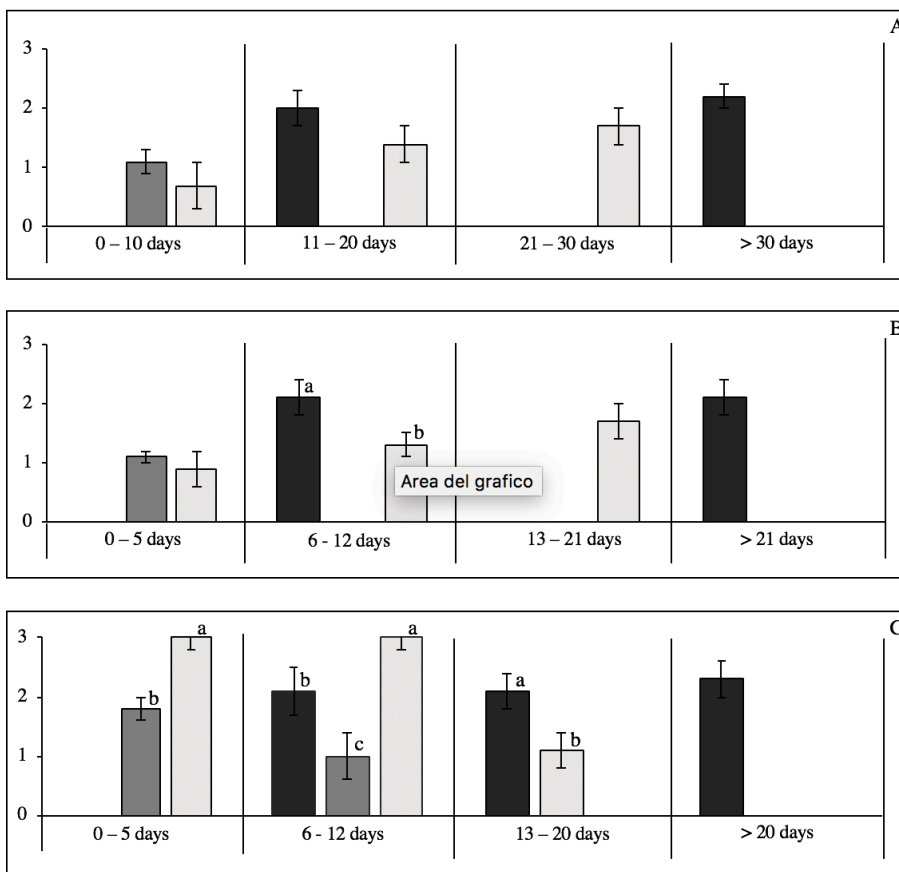

Fig. 5B – Graphical representation of the effect of decalcification solution and time combined on tissue morphology for mammals. A: dog; B: sheep; C: pig. Black: solution A; dark grey: solution B; light grey: solution C. Values have been standardized for sample weight and are expressed as mean±ES. Columns with different letters are significantly different (P<0,05).
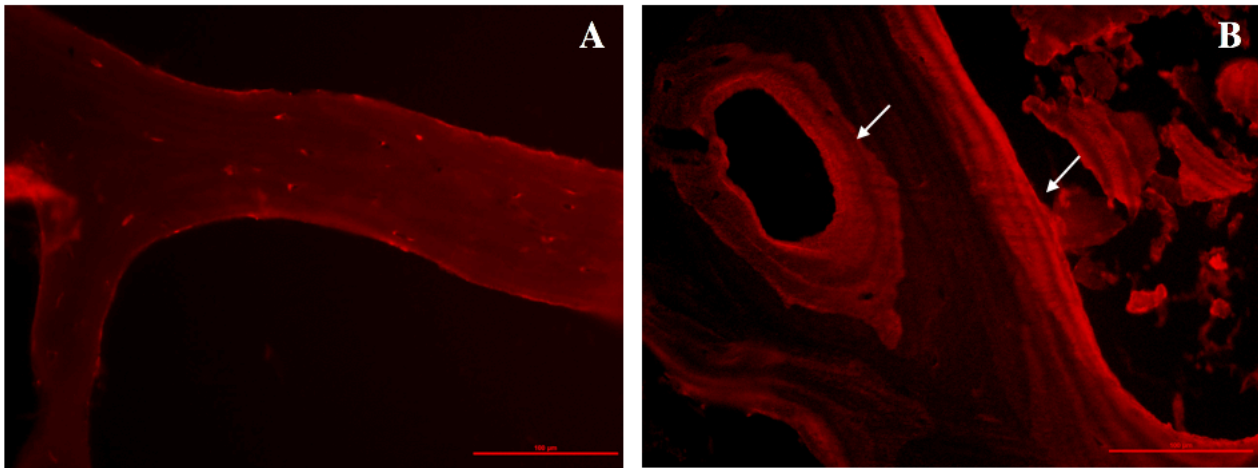
Fig. 6 – Immunolocalization of collagen I in canine samples decalcified with solution A (A) and solution C (B) for 20 days. Better tissue detail (visualization of collagen fibres deposition, white arrows) is obtained with solution C. Bar=100 μm

Discussion

This study compared three acid solutions (strong acid, weak acids, strong and weak acids combined) for the decalcification of trabecular bone from 5 animal species often used in bone-related research. It is commonly believed that strong acid solutions deteriorate the bone, but in this study excellent tissue morphology (tissue/lamellar integrity, consistent HE staining, presence of 100% of osteocytes' nuclei) was achieved with hydrochloric acid, when combined with formic acid, as previously described in rats' femur (Liu et al., 2017) and marmosets' teeth (Silva et al., 2012). Solution C (1,85% hydrochloric acid, 4% formic acid in distilled water), in fact, allowed to obtain excellent tissue morphology in mice in 0-4 days, in rats in 0-8 days and in pigs in 0-12 days. We consider this result relevant because it might support researchers in their activity by shortening experimental time as well as cutting the expenses due to solution renewal. Although occasionally (0-4days in mice), excellent tissue morphology was also obtained with 10% hydrochloric acid.

Concerning decalcification time, canine bone was decalcified significantly more slowly compared to the other species. The age of animals could be one of the reasons for this result: in fact, small islets of cartilage were found within the lamellae of rodents' and pigs' samples. These animals are considered adults (and enrolled in experimental trials) when they reach sexual maturity, which does not match skeletal maturity skeletal maturity (Roach et al., 2003; Fukuda and Matsuoka, 1979). The mice and rats included in this study were six months old (considered adult) the age of pigs, on the other hand, was uncertain, but their slaughtering weight (80-100 kg) suggests that they were skeletally immature as well (growth plate closure is reported to occur in pigs between two and four years of age (Cone, 2017). This "young" and metabolically active bone may have been more sensitive to the action of decalcification solutions, because it contains minerals that are more soluble and less crystallin than they are in "old" bone (Horvath, 2006). Anyway, although skeletally mature, sheep samples were decalcified in a significantly lower time when compared to dogs. The reason for this result is not known, but it could be due to the fact that bone mineral density (BMD) changes in sheep based on the season (Arens et al., 2007); it could be speculated that the sheep we used for

this experiment were euthanized at the end of the winter, when the BMD is lower (Arens et al., 2007); however, no BMD analysis was performed.

It is worth noticing that a high standard error in decalcification time was obtained with all solutions in all species, so it was possible to define only approximate time protocols. This high standard error could be due to high interindividual variability, which was not tested due to the insufficient sample size. If this was true, however, the standard error should be higher in dogs, which came from a less homogeneous population as compared to experimental animals (mice, rats, sheep) or livestock (pigs), which are usually more uniform as a population and as for the environment they live in and the diet they are fed. The high standard error could be also due to intraindividual regional (femur *vs* tibia) differences in bone features and density; although improbable, this difference was not tested. However, it cannot be completely ruled out that it could be caused by an internal bias in subjectively determining when the sample was ready to be processed. In fact, even if different options exist for such evaluation (X-ray techniques, chemical testing, Mattuella et al., 2007; Verdenius and Alma, 1958; Guibas et al., 2014), we choose to use a type of test (visual inspection, cutting with blade) which could be costless, fast and easily repeatable in everyday laboratory practice.

The results of our study confirm that hydrochloric acid alone, although significantly faster than weak acids alone, is generally not recommended for the decalcification of bone samples, as demonstrated by the significantly lower scores obtained in most species. In fact, it proved to be aggressive and deteriorate the bone faster than other solutions. It is worth noticing, anyway, that occasional excellent score was achieved with 10% hydrochloric acid in mice: this solution might therefore represent a valid alternative in this species, but it should be considered that very strict monitoring would be required (e.g. hourly). On the other hand, hydrochloric acid proved to be a fast and reliable agent when combined with formic acid, as previously described for teeth (Silva et al., 2012): this mix, in fact, allowed to obtain excellent morphology in mice, rats, and pigs. Weak acids, finally, constantly allowed to obtain a high score in all species, significantly higher than other solutions in rats and sheep, at the expense of decalcification time. This result should be carefully considered during experimental planning, as these solutions could take longer than one month (e.g. in dogs) and multiple renewals to achieve appropriate decalcification, and a decalcification time lower than 12 days should not be expected in any of the examined species.

To better evaluate the obtained results, the effect of the combination of decalcification solution and time on tissue morphology was evaluated, to be able to suggest a protocol based on the specific time requirements of different experiments. Significantly higher scores were obtained in rodents with solution C in relatively short time (0-4 days in mice, 0-8 days in rats). As mentioned earlier, excellent morphology was also obtained with solution B for 0-4 days in mice; anyway, a very fast decline in score is evident for this solution in all species as time progresses, confirming its difficult handling. Results of solution C in pigs are similar to the ones obtained in rodents, with significantly higher scores up until 12 days, that then rapidly decrease. As mentioned before, this could be related to the skeletal immaturity of the animals, which could have led to a higher sensitivity of the bone to decalcification solutions. An opposite result was obtained in sheep and dog samples, in which this solution provided better results in longer times. Lower initial scores caused by under-

decalcification instead of over-decalcification could explain this result. High scores were obtained with solution A in all species in longer times, although the difference when compared to solution C is only significant for solution A in sheep in 6-12 days and in pigs in 13-21 days. Anyway, the scores obtained with solution A proved to be more constant when compared to other solutions and confirmed easier handling, probably due to its slow and delicate action. Finally, solution B proved to be unable to give high scores in mammals at any time.

Microwave incubation resulted in tissue detachment from the slides. Based on our laboratory experience, slices adhesion to slides is a common problem when working with hard tissues, which tend to be more rigid than soft tissues and more likely are lost during processing. EDTA incubation proved to be a valid alternative to microwave, avoiding slices detachment and exposing collagen I. Although preliminary, the results obtained with immunolocalization of collagen I are substantially in agreement with the morphologic score; however, unexpectedly, collagen I signal was more intense for the samples decalcified with solution C (strong and weak acids) when compared to those decalcified with solution A (weak acids only). It can be hypothesized that solution C is comprehensively less aggressive, as the longer decalcification time required for solution A might have enhanced tissue sensibility to EDTA. EDTA, in fact, is a calcium chelator (Roger Hart, 2005) and its effect might have been boosted by incubation temperature. This would also explain the negative results obtained in rats and mice samples, which seem more prone to overdecalcification, based on the results of this study. Further experiments, however, need to be performed to confirm immunofluorescence results, especially in order to verify the effects of EDTA. Moreover, further polyclonal antibodies may be employed, which could be able to recognise different epitopes when compared to the one we used

This study has several limits. Although the high number of samples examined, the number per group was uneven and this may have limited the power of the statistical analysis, for example in rodents. Moreover, interindividual differences in the results related to animals age and gender, as well as intraindividual regional differences, were not statistically evaluated. A subjective method was used to determine when the samples were ready to be processed and this may have influenced the results; the choice was driven by the desire to mimic basic laboratory resources, using fast, cheap and user-friendly techniques. Finally, factor unrelated to the presence of mineral content, such as the characteristics of bone organic components in different species and sites, were not considered, but it is not unlikely that they might influence the efficacy of decalcification solutions and therefore the final results.

Conclusion

This study provided basic protocols for bone decalcification in different species with different solutions and showed that excellent morphologic results can be achieved with solution containing strong acids in rodents, sheep and pig. As a general rule, 10% hydrochloric acid solution is not recommended for tissue decalcification; 1,85% hydrochloric acid, 4% formic acid proved to be a good compromise, shortening experimental time and preserving tissue morphology and antigenicity; 7,5% citric acid + 25% formic acid

provided good tissue morphology, at the expenses of decalcification time, and only fair antigenicity. Further studies are needed to further test antigen preservation after decalcification and better define these protocols.

References

1. Alers JC, Krijtenburg PJ, Vissers KJ, van Dekken H. Effect of bone decalcification procedures on DNA in situ hybridization and comparative genomic hybridization. EDTA is highly preferable to a routinely used acid decalcifier. J Histochem Cytochem. 1999 May;47(5):703-10.

2. An HY, Martin KL. Handbook of histology methods for bone and cartilage. Totowa, NJ: Humana Press, 2003.

3. Arens D, Sigrist I, Alini M, Schawalder P, Schneider E, Egermann M. Seasonal changes in bone metabolism in sheep. Vet J. 2007 Nov;174(3):585-91. Epub 2006 Dec 1.

4. Athanasou NA, Quinn J, Heryet A, Woods CG, McGee JO. Effect of decalcification agents on immunoreactivity of cellular antigens. J Clin Pathol. 1987 Aug;40(8):874-8.

5. Bancroft JD, Gamble M. Theory and practice of histological techniques. 5th ed. Edinburgh: Churchill Livingstone; 2002.

6. Begum F, Zhu W, Namaka MP, Frost EE. A novel decalcification method for adult rodent bone for histological analysis of peripheral-central nervous system connections. J Neurosci Methods. 2010 Mar 15;187(1):59-66. doi: 10.1016/j.jneumeth.2009.12.013. Epub 2009 Dec 28.

7. Callis G, Sterchi D (1998) Decalcification of Bone: Literature Review and Practical Study of Various Decalcifying Agents. Methods, and Their Effects on Bone Histology, Journal of Histotechnology, 21:1, 49-58, DOI: 10.1179/his.1998.21.1.49

8. Castania VA, Silveira JW, Issy AC, Pitol DL, Castania ML, Neto AD, Bel EA, Defino HL. Advantages of a combined method of decalcification compared to EDTA. Microsc Res Tech. 2015 Feb;78(2):111-8. doi: 10.1002/jemt.22451. Epub 2014 Nov 28.

9. Cone S.G., Warren P.B., Fisher M.B. Rise of the Pigs: Utilization of the Porcine Model to Study Musculoskeletal Biomechanics and Tissue Engineering During Skeletal Grow. Tissue Engineering: Part C, (2017); 23.

10. Culling CFA, Allison R, Barr W. Cellular pathology technique. 1985; Butterworths London.

11. Ehrlich H, Koutsoukos PG, Demadis KD, Pokrovsky OS. Principles of demineralization: modern strategies for the isolation of organic frameworks. Part II. Decalcification. Micron. 2009 Feb;40(2):169-93. doi: 10.1016/j.micron.2008.06.004. Epub 2008 Jul 11.

12. Emans PJ, Bulstra SK, Kuijer R. The effects of different decalcification protocols on TUNEL and general cartilage staining. Biotech Histochem. 2005 May-Aug;80(3-4):111-5.

13. Farrell SF, Osmotherly PG, Rivett DA, Cornwall J. Formic acid demineralization does not affect the morphometry of cervical zygapophyseal joint meniscoids. Anat Sci Int. 2015 Jan;90(1):57-63. doi: 10.1007/s12565-014-0248-8. Epub 2014 Jul 3.

14. Frank JD, Balena R, Masarachia P, Seedor JG, Cartwright ME (1993). The effects of three different demineralization agents on osteopontin localization in adult rat bone using immunohistochemistry. Histochemistry 99: 295-301.

15. González-Chávez SA, Pacheco-Tena C, Macías-Vázquez CE, Luévano-Flores E. Assessment of different decalcifying protocols on Osteopontin and Osteocalcin immunostaining in whole bone specimens of arthritis rat model by confocal immunofluorescence. Int J Clin Exp Pathol. 2013; 6(10): 1972–1983. Published online 2013 Sep 15.

16. Guibas GV, Lakis S, Gkimpas C, Manda M, Kapoukranidou D, Spandou E. Efficiency of different decalcification protocols for nasal osseous structures in a rat experimental model of allergic rhinitis, and their effects on epithelial histology: an attempt at standardization. Exp Toxicol Pathol. 2014 Dec;66(9-10):469-75. doi: 10.1016/j.etp.2014.09.001. Epub 2014 Sep 18.

17. Gül M, Bayat N, Gül S, Hüz M, Yıldız A, Otlu Al. A Comparison of Three Different Agents of Decalcification for a Histological Examination of Bone Tissues. Journal of Turgut Ozal Medical Center. 2014, Vol. 21 Issue 4, p274-279. 6p.

18. Gupta S, Jawanda MK, Sm M, Bharti A. Qualitative histological evaluation of hard and soft tissue components of human permanent teeth using various decalcifying agents - a comparative study. J Clin Diagn Res. 2014 Sep;8(9):ZC69-72. doi: 10.7860/JCDR/2014/10195.4874. Epub 2014 Sep 20.

19. Hatta H, Tsuneyama K, Nomoto K, Hayashi S, Miwa S, Nakajima T, Nishida T, Nakanishi Y, Imura J. A simple and rapid decalcification procedure of skeletal tissues for pathology using an ultrasonic cleaner with D-mannitol and formic acid. Acta Histochem. 2014 Jun;116(5):753-7. doi: 10.1016/j.acthis.2014.01.006. Epub 2014 Feb 21.

20. Horvath AL. Solubility of structurally complicated materials: II. Bone. J Phys Chem Ref Data 2006; 35(1653).

21. Imaizumi K, Taniguchi K, Ogawa Y. An evaluation of the effect of microwave irradiation on bone decalcification aimed to DNA extraction. Leg Med (Tokyo). 2013 Sep;15(5):272-7. doi: 10.1016/j.legalmed.2013.06.001. Epub 2013 Jul 6.

22. Kapila SN, Natarajan S, Boaz K, Pandya JA, Yinti SR. Driving the Mineral out Faster: Simple Modifications of the Decalcification Technique. J Clin Diagn Res. 2015 Sep;9(9):ZC93-7. doi:10.7860/JCDR/2015/14641.6569. Epub 2015 Sep 1.

23. Katoh K. Microwave-Assisted Tissue Preparation for Rapid Fixation, Decalcification, Antigen Retrieval, Cryosectioning, and Immunostaining. J Cell Biol. 2016;2016:7076910. Epub 2016 Oct 20.

24. Kiviranta I, Tammi M, Lappalainen R, Kuusela T, Helminen HJ. The rate of calcium extraction during EDTA decalcification from thin bone slices as assessed with atomic absorption spectrophotometry. Histochemistry. 1980;68(2):119-27.

25. Kok LP, Boon ME. Microwaves for declcification. In: Microwave cookbook for microscopists: art and science of visualization. Leyden: Coulomb Press; 1992 (Chapter 13).

26. Leong, A.S.-Y. (2009). Microwave applications in pathology. Microwave Applications in Pathology. 1-162.

27. Liu H, Zhu R, Liu C, Ma R, Wang L, Chen B, Li L, Niu J, Zhao D, Mo F, Fu M, Brömme D, Zhang D, Gao S. Evaluation of Decalcification Techniques for Rat Femurs Using HE and Immunohistochemical Staining. Biomed Res Int. 2017;2017:9050754. doi: 10.1155/2017/9050754. Epub 2017 Jan 26.

28. Matthews JB, Mason GI. Influence of decalcifying agents on immunoreactivity of formalin-fixed, paraffin-embedded tissue. Histochem J. 1984 Jul;16(7):771-87.

29. Mattuella LG, Bento LW, Vier-Pelisser FV, Araujo FB, Fossati ACM. Revista Odonto Ciência – Fac. Odonto/PUCRS, v. 22, n. 56, abr./jun. 2007

30. Mori S, Sawai T, Teshima T, Kyogoku M. A new decalcifying technique for immunohistochemical studies of calcified tissue, especially applicable to cell surface marker demonstration. J Histochem Cytochem. 1988 Jan;36(1):111-4.

31. Morse A. Formic Acid-Sodium Citrate Decalcification and Butyl Alcohol Dehydration of Teeth and Bones for Sectioning in Paraffin. Journal of Dental Research Vol 24, Issue 3-4, pp. 143 – 153 First Published June 1, 1945 https://doi.org/10.1177/00220345450240030501.

32. Neves, Juliana & Omar, Nádia & Aparecida Orsini Narvaes, Eliene & Gomes, Jose & Novaes, Pedro. (2011). Influence of different decalcifying agents on EGF and EGFR immunostaining. Acta histochemica. 113. 484-8. 10.1016/j.acthis.2010.04.006.

33. Pitol DL, Caetano FH, Lunardi LO. Microwave-induced fast decalcification of rat bone for electron microscopic analysis: an ultrastructural and cytochemical study. Braz Dent J. 2007;18(2):153-7.

34. Reineke T, Jenni B, Abdou MT, Frigerio S, Zubler P, Moch H, Tinguely M. Ultrasonic decalcification offers new perspectives for rapid FISH, DNA, and RT-PCR analysis in bone marrow trephines. Am J Surg Pathol. 2006 Jul;30(7):892-6.

35. Roach HI[1], Mehta G, Oreffo RO, Clarke NM, Cooper C. Temporal analysis of rat growth plates: cessation of growth with age despite presence of a physis. J Histochem Cytochem. 2003 Mar;51(3):373-83.

36. Roger Hart J, Ethylenediaminetetraacetic Acid and Related Chelating Agents, in Ullmann's Encyclopedia of Industrial Chemistry, Weinheim, Wiley-VCH, 2005.

37. Sangeetha R, Uma K, Chandavarkar V. Comparison of routine decalcification methods with microwave decalcification of bone and teeth. J Oral Maxillofac Pathol. 2013 Sep;17(3):386-91. doi: 10.4103/0973-029X.125204.

38. Sangeetha R, Uma K, Chandavarkar V. Comparison of routine decalcification methods with microwave decalcification of bone and teeth. J Oral Maxillofac Pathol. 2013 Sep;17(3):386-91. doi: 10.4103/0973-029X.125204.

39. Sanjai K, Kumarswamy J, Patil A, Papaiah L, Jayaram S, Krishnan L. Evaluation and comparison of decalcification agents on the human teeth. *Journal of Oral and Maxillofacial Pathology : JOMFP*. 2012;16(2):222-227. doi:10.4103/0973-029X.99070.

40. Sanjeet S, Keya S. Evaluation of efficacy of various chemicald for decalcification of dental hard tissues-an in-vitro study. I Orofac Sci. 2010;1(1):5-10.

41. Savi FM, Brierly GI, Baldwin J, Theodoropoulos C, Woodruff MA. Comparison of Different Decalcification Methods Using Rat Mandibles as a Model. J Histochem Cytochem. 2017 Dec;65(12):705-722. doi: 10.1369/0022155417733708. Epub 2017 Sep 29.

42. Schajowicz F, Cabrini RL. The effect of acids (decalcifying solutions) and enzymes on the histochemical behavior of bone and cartilage. J Histochem Cytochem. 1955 Mar;3(2):122-9.

43. Silva A, Rici REG, Neto AA: Techniques used for morphological and ultrastructural description from teeth white-tufted.ear-marmosets (Callithrix jacchus), 2012.

44. Verdenius HH; Alma L. A quantitative study of decalcification methods in histology. J Clin Pathol. 1958 May;11(3):229-36.

45. Yamamoto-Fukud T, Shibata Y, Hishikawa Y, Shin M, Yamaguchi A, Kobayashi T and Koji T. Effects of various decalcification protocols on detection of DNA strand breaks by terminal dUTP nick end labelling. Histochem J 2000; 32: 697-702.

46. Yoshioka M, Yoshida Y, Inoue S, Lambrechts P, Vanherle G, Nomura Y, Okazaki M, Shintani H, Van Meerbeek B. Adhesion/decalcification mechanisms of acid interactions with human hard tissues. J Biomed Mater Res. 2002 Jan;59(1):56-62.

3. MULTI-DISCIPLINARY APPROACH TO SWINE AND OVINE BONE TISSUE: HISTOLOGIC, DENSITOMETRIC, MICRO-COMPUTED TOMOGRAPHIC AND BIOMECHANICAL CHARACTERIZATION

M. E. Andreis[1], F. Boschetti[2], M. Cummaudo[3], C. Cattaneo[3], A. Crovace[4], C. F. Wolschrijn[5], M. Di Giancamillo[6], S. C. Modina[1]

[1]Department of Health, Animal Science and Food Safety, Università degli Studi di Milano, Milano, Italy

[2]Department of Chemistry, Materials and Chemical Engineering "Giulio Natta", Politecnico di Milano, Italy

[3]Laboratory of Forensic Anthropology and Odontology, Department of Biomedical Science for Health, Università degli Studi di Milano, Italy

[4]Istituto di Clinica Chirurgica Veterinaria, Università degli Studi di Bari, Italy

[5]Department of Pathobiology – Anatomy and Physiology, Universiteit Utrecht, Utrecht, The Netherlands

[6]Department of Veterinary Medicine, Università degli Studi di Milano, Milano, Italy

Introduction

Artificial bone substitues are widely used for bone reconstruction and regeneration (Wu et al., 2014). Although autologous grafting is still considered the gold standard, in fact, significant advances in the development of synthetic substitutes have been reached in the recent years (Campana et al., 2014). Bone substitutes are defined as "synthetic, inorganic or biologically organic combinations which can be inserted for the treatment of a bone defect instead of autogenous or allogenous bone" (Schlickewie and Schlickewie; 2007); they can be divided into grafts, ceramics and growth factors (Campana et al., 2014). Because of their role in bone defect therapy, bone substitutes ideally need to satisfy different requirements, such as biocompatibility and absence of adverse inflammatory response at their use, optimal osteoconduction and osteoinduction, resorbability, ready availability and reasonable cost (Campana et al., 2014). To date, synthetic bone substitutes exhibit several satisfactory properties, such as mechanical properties and biocompatibility (Wu et al., 2014); however, there are specific deficiencies for different types of substitutes (friability of ceramic scaffolds (Gotman et al., 2013), poor strength of polymeric scaffolds (Hutmacher, 2000), uncontrollable degradability (Wang et al, 2007), among others) (Wu et al., 2014). A deep knowledge and full understanding of structural, biomechanical and compositional bone properties is mandatory to design ideals biomimetic synthetic scaffolds (Wu et al., 2014). In fact, the physico-chemical and structural features of scaffold seem to influence significantly their performance *in vivo*, and three-dimensional scaffold might have important clinical application in regenerative medicine (Gramanzini et al., 2015; Velasquez et al. 2013). The bone is a highly specialized connective tissue, specifically designed for structural, mechanical and metabolic functions. It is composed of 60-70% mineral, 10-20% collagen and 9-20% water (Park, 1987); small quantities of other organic components (e.g. proteins, lipids, polysaccharides) are also present

(Gunderson et al., 1991). Based on its microscopic organization, mammalian bone tissue is classified as cortical or trabecular. Cortical bone is traditionally considered to be hierarchically organized in functional units called osteons, formed by circumferential lamellae arranged around a longitudinal vascular channel (Haversian canal) (Webster, 1988). Despite these shared features, cortical bone shows a different organisation mainly based on animal species, size, age and functional moment (Hillier and Bell, 2007; Sawada et al., 2014; Matiniakova et al., 2006; Martiniakova et al., 2006). In adult pigs and sheep, femoral cortical bone is mainly vascular plexiform, a highly organized pattern which reflects rapid increase in size (Currey, 1984; Martiniakova 2006; Martiniakova, 2007) many primary osteons and scattered dense Haversian systems are also present, together with several resorption lacunae (Martiniakova, 2006; Martiniakova, 2007). Histomorphometric parameters (area, perimeter, maximum and minimum diameter of Haversian canals and Haversian systems, as well as primary osteon's vascular canals parameters) have also been described in these two species (Martiniakova, 2006; Martiniakova, 2007). Trabecular bone, on the other hand, consists of a network of anastomosing trabeculae, containing bone marrow within their pores. Parallel sheets of lamellae form angular segments called trabecular packets, the functional analogous of osteons (Webster, 1988). The amount of mineral inorganic components of the bone is represented by Bone Mineral Density (BMD). Besides more invasive techniques (e.g. measurements of ashes and mineral content), the most accurate way to determine BMD is considered Dual-energy X-Rays Absorptiometry (DXA), which has been validated for the study of BMD in pigs and sheep (Nielsen et al., 2004). Although several studies focus on the consequences of drugs or specific diets (Duffy et al., 2018; Kolp et al., 2017; Skiba et al., 2017) on BMD, few of them exist which evaluate BMD in normal conditions (Mitchell et al., 2001; Turner et al, 1995; Teo et al., 2006). BMD contributes significantly to the mechanical properties of bone (Wu et al., 2014); however, it has been proven that microarchitecture can be accounted for the majority of bone biomechanical behaviour (Parfitt, 1992; Kleerekoper et al., 1985; Parfitt et al., 1983; Jensen et al., 1990). Although the possibility to deduce the three-dimensional organization of trabecular bone from two-dimensional histologic sections is possible through histomorphometric analysis, the most reliable method to assess trabecular bone microscopic structure is micro-computed tomography (μCT) (Müller et al., 1998; Hildebrand, et al., 1999; Chappard et al., 2005). Microarchitectural parameters such as Bone Volume to Tissue Volume fraction (BV/TV, %), Trabecular Number (Tb.N/mm) and Thinckness (Tb.Th, mm) and Structural Model Index (SMI), among others, have a fundamental role in bone quality (Fazzalari et al., 1998; Hernandez and Keaveny, 2006). Since the use of this μCT for the evaluation of cortical bone, on the other hand, is still limited (Britz et al., 2010), histology is still widely used, especially on undecalcified samples. Bone quality has been quantitatively described by its mechanical properties (Bailey and Vashishth, 2018), which reflect its organisation and function, combining the features of its inorganic and organic components. They are critical for the assessment of its load-bearing capacity and functionality, which is affected by aging, disease and pharmacological intervention (Osterhoff et al., 2016; Donnelly, 2011). From a biomechanical point of view, bone is a heterogeneous material characterised by anisotropic behaviour, mostly due to its hierarchical organization. Cortical bone is characterized by excellent toughness at low strain rates, but at high rates it

behaves like a brittle material (Park, 1987). Trabecular bone, on the other hand, exhibits three behavioural regimens: a small strain linear-elastic response, which ends when the cell walls of low-density bone collapse, a plateau, which continues until opposite cell walls touch, causing a steep increase in stress (Hayes and Carter, 1976; Pugh et al, 1973; Stone et al., 1983; Gibson, 1985; Wu et al., 2014).

Since each of these features has an influence on the final performance of the bone tissue as a whole, they should all be carefully considered in the light of bone substitutes design.

The aim of this work is therefore to comprehensively describe normal cortical and cancellous bone (femur and tibia) features in swine and sheep, which are often used as model to test bone substitutes' biocompatibility and mechanical stability. Basic densitometric, morphological, microarchitectural and biomechanical bone features will be described, in order to provide multi-disciplinary information for bone substitues' design and evaluation in pre-clinical trials.

Methods

Animals

Left swine hindlimbs were collected from the slaughterhouse. The medio-distal femur and medio-proximal tibia of Landrance x Large White crosses weighting 80-90 kg were evaluated. Nine left hindimbs from 3-year-old Bergamasca sheep were collected from an external laboratory, after euthanasia as part of experiments unrelated to the present study. The experiments were approved by Italian Ministry of Health (Permit N. 264/2013-B).

Macroscopic and radiographic evaluation

After complete soft tissue removal, bones underwent a visual inspection and radiographic examination (orthogonal views) to exclude potential abnormalities (e.g. osteochondrosis) and were stored at -20°C until use. Animals with homogeneous skeletal age at the radiographic exam (growth plates) were selected.

Dual-energy X-rays Absorptiometry

All bones underwent a Dual-energy X-rays Absorptiometry (DXA) (Hologic QDR-1000 Plus, Hologic, Waltham, MA, USA) exam as a whole, and Bone Mineral Density (BMD) was recorded at 12 different anatomic sites (femur: cranial diaphysis, caudal diaphysis, medial diaphysis, lateral diaphysis, medial condyle, lateral condyle; tibia: cranial diaphysis, caudal diaphysis, medial diaphysis, lateral diaphysis, medial condyle, lateral condyle) through the placement of a Region Of Interest (ROI). Each measure was repeated three times and mean values were used for statistical analysis. A calibration scan of a phantom was performed weekly to ensure accurate results. DXA analysis was repeated after sampling on isolated cortical and trabecular samples (see below).

Sampling

For each femur and tibia, the following samples were obtained: 4 cortical bone stripes (medial, lateral, cranial and caudal); 1 cortical circumferential slice; 2 trabecular bone cubes (medial condyle, lateral condyle) (Fig. 1). Cortical stripes underwent DXA and biomechanical evaluation; cortical circumferential slices underwent undecalcified histologic evaluation; trabecular bone cubes underwent DXA, micro-CT and biomechanical analysis; a thin slice was sampled from each cube, which underwent histological analysis.
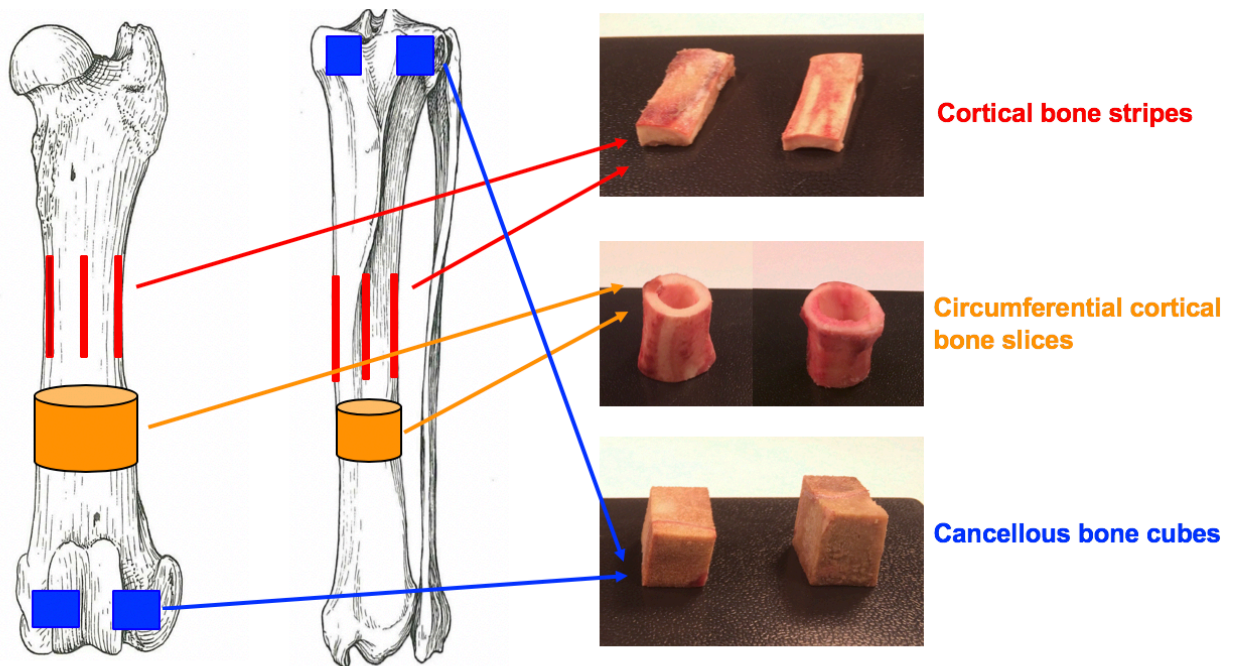
Fig. 1 – Sampling: For each femur and tibia, the following samples were obtained: 4 cortical bone stripes (medial, lateral, cranial and caudal); 1 cortical circumferential slice; 2 trabecular bone cubes (medial condyle, lateral condyle).

Cortical Bone histology

Bones were then cut with a band saw to obtain cancellous bone (≈2 cm x 2 cm x 2 cm for swine; ≈1,5 cm x 1,5 cm x 1,5 cm for sheep) and full cortical bone specimens (≈1 cm x 7 cm), corresponding to the 12 ROIs. The circumferential slices of cortical bone were degreased in ammonia water solution, polished with grinding/abrasive paper on a grinding wheel for geologists (Struers DAP-7) (Caccia et al., 2016) and microscopically evaluated to determine their thickness and microarchitecture (prevalent type of bone, Haversian systems' and canals' number, minimum and maximum diameter, perimeter and area).

Trabecular Bone histology

Corresponding 2-mm-thick thin sections of trabecular bone were obtained at each site for microscopic analysis; 2-cm-thick circumferential slices from the bone adjacent to the cortical stripes were also sampled for undecalcified microscopic examination. The thin slices of cancellous bone were fixed in neutral buffered formalin for 48 hours, rinsed in running tap water for 5 hours and decalcified in acid solution (1,85% hydrochloric acid, 4% formic acid in distilled water) for 6 days (swine) and 15 days (sheep). All samples were then dehydrated in a graded 50% (v/v), 70% (v/v), 95% (v/v) and 100% (v/v) ethanol series, embedded in paraffin and transversally cut into 4-lm-thick sections. The obtained sections were dewaxed and rehydrated and routinely stained with hematoxilin and eosin (HE) and Safranin O (specific for cartilage). Immunolocalization of collagen I was performed with a polyclonal anti collagen I antibody (EPR7785 ab138492 abcam) incubated overnight at room temperature in a humid chamber. The antigen–antibody complex was detected with a TRITC-labeled donkey anti-rabbit (1:100; Vector Laboratories, Inc.) incubated for 30 min at room temperature. After incubation with secondary antibodies sections were washed and finally mounted on slides in the antifade medium Vecta Shield (Vector Laboratories, Inc). Samples were analysed on an epifluorescence microscope (Eclipse E600; Nikon) also equipped for epifluorescence and a digital camera (Nikon digital sight, DS-U3) and software (NIS elements Imaging Software; Nikon) with a 20 X objective. Immunofluorescence negative controls, which were performed by omitting the primary antibodies, did not show any staining under the same exposure settings.

Micro-Computed Tomography

Each of the collected specimen of trabecular bone underwent micro-computed tomographic examination (μCT 100, Scanco Medical AG, Switzerland, EU). Scanning was performed in air, with a peak voltage of 70 kV and intensity (current) of 114 μA; the scanner was equipped with an aluminium filter to reduce beam hardening. Trabecular microarchitecture was quantitatively determined in manually-drawn volumes of interest (VOIs). Due to the presence of growth plates in porcine samples (femoral condyles and tibial plateau), the epiphyseal (Epiphyseal Trabecular Bone, ETB) and diaphyseal (Metaphyseal Trabecular Bone, MTB) portions of each sample were evaluated separately.

Biomechanical testing

Swine trabecular specimens were cut with a band saw immediately before biomechanical testing, to obtain smaller specimens of uniform tissue, one at each side of the growth plate (Epiphyseal Trabecular Bone, ETB and Diaphyseal Trabecular Bone, DTB). Sheep trabecular specimens were tested as a whole. A four-point bending test, with four preload cycles and until facture, was applied on the cortical specimens. A strain gage rosette was glued on each sample and connected to a Quantum X control unit in order to record the values of deformation. The maximum stress was evaluated as well. From the three SG that compose the rosette, the maximum and minimum values of the deformation were calculated as $\varepsilon_{MAX,min}(i) = \frac{\varepsilon_1(i)+\varepsilon_3(i)}{2} \pm$

$\frac{1}{\sqrt{2}}\sqrt{(\varepsilon_1(i) - \varepsilon_2(i))^2 + (\varepsilon_2(i) - \varepsilon_3(i))^2}$ and the Poisson ratio was computed as $\nu = -\frac{\varepsilon_{min}}{\varepsilon_{MAX}}$. From the stress-strain curve of the last cycle of load, the slope of the linear part was evaluated: this was the elastic modulus. Six preload cycles until 2 MPa of compression with end-caps were applied to ETB and DTB specimens. A steel sample was tested with the same procedure in order to obtain the load-displacement curve of the set-up and use it to correct the data and achieve the real displacement of the bone specimens. With the so-obtained data, the values of stress and strain of the last cycle of load were calculated and, it was then possible to obtain the value of the elastic modulus, defined by the Hookes law as $E = \frac{\sigma}{\varepsilon}$. The Young modulus was extracted by evaluating the initial and final slopes of the curve. Specimens were tested with a compression procedure with end-caps until failure; after correcting the displacement taking into account the machine compliance, the elastic modulus was computed and the failure and yielding behaviours were evaluated by computing, for each situation, the stress and strain.

Statistical analysis

Statistical analysis was performed with the IBM SPSS Statistics 25.0 (IBM SPSS Inc., Armonk, USA). Descriptive statistics was performed for BMD, micro-CT and biomechanical parameters.

Results

Macroscopic and radiographic evaluation

Five pigs were excluded from the study due to macroscopic abnormalities compatible with osteochondritis dissecans of the medial femoral condyle (Fig. 2); three pigs were excluded due to radiographic abnormalities of the medial femoral condyle compatible with osteochondrosis (Fig. 3). Ten pigs and all nine sheep were finally included in the study.

Dual-energy X-rays absorptiometry

The results of bone density analysis on the whole bone and on isolated specimens are reported in App. 1, 2 and App. 3-5 respectively.

Cortical Bone histology

Histomorphological analysis of cortical bone revealed several different patterns, as previously reported (Martiniakova et al., 2006) (Fig. 4). In the femur, plexiform bone was found in association with mostly primary osteons towards the endosteal surfaces mainly in the cranio-medial portions of the diaphysis, while a larger proportion of fibrolamellar bone with both primary and secondary osteon was found in the caudolateral diaphyseal portions, mainly towards the endosteal region. In the tibia, plexiform bone was primarily accompanied by primary and secondary osteons towards the endosteum in the cranial, medial and lateral portions of the diaphysis, with occasional areas of fibrous tissue; in the caudal diaphyseal portion, plexiform bone was accompanied by several areas of mixed pattern, including fibrolamellar, differently-

arranged vascular canals and primary/secondary osteons, with occasional osteon banding (App. 6-9). The results of Haversian systems' and canals' measures are reported in App. 10-13.

Trabecular Bone histology

Histological analysis confirmed morphologic preservation of all samples after decalcification (Fig. 5). In all porcine samples intra-trabecular basophilic areas were found, which appeared red at Safranin O' staining (cartilage) (Fig. 5); these areas seemed larger and more numerous in MTB. Immunolocalisation of collagen I confirmed antigenicity preservation; in sheep samples, as expected, different levels of collagen deposition were evident. In swine samples, no signal was present in the areas corresponding to positive staining at Safranin O (cartilage) (Fig. 6).

Micro-Computed Tomography

The results of micro-CT analysis are reported in App. 14 for pigs (MTB and ETB) and App. 15 for sheep. Differences in micro-CT parameters between MTB and ETB in swine bone are depicted in Fig. 7. Micro-CT images for sheep are showed in Fig. 8

Biomechanical Testing

The results of biomechanical evaluation are reported in App. 16-21. Significant difference in US was found between ETB and MTB in pigs (Fig. 9)
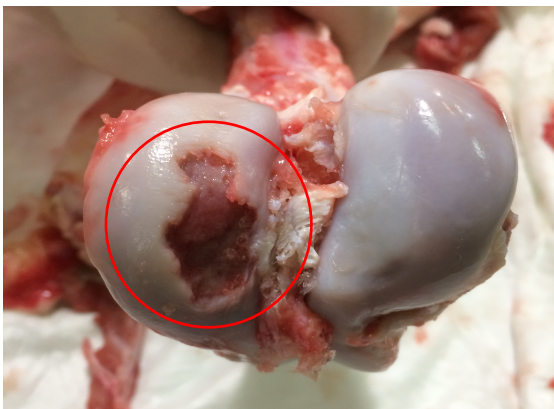
Fig. 2 - Distal epiphysis of swine femur: macroscopic pathologic alterations compatible with osteocondrosis dissecans of the medial femoral condyle (red circle).

Fig. 3 - Distal epiphysis of swine femur: a curvilinear radiolucent subchondral defect, compatible with osteocondrosis, is visible at the level of the medial femoral condyle (red circle).

Fig. 4 – Histomorphological characterization. Large areas of plexiform bone are visible, together with small areas of laminar bone and isolated osteons. Pig, femoral diaphysis, undecalcified (10X).
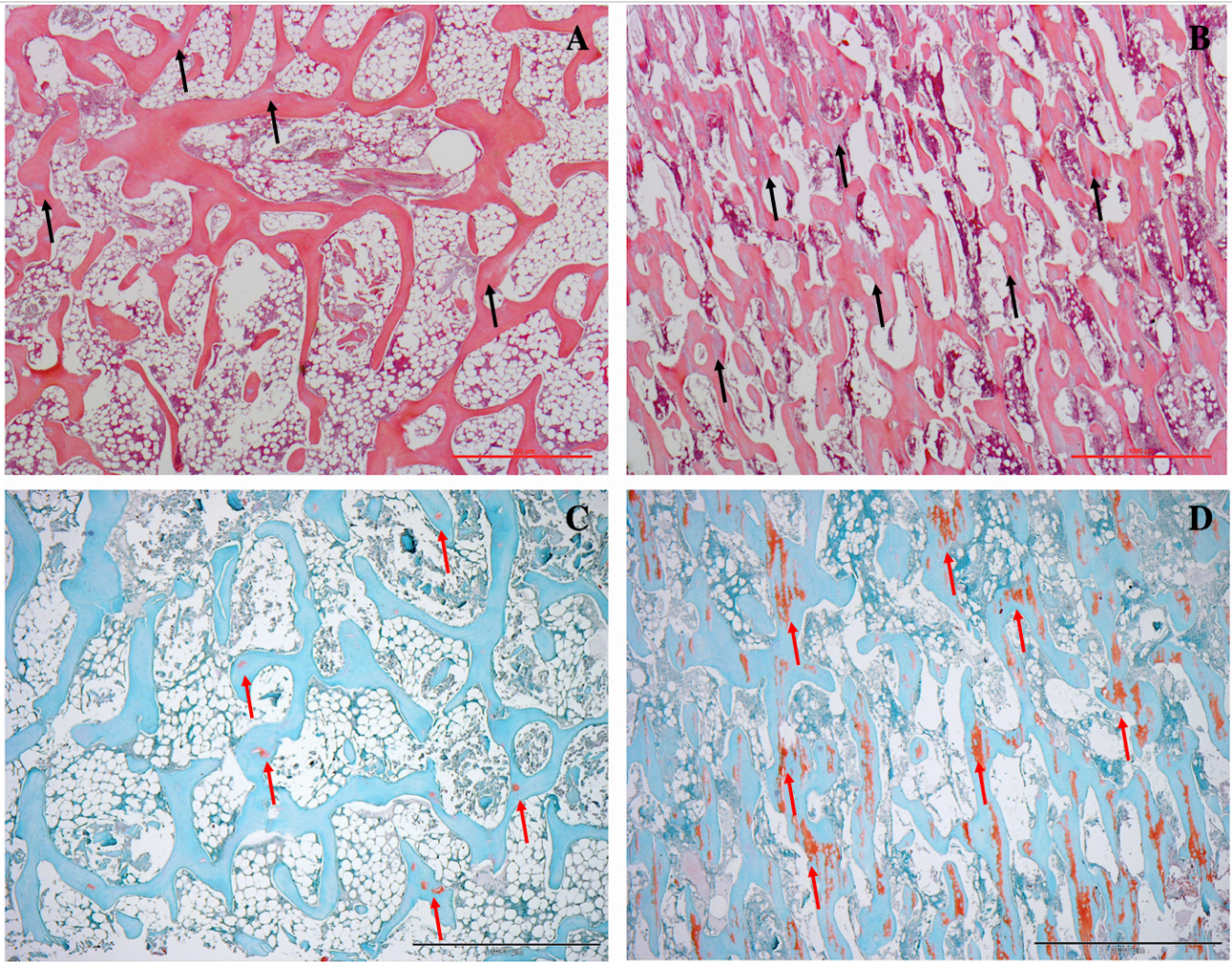
Fig. 5 - Histological characterization of swine trabecular bone. Intra-trabecular basophilic areas at hematoxylin and Eosin staining (black arrows) are confirmed to be cartilage at Safranin O staining, where they appear intensely red (red arrowws). These areas seem larger and more numerous in ETB (A) when compared to MTB (B). A, B: Hematoxylin and Eosin; C, D: Safranin O; pig, femoral condyle, decalcified. Bar=1mm.
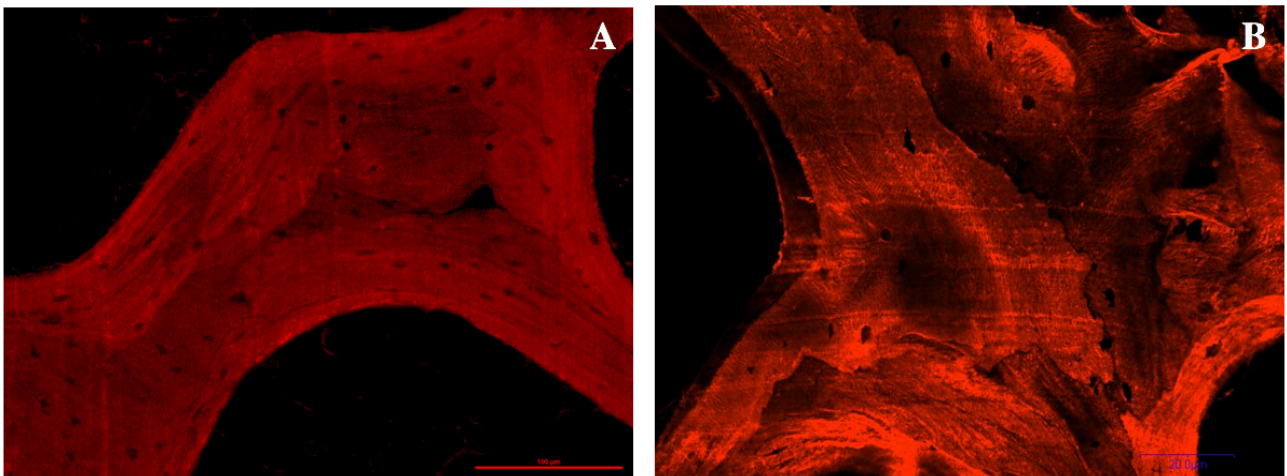
Fig. 6 – Immunoflourescence characterization of swine and ovine trabecular bone. In swine samples (A), no signal was present in the areas corresponding to cartilage. In ovine samples (B), different levels of collagen deposition were evident; this is typical of adult bone. Bar=
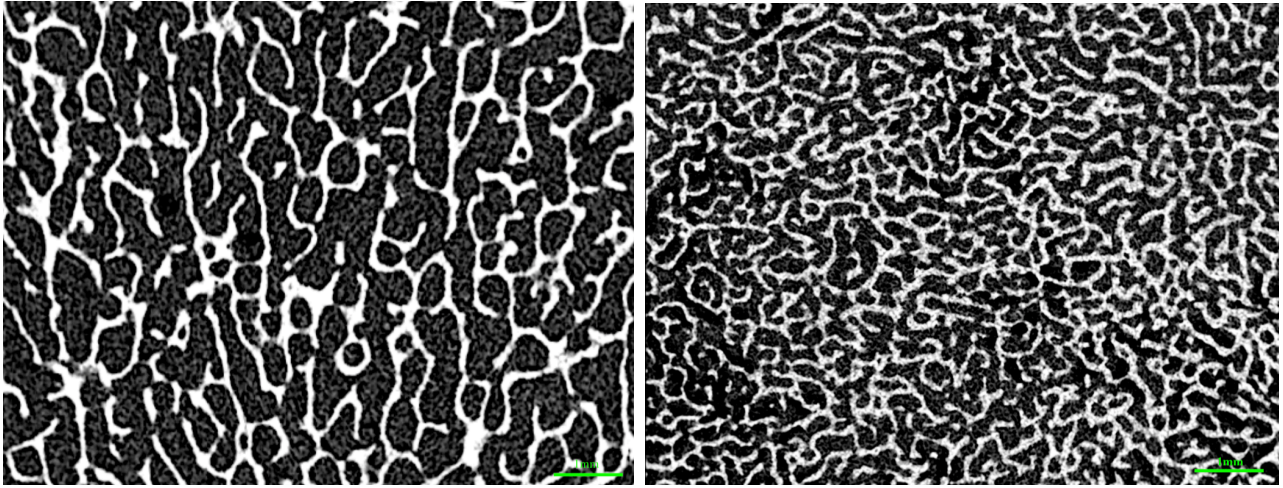
Fig. 7– Micro-CT thin slices of swine trabecular bone. left: ETB; right: MTB. ETB shows a lower number of trabeculae, separated by larger marrow cavities when compared to ETB. Bar=1mm.
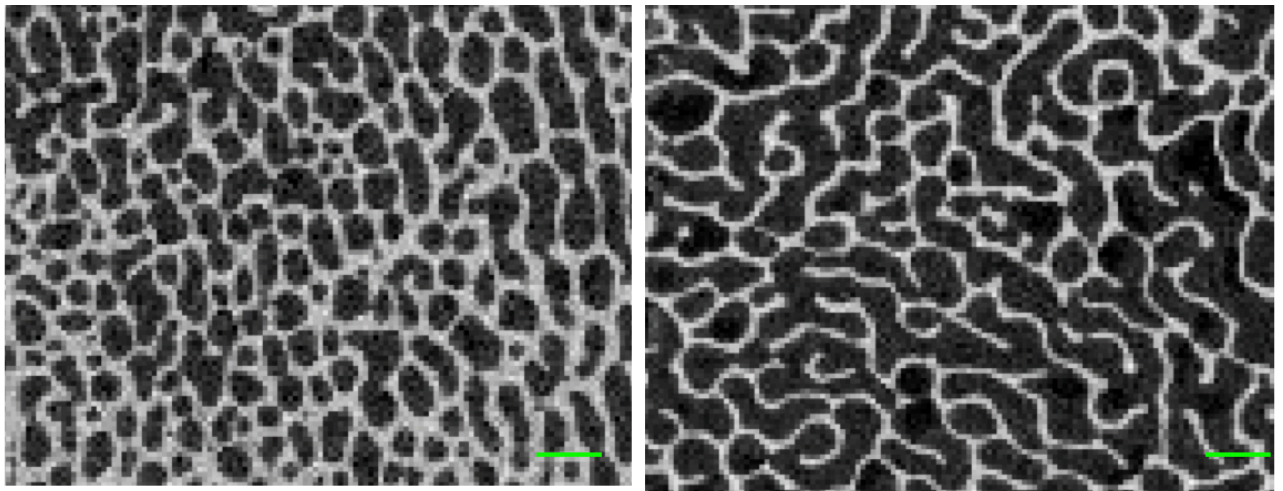
Fig. 7– Micro-CT thin slices of ovine trabecular bone. Left: femoral condyle; right: tibial condyle. Bar=1mm
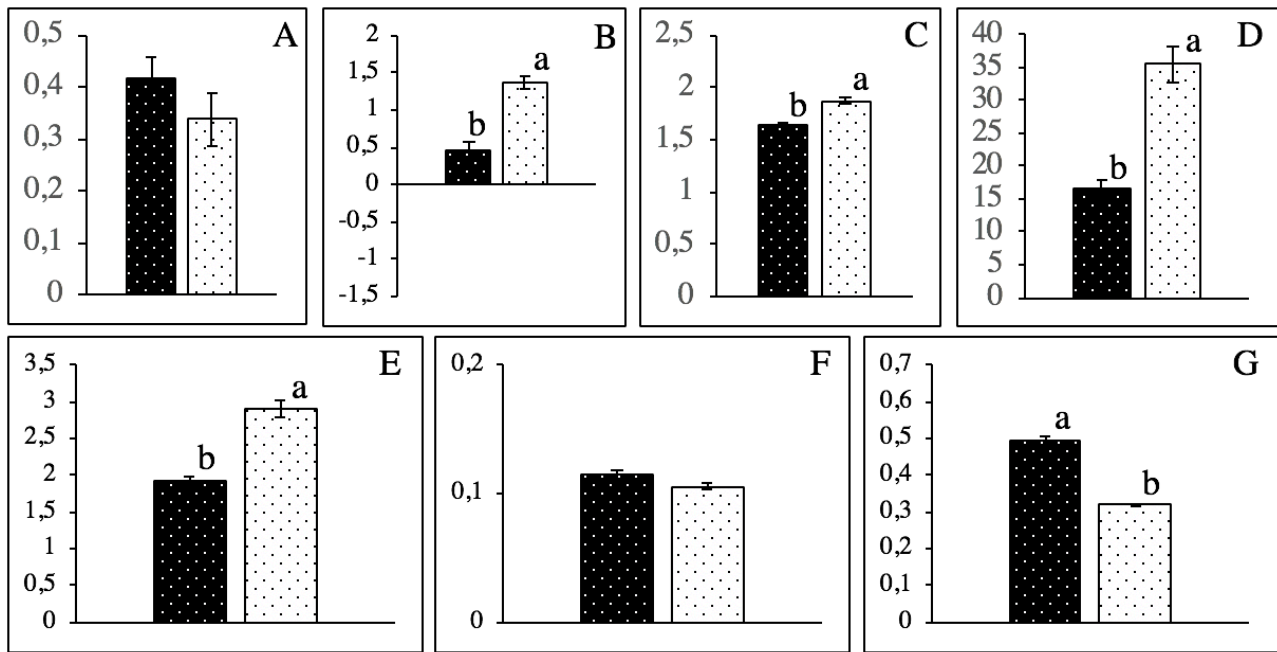
Fig. 8 – Graphical representation of the differences in micro-CT parameters of swine trabecular bone between ETB (left) and MTB (right). A: BV/TV (%); B: SMI; C: DA; D: Conn; E: Tb.N (1/mm); F: Tb.Th (mm); G: Tb.Sp (mm). Values are expressed as mean±standard. Column with different letters are significantly different (p<0,05).

Discussion

When approaching the design of bone substitutes or the evaluation of the efficacy, safety and biocompatibility of such synthetic materials in preclinical trials, none of basic bone features such as morphology, composition, mineral density and biomechanics can be left behind without the risk of precluding the reliability of the obtained results. The bone is a very complex and metabolically active tissue, and each of its properties and function can be optimally tested with a specific method; to date, no single technique exists that allows to provide information simultaneously all the basic characteristics of bone quality. In this work we propose a multidisciplinary approach to swine and ovine bone tissue, through the study of different bone features with different techniques on the same specimens. Pigs and sheep have been selected for this study because they represent common models in orthopaedic research. Pigs are reported as the subject of choice in a variety of studies, such as femoral head osteonecrosis, cartilage and bone fractures and bone ingrowth studies (An and Friedman, 1999; Buser et al., 1991; Sun et al., 1999); they have been also employed to test fixation devices and investigate trauma (Seil et al., 1998; Massengill et al., 1982; Kousa et al., 2003; Kousa et al., 2003; Humphrey et Hutchinson, 2001; Southern et al., 1990). Since swine commercial breeds are characterized by very high growth rate and excessive final body weight (Pearce et al., 2007), however, pigs weighting 70-80 kg were selected at the slaughterhouse. Sheep, on the other hand, are becoming more and more diffuse especially in studies involving fractures, osteoporosis and osteoarthritis (Decker et al., 2014; Dias et al. 2018; McCoy, 2015), probably due to their body weight and hindlimb long bones dimension and biomechanics, which are similar to humans (Pearce et al, 2007). All bone features were studied at different regions of both femur and tibia (medial, lateral, crabnial, caudal diaphysis; medial and lateral condyles). In fact, regional differences in bone microscopic and biomechanical features have been

previously described is some species (Mason et al, 1995; Martin et al., 1996; Zedda et al., 2015; Bonney et al., 2011), which are likely to correspond to the loading strain patterns of the bone during normal locomotion (Bonney et al., 2011).

Microscopic analysis of cortical bone revealed plexiform bone as the overall major component in pigs both for the femur and the tibia, in accordance with previous studies (Martiniakova 2006, 2007; Hillier et al., 2007). Plexiform bone is a type of primary bone which is typically found in the long bone of large, fast-growing animals, morphologically characterised by a "brick-wall appearence" (Martin, 1998; Hillier et al., 2007). Previous studies enlighted a connection between osteon density and mechanical load, with a decrease of density on the sides of the bone where tensile strains are predominant (Mason et al., 1995). Similarly, a relation between osteon diameter and strain magnitude has been described (Frost, 1990; Skedros, 2001). In our study a purely qualitative analysis of cortical bone morphometric parameters was performed, which does not suggest the presence of such differences at different anatomical sites. However, a quantitative analysis of these parameters would be very interesting, potentially revealing significant differences due to muscular and joint anatomy and loadbearing patterns.

Microscopic analysis of trabecular bone samples revealed typical features in all sheep samples. In all swine samples, small intra-trabecular areas of mineralized cartilage, confirmed with Safranin O staining were evident, which seem larger and more abundant in MTB when compared to ETB. Although expected, it is very important to remark these results: in fact, it is important to remark that pigs weighting 70-80 kg, often used as orthopaedic models, are far from being skeletally adult, and this has important implication on results interpretation. In fact, the normal rate of bone regeneration and remodelling is very high in young animals and decreases with ageing, and this could very likely influence the outcome of studies aimed, for example, to evaluate fracture healing, fixation devices and bone regeneration, with potential misinterpretation of the results. The primary diagnostic value of bone histomorphometry is the assessment of osteoid and bone cells, and three-dimensional techniques such as microCT do not provide information on bone dynamics (e.g. forming, resorbing and resting bone surfaces) (Müller et al., 1998). Moreover, mineralization of these cartilage areas would not be evident at micro-CT analysis, which is often employed in this type of studies, but would probably have an influence on bone biomechanical analysis, possibly leading to imprecise data interpretation. The reason for a higher mineralization at the metaphyseal region is not clear, but this difference could be due to the higher apposition rate when compared to the epiphyseal ossification centre. Few densitometric study exist on pigs, especially whole-body examinations aimed to non-invasive evaluation of carcasses' composition (Kremer et al., 2011; Bernau et al., 2015; Soladoye et al., 2016). Concerning sheep, together with carcasses' evaluation (Pearce et al., 2009), DXA has been employed to quantitatively analyse bone healing and regeneration, osteoporosis (den Boer et al., 1999; Floerkemeier et al., 2010; Heiss et al., 2017), and in normal conditions both on live animals and *ex vivo* (Turner et al. 1995; Pouilles et al., 2000). To our knowledge, no precise regional information about the femur and tibia in this species exist. Despite the small sample size, BMD analysis provided basic regional parameters in 70-80 kg pigs and adult sheep. Such results may serve as basic comparison with new researches about the tibia and the

femur in these species, providing a set of normal references. On the other way, the BMD analysis performed on isolated specimens, corrected for their size, aimed to provide standard densitometric parameters for the realization of scaffold materials designed for specific regions. In fact, BMD significantly contributes to the mechanical properties of bone (Wu et al., 2014), and regional differences in this parameter could potentially influence the efficacy of a non-specific synthetic substitute. It is important to notice that no precise information was available about the age and rearing conditions of the pigs included in the study. Accurate age determination, in fact, is not possible with radiography; moreover, growth plates closure is very variable in pigs (Cone, 2017) and only two bones were available for radiographic interpretation. Anyway, subjective radiographic evaluation of the available growth plates suggested a homogeneous sample. Also, no precise information about conditions that may have influenced bone metabolism were available (e.g. diet; non-skeletal orthopaedic disease; metabolic disease); anyway, diet is generally standardized for these animals and no remarks at the pre-mortem inspection were reported. On the other hand, sheep came from a control experimental group, so the variables potentially affecting BMD were likely reduced.

MicroCT analysis provided basic results about bone microarchitecture, bypassing the possible error involved in traditional histomorphometric analysis. In fact, basic parameters, such as relative bone volume density (BV/TV), mean trabecular thickness (Tb.Th), mean trabecular separation (Tb.Sp) and trabecular number (Tb.N) can be computed directly from three-dimensional images without underlying model assumption (Hildebrand and Rüegsegger, 1997). Trabecular bone is organized in a three-dimensional network of rods and plates, and the extrapolation of three-dimensional values from two-dimensional sections assumes a plate-like organization (Stauber and Müller, 2005), which is not always the case. MicroCT results in the pig showed higher BV/TV in MTB when compared to ETB, explained by a higher Tb.N and lower Tb.Sp, without differences in Tb.Th; therefore, MTB can be considered more porous with respect to ETB. Analysing the Structural model index (SMI), a parameter which estimates the plate-rod organization of bone, both ETB and MTB showed a plate-like structure, which was more pronounced in ETB. SMI, in fact, varies from 0 (ideal plate structure) to 3 (ideal rod structure), lying between 0 and 3 for structures with both plates and rods (Hildebrand and Rüegsegger, 1997). Although some Authors recently proposed ellipsoid factor (EF) as an alternative to SMI, arguing that SMI is unavoidably influenced by the assumption that the entire trabecular bone surface is convex and that SMI values in literature should be considered with suspicion (Salmon et al., 2015), SMI is still widely used to describe microarchitectural bone features. Few negative SMI results were also obtained in ETB, in samples with higher BV/TV, confirming the hypothesis of close relation of between these two parameters (Salmon et al., 2015).

No precise information is available at the moment about species-specific biomechanical parameters of cortical and cancellous bone. In this project, the elastic modulus and ultimate strength were measured both for cortical and cancellous bone with bending tests (cortical bone) and compression test (cancellous bone) with strain gages. The results obtained for all samples are in rough agreement with those reported for humans, sheep and cows in other studies (Zhang et al., 2014; Ding et al., 2012; Endo et al., 2016; Wu et al., 2014). The elastic modulus of cortical bone in sheep was higher when compared to the pig and to the

available parameters for humans (Ding et al., 2012; Wu et al., 2014). The reason for this difference is unclear, but since BMD analysis showed similar results for both species, the different morphometric features (e.g. different amount of plexiform bone) might be responsible for it. However, it must be specified that several different techniques can be employed to measure the biomechanical properties of bone, and not all of them provide the same results (Bayley and Vashishth, 2018). Therefore, a precise comparison is difficult to perform.

This study has several limits. It was not possible to establish precisely the age of the animals. Sample size was small, but animals were homogeneous. No precise information was available about the diet the animals were fed, and the skeletal consequences on different diets on bone metabolism are well-known. Anyway, all animals were fed the same diet. The results of this study confirmed the advantages and limitations of each employed technique, highlighting the importance of a consistent and combined approach to such a problematic tissue.

Conclusion

In conclusion this study allowed to develop a multidisciplinary approach to the study of the bone in pigs and sheep, evaluating several different parameters with different techniques on the same samples. This approach is crucial because it allows to elucidate all the fundamental features of such a complex tissue at once. In fact, omitting one or more of these aspects during preclinical trials could result in inaccurate study design or imprecise estimation and interpretation of the results, with serious consequences. Finally, reference parameters for normal swine and ovine bone features were provided.

References

1. An YH, Friedman RJ. Animal selections in orthopedic research. In: Animal models in orthopedic research (An YH; Friedman RJ, eds), CRC Press LLC, Boca Raton, 1999)
2. Bailey S, Vashishth D. Mechanical Characterization of Bone: State of the Art in Experimental Approaches-What Types of Experiments Do People Do and How Does One Interpret the Results? Curr Osteoporos Rep. 2018 Jun 18. doi: 10.1007/s11914-018-0454-8.
3. Bernau M[1], Kremer PV[2], Lauterbach E[3], Tholen E[4], Petersen B[4], Pappenberger E[3], Scholz AM[3]. Evaluation of carcass composition of intact boars using linear measurements from performance testing, dissection, dual energy X-ray absorptiometry (DXA) and magnetic resonance imaging (MRI). Meat Sci. 2015 Jun;104:58-66. doi: 10.1016/j.meatsci.2015.01.011. Epub 2015 Feb 7.
4. Bonney H, Colston BJ, Goodman AM. Regional variation in the mechanical properties of cortical bonefrom the porcine femur. Med Eng Phys. 2011 May;33(4):513-20. doi: 10.1016/j.medengphy.2010.12.002. Epub 2011 Jan 6.
5. Britz HM[1], Jokihaara J, Leppänen OV, Järvinen T, Cooper DM. 3D visualization and quantification of rat cortical bone porosity using a desktop micro-CT system: a case study in the tibia. J Microsc. 2010 Oct;240(1):32-7. doi: 10.1111/j.1365-2818.2010.03381.x.
6. Buser D[1], Schenk RK, Steinemann S, Fiorellini JP, Fox CH, Stich H. Influence of surface characteristics on bone integration of titanium implants. A histomorphometric study in miniature pigs. J Biomed Mater Res. 1991 Jul;25(7):889-902.
7. Caccia G, Magli F, Tagi VM, Porta DGA, Cummaudo M, Marquez-Grant N, Cattaneo C. Histological determination of the human origin from dry bone: a cautionary note for subadults. Int J Legal Med (2016) 130:299–307 DOI 10.1007/s00414-015-1271-6
8. Campana V, Milano G, Pagano E, Barba M, Cicione C, Salonna G, Lattanzi W, Logroscino G. Bone substitutes in orthopaedic surgery: from basic science to clinical practice. J Mater Sci Mater Med. 2014 Oct;25(10):2445-61. doi: 10.1007/s10856-014-5240-2. Epub 2014 May 28.
9. Carter DR, Hayes WC. Bone compressive strength: the influence of density and strain rate. Science. 1976 Dec 10;194(4270):1174-6.
10. Chappard D, Retailleau-Gaborit N, Legrand E, Baslé MF, Audran M. Comparison insight bone measurements by histomorphometry and microCT. J Bone Miner Res. 2005 Jul;20(7):1177-84. Epub 2005 Feb 14.
11. Cone S.G., Warren P.B., Fisher M.B. Rise of the Pigs: Utilization of the Porcine Model to Study Musculoskeletal Biomechanics and Tissue Engineering During Skeletal Grow. Tissue Engineering: Part C, (2017); 23.
12. Currey J, 1984. The mechanical adaptations of bones. Princeton, NJ: Princeton University Press.
13. Decker S[1], Reifenrath J[2], Omar M[1], Krettek C[1], Müller CW[1]. Non-osteotomy and osteotomy large animal fracture models in orthopedic trauma research. Orthop Rev (Pavia). 2014 Dec 17;6(4):5575. doi: 10.4081/or.2014.5575. eCollection 2014 Oct 27.
14. den Boer FC, Patka P, Bakker FC, Wippermann BW, van Lingen A, Vink GQ, Boshuizen K, Haarman HJ. New segmental long bone defect model in sheep: quantitative analysis of healing with dual energy x-ray absorptiometry. J Orthop Res. 1999 Sep;17(5):654-60.
15. Dias IR, Camassa JA, Bordelo JA, Babo PS, Viegas CA, Dourado N, Reis RL, Gomes ME. Preclinical and Translational Studies in Small Ruminants (Sheepand Goat) as Models for Osteoporosis Research. Curr Osteoporos Rep. 2018 Apr;16(2):182-197. doi: 10.1007/s11914-018-0431-2. Review.
16. Ding M[1], Danielsen CC, Overgaard S. The effects of glucocorticoid on microarchitecture, collagen, mineral and mechanical propertiesof sheep femur cortical bone. J Tissue Eng Regen Med. 2012 Jun;6(6):443-50. doi: 10.1002/term.448. Epub 2011 Jul 13.
17. Donnelly E. Methods for assessing bone quality: a review. Clin Orthop Relat Res. 2011 Aug;469(8):2128-38. doi: 10.1007/s11999-010-1702-0.
18. Duffy SK, Kelly AK, Rajauria G, Clarke LC, Gath V, Monahan FJ, O'Doherty JV. The effect of 25-hydroxyvitamin D_3 and phytase inclusion on pig performance, bone parameters and pork quality in finisher pigs. J Anim Physiol Anim Nutr (Berl). 2018 Oct;102(5):1296-1305. doi: 10.1111/jpn.12939. Epub 2018 Jul 5.

19. Endo K[1], Yamada S[2], Todoh M[2], Takahata M[1], Iwasaki N[1], Tadano S[2]. Structural strength of cancellous specimens from bovine femur under cyclic compression. PeerJ. 2016 Jan 25;4:e1562. doi: 10.7717/peerj.1562. eCollection 2016.

20. Fazzalari NL, Forwood MR, Smith K, Manthey BA, Herreen P. Assessment of cancellous bone quality in severe osteoarthrosis: bone mineral density, mechanics, and microdamage. Bone. 1998 Apr;22(4):381-8.

21. Floerkemeier T, Wellmann M, Thorey F, Hurschler C, Witte F, Windhagen H. Comparison of bone mineral parameter measurements by dual-energy x-ray absorptiometry with bone stiffness measurements as indicators of the load-bearing capacity of regenerating bone. J Orthop Trauma. 2010 Mar;24(3):181-7. doi: 10.1097/BOT.0b013e3181bae887.

22. Gibson LJ. The mechanical behaviour of cancellous bone. J Biomech. 1985;18(5):317-28.

23. Gramanzini M, Gargiulo S, Zarone F, Megna R, Apicella A, Aversa R, Salvatore M, Mancini M, Sorrentino R, Brunetti A. Combined microcomputed tomography, biomechanical and histomorphometric analysis of the peri-implant bone: a pilot study in minipig model. Dental materials June 2016 Vol 32, Issue 6, Pag 794-806 doi: https://doi.org/10.1016/j.dental.2016.03.025

24. Heiss C, Kern S, Malhan D, Böcker W, Engelhardt M, Daghma DES, Stoetzel S, Schmitt J, Ivo M, Kauschke V, Lips KS, Tushtev K, Rezwan K, El Khassawna T. A New Clinically Relevant T-Score Standard to Interpret Bone Status in a Sheep Model. Med Sci Monit Basic Res. 2017 Oct 2;23:326-335.

25. Hernandez CJ, Keaveny TM. A biomechanical perspective on bone quality. Bone. 2006 Dec;39(6):1173-81. Epub 2006 Jul 28.

26. Hildebrand T, Laib A, Müller R, Dequeker J, Rüegsegger P. Direct three-dimensional morphometric analysis of human cancellous bone: microstructural data from spine, femur, iliac crest, and calcaneus. J Bone Miner Res. 1999 Jul;14(7):1167-74.

27. Hillier ML[1], Bell LS. Differentiating human bone from animal bone: a review of histological methods. J Forensic Sci. 2007 Mar;52(2):249-63.

28. Humphrey JH[1], Hutchinson DL. Macroscopic characteristics of hacking trauma. Forensic Sci. 2001 Mar;46(2):228-33.

29. Hutmacher DW. Scaffolds in tissue engineering bone and cartilage. Biomaterials. 2000 Dec;21(24):2529-43.

30. Jensen KS, Mosekilde L, Mosekilde L. A model of vertebral trabecular bone architecture and its mechanical properties. Bone. 1990;11(6):417-23.

31. Kleerekoper M, Villanueva AR, Stanciu J, Rao DS, Parfitt AM. The role of three-dimensional trabecular microstructure in the pathogenesis of vertebral compression fractures. Calcif Tissue Int. 1985 Dec;37(6):594-7.

32. Kolp E, Wilkens MR, Pendl W, Eichenberger B, Liesegang A. Vitamin D metabolism in growing pigs: influence of UVB irradiation and dietary vitamin D supply on calcium homeostasis, its regulation and bone metabolism. J Anim Physiol Anim Nutr (Berl). 2017 Jun;101 Suppl 1:79-94. doi: 10.1111/jpn.12707.

33. Kousa P, Järvinen TL, Vihavainen M, Kannus P, Järvinen M. The fixation strength of six hamstring tendon graft fixation devices in anterior cruciate ligament reconstruction. Part II: femoral site. Am J Sports Med. 2003 Mar-Apr;31(2):174-81.

34. Kousa P, Järvinen TL, Vihavainen M, Kannus P, Järvinen M. The fixation strength of six hamstring tendon graft fixation devices in anterior cruciate ligament reconstruction. Part II: tibial site. Am J Sports Med. 2003 Mar-Apr;31(2):182-8.

35. Martin RB, Lau ST, Mathews PV, Gibson VA, Stover SM. Collagen fiber organization is related to mechanical properties and remodeling in equine bone. A comparison of two methods. J Biomech. 1996 Dec;29(12):1515-21.

36. Martin RB. Skeletal biology. In: Martin RB, Burr DB, Sharkey NA, editors. Skeletal tissue mechanics. New York: Springer, 1998

37. Martiniaková M, Grosskopf B, Omelka R, Vondráková M, Bauerová M. Differences among species in compact bone tissue microstructure of mammalian skeleton: use of a discriminant function analysis for species identification. J Forensic Sci. 2006 Nov;51(6):1235-9

38. Martiniaková M, Grosskopf B, Vondráková M, Omelka R, Fabis M. Differences in femoral compact bone tissue microscopic structure between adult cows (Bos taurus) and pigs (Sus scrofa domestica). Anat Histol Embryol. 2006 Jun;35(3):167-70.

39. Martiniaková M, Grosskopf B, Vondráková M, Omelka R, Fabis M. Differences in femoral compact bone tissue microscopic structure between adult cows (Bos taurus) and pigs (Sus scrofa domestica). Anat Histol Embryol. 2006 Jun;35(3):167-70.

40. Mason MW, Skedros JG, Bloebaum RD. Evidence of strain-mode-related cortical adaptation in the diaphysis of the horse radius. Bone. 1995 Sep;17(3):229-37.

41. Massengill JB, Alexander H, Langrana N, Mylod A. A phalangeal fracture model--quantitative analysis of rigidity and failure. J Hand Surg Am. 1982 May;7(3):264-70.

42. McCoy AM. Animal Models of Osteoarthritis: Comparisons and Key Considerations.Vet Pathol. 2015 Sep;52(5):803-18. doi: 10.1177/0300985815588611. Epub 2015 Jun 10. Review.

43. Mitchell AD, Scholz AM, Pursel VG. Total body and regional measurements of bone mineral content and bone mineral density in pigs by dual energy X-ray absorptiometry. J Anim Sci. 2001 Oct;79(10):2594-604.

44. Müller R, Van Campenhout H, Van Damme B, Van Der Perre G, Dequeker J, Hildebrand T, Rüegsegger P. Morphometric analysis of human bone biopsies: a quantitative structural comparison of histological sections and micro-computed tomography. Bone. 1998 Jul;23(1):59-66.

45. Nielsen DH[1], McEvoy FJ, Poulsen HL, Madsen MT, Buelund LE, Svalastoga E. Dual-energy X-ray absorptiometry of the pig: Protocol development and evaluation. Meat Sci. 2004 Oct;68(2):235-41. doi: 10.1016/j.meatsci.2004.03.002.

46. Osterhoff G, Morgan EF, Shefelbine SJ, Karim L, McNamara LM, Augat P. Bone mechanical properties and changes with osteoporosis. Injury. 2016 Jun;47 Suppl 2:S11-20. doi: 10.1016/S0020-1383(16)47003-8.

47. Parfitt AM. Compact bone and fracture risk. Calcif Tissue Int. 1992 Jan;50(1):97-8.

48. Parfitt AM. Recent developments in bone physiology. Henry Ford Hosp Med J. 1983;31(4):209-10. No abstract available.

49. Park JB, Biomaterials Science and Engineering, Plenum Press, New York, 1987.

50. Pearce AI, Richards RG, Milz S, Schneider E, Pearce SG. Animal models for implant biomaterial research in bone: a review. Eur Cell Mater. 2007 Mar 2;13:1-10.

51. Pouilles JM[1], Collard P, Tremollieres F, Frayssinet P, Railhac JJ, Cahuzac JP, Autefage A, Ribot C. Accuracy and precision of *in vivo* bone mineral measurements in sheep using dual-energy X-ray absorptiometry. Calcif Tissue Int. 2000 Jan;66(1):70-3.

52. Pugh JW, Rose RM, Radin EL. A structural model for the mechanical behavior of trabecular bone. J Biomech. 1973 Nov;6(6):657-70.

53. Sawada J, Nara T, Fukui J, Dodo Y, Hirata K. Histomorphological species identification of tiny bone fragments from a Paleolithic site in the Northern Japanese Archipelago, Journal of Archaeological Science, Volume 46, 2014, Pages 270-280

54. Schlickewei, Wolfgang & Schlickewei, Carsten. The Use of Bone Substitutes in the Treatment of Bone Defects – the Clinical View and History. Macromolecular Symposia (2007). 253. 10 - 23. 10.1002/masy.200750702.

55. Seil R, Rupp S, Krauss PW, Benz A, Kohn DM. Comparison of initial fixation strength between biodegradable and metallic interference screws and a press-fit fixation technique in a porcine model. Am J Sports Med. 1998 Nov-Dec;26(6):815-9.

56. Skiba G, Sobol M, Raj S. Femur morphometry, densitometry, geometry and mechanical properties in young pigs fed a diet free of inorganic phosphorus and supplemented with phytase. Arch Anim Nutr. 2017 Feb;71(1):81-92. Epub 2016 Nov 14.

57. Soladoye OP, López Campos Ó, Aalhus JL, Gariépy C, Shand P, Juárez M.Accuracy of dual energy X-ray absorptiometry (DXA) in assessing carcass composition from different pig populations. Meat Sci. 2016 Nov;121:310-316. doi: 10.1016/j.meatsci.2016.06.031. Epub 2016 Jul 1.

58. Southern EP, Oxland TR, Panjabi MM, Duranceau JS. Cervical spine injury patterns in three modes of high-speed trauma: a biomechanical porcine model. J Spinal Disord. 1990 Dec;3(4):316-28.

59. Stone JL, Beaupre GS, Hayes WC. Multiaxial strength characteristics of trabecular bone. J Biomech. 1983;16(9):743-52.

60. Sun C, Huang G, Christensen FB, Dalstra M, Overgaard S, Bünger C. Mechanical and histological analysis of bone-pedicle screw interface *in vivo*: titanium versus stainless steel. Chin Med J (Engl). 1999 May;112(5):456-60.

61. Teo JC, Si-Hoe KM, Keh JE, Teoh SH. Relationship between CT intensity, micro-architecture and mechanical properties of porcine vertebral cancellous bone. Clin Biomech (Bristol, Avon). 2006 Mar;21(3):235-44. Epub 2005 Dec 13.

62. Turner AS, Mallinckrodt CH, Alvis MR, Bryant HU. Dual-energy X-ray absorptiometry in sheep: experiences with *in vivo* and ex vivo studies. Bone. 1995 Oct;17(4 Suppl):381S-387S.

63. Turner AS, Mallinckrodt CH, Alvis MR, Bryant HU. Dual-energy X-ray absorptiometry in sheep: experiences with *in vivo* and ex vivo studies. Bone. 1995 Oct;17(4 Suppl):381S-387S.

64. Velasquez P, Luklinska ZB, Meseguer-Olmo L, Mate-Sanchez de Val JE, Delgado-Ruiz RA, Calvo-Guirado JL, Ramirez-Fernandez MP, de Aza PN. αTCP ceramic doped with dicalcium silicate for bone regeneration applications prepared by powder metallurgy method: in vitro and *in vivo* studies. J Biomed Mater Res A. 2013 Jul;101(7):1943-54. doi: 10.1002/jbm.a.34495. Epub 2012 Dec 5.

65. Wang P, Liu P, Xu P, Fan X, Yuan X, Li H, Yan Y. Controlling the degra- dation of dicalcium phosphate/calcium sulfate/poly(amino acid) bio- composites for bone regeneration, Polym Compos. (2016), https://doi.org/ 10.1002/pc.24049.

66. Webster S. S. J. The skeletal tissue; in Cell and tissue biology. Leon Weiss Editor, 1988, sixth edition, Urban and Schwarzenberg, Germany

67. Wu S, Liu X, Yeung K, Liu C, Yang X. Biomimetic porous scaffolds for bone tissue engineering. Materials Science and Engineering, 2014: R: Reports. 80. 1–36. 10.1016/j.mser.2014.04.001.

68. Zedda M, Lepore G, Biggio GP, Gadau S, Mura E, Farina V. Morphology, Morphometry and Spatial Distribution of Secondary Osteons in Equine Femur. Anat Histol Embryol. 2015 Oct;44(5):328-32. doi: 10.1111/ahe.12141. Epub 2014 Aug 21.

69. Zhang Y[1], Li Y[1], Gao Q[2], Shao B[1], Xiao J[3], Zhou H[4], Niu Q[5], Shen M[5], Liu B[1], Hu K[1], Kong L[6]. The variation of cancellous bones at lumbar vertebra, femoral neck, mandibular angle and rib in ovar iectomized sheep. Arch Oral Biol. 2014 Jul;59(7):663-9. doi: 10.1016/j.archoralbio.2014.03.013. Epub 2014 Apr 2.

Tables

Bone	Region		mean±ES	min	max	LIC 95%	UIC 95%
Femur	Diaphysis	Medial	1,47±0,11	1,16	2,22	1,22	1,72
		Lateral	1,41±0,09	1,15	1,93	1,20	1,62
		Cranial	1,50±0,09	1,20	2,04	1,30	1,70
		Caudal	1,42±0,06	1,15	1,65	1,28	1,56
	Condyles	Medial	1,14±0,04	0,98	1,31	1,05	1,24
		Lateral	1,06±0,06	0,92	1,43	0,94	1,19
Tibia	Diaphysis	Medial	1,45±0,08	1,19	1,90	1,28	1,63
		Lateral	1,13±0,04	0,99	1,33	1,03	1,23
		Cranial	1,58±0,11	1,22	2,23	1,34	1,82
		Caudal	1,51±0,12	1,20	2,40	1,22	1,80
	Condyles	Medial	1,02±0,045	0,90	1,29	0,91	1,12
		Lateral	0,95±0,05	0,80	1,29	0,83	1,08

Table 1 – BMD values (g/cm^2) for swine femur and tibia (whole bone) at different locations.

Bone	Region		mean±ES	min	max	95%LIC	95%UIC
Femur	Diaphysis	Medial	1,51±0,06	1,19	1,75	1,38	1,63
		Lateral	1,37±0,04	1,08	1,46	1,28	1,45
		Cranial	1,38±0,04	1,19	1,49	1,29	1,47
		Caudal	1,19±0,05	1,03	1,46	1,06	1,32
	Condyles	Medial	1,48±0,04	1,17	1,64	1,38	1,58
		Lateral	1,29±0,05	1,03	1,49	1,17	1,41
Tibia	Diaphysis	Medial	1,55±0,05	1,34	1,77	1,44	1,66
		Lateral	1,37±0,04	1,24	1,58	1,29	1,45
		Cranial	1,54±0,04	1,42	1,68	1,46	1,62
		Caudal	1,49±0,05	1,31	1,77	1,37	1,60
	Condyles	Medial	1,27±0,065	0,93	1,59	1,12	1,42
		Lateral	1,11±0,05	0,89	1,37	1,00	1,22

Table 2 – BMD values (g/cm^2) for ovine femur and tibia (whole bone) at different locations.

Bone	Region		mean±ES	min	max	95%LIC	95%UIC
Femur	Diaphysis	Medial	1,23±0,05	0,96	1,43	1,12	1,34
		Lateral	1,15±0,05	0,93	1,36	1,04	1,26
		Cranial	1,18±0,05	0,98	1,43	1,07	1,29
		Caudal	1,24±0,05	1,01	1,41	1,13	1,35
Tibia	Diaphysis	Medial	1,21±0,04	1,01	1,35	1,13	1,30
		Lateral	1,32±0,03	1,20	1,53	1,24	1,40
		Cranial	1,33±0,05	1,05	1,57	1,22	1,44
		Caudal	1,25±0,05	0,97	1,49	1,13	1,38

Table 3 – BMD values (g/cm³) for swine femur and tibia (cortical bone, isolated specimens) at different locations, corrected for sample size (height).

	mean±ES	min	max	95%LIC	95%UIC
ETB	0,34±0,01	0,27	0,41	0,31	0,36
MTB	0,39±0,02	0,27	0,48	0,35	0,43

Table 4 – BMD values (g/cm³) for swine trabecular bone (isolated specimens), corrected for sample size (height). ETB= epiphyseal trabecular bone; MTB: metaphiseal trabecular bone.

Bone	Region		mean±ES	min	max	95%LIC	95%UIC
Femur	Diaphysis	Medial	1,63±0,02	1,51	1,70	1,57	1,68
		Lateral	1,57±0,07	1,33	1,98	1,40	1,73
		Cranial	1,52±0,03	1,43	1,65	1,46	1,58
		Caudal	1,68±0,05	1,46	1,85	1,57	1,79
	Condyles	Medial	0,80±0,05	0,60	1,02	0,68	0,92
		Lateral	0,60±0,04	0,40	0,77	0,51	0,69
Tibia	Diaphysis	Medial	1,60±0,05	1,43	1,91	1,47	1,73
		Lateral	1,68±0,09	1,45	2,27	1,45	1,89
		Cranial	1,59±0,07	1,39	2,02	1,42	1,75
		Caudal	1,57±0,04	1,44	1,80	1,47	1,67
	Condyles	Medial	0,64±0,06	0,36	0,90	0,50	0,78
		Lateral	0,59±0,06	0,31	0,94	0,45	0,72

Table 5 –BMD values (g/cm³) for ovine femur and tibia (isolated specimens) at different locations, corrected for sample size (height).

Animal	Medial	Lateral	Cranial	Caudal
1	plexiform	plexiform	- plexiform (subperiosteum) - radial vascular canals and primary osteons (towards the endosteum)	- plexiform - area of isolated secondary osteons
2	plexiform	plexiform	plexiform	- plexiform - primary osteons (towards the endosteum)
3	plexiform	plexiform	plexiform	- plexiform (subperiosteum) - isolated secondary osteons (towards the endosteum)
4	plexiform	plexiform	- plexiform - primary osteons (towards the endosteum)	- fibrolamellar with primary osteons
5	- plexiform (subperiosteum) - reticular vascular canals (towards the endosteum)	primary osteons (towards the endosteum)	- plexiform (subperiosteum) - fibrolamellar with primary osteons (towards the endosteum)	- fibrolamellar with longitudinal and reticular vascular canals
6	plexiform	- plexiform – primary osteons (towards the endosteum)	plexiform	fibrous
7	- plexiform - primary (and secondary) osteons towards the endosteum	- plexiform - rare primary and secondary osteons towards the endosteum	plexiform	- primary and secondary osteons - resorption lacunae
8	plexiform	- plexiform - primary and secondary osteons (towards the endosteum) - resorption lacunae (towards the endosteum)	- plexiform - secondary osteons towards the endosteum)	plexiform
9	- plexiform - primary (and secondary) osteons (towards the endosteum)	- fibrous (towards the periosteum) - primary and secondary osteons (towards the endosteum)	- plexiform - primary osteons (towards the endosteum)	- plexiform - primary and secondary osteons (towards the endosteum)
10	- plexiform - fibrous with primary osteons (towards the endosteum)	fibrous with primary and secondary osteons	- plexiform - fibrous with primary osteons (towards the endosteum)	- plexiform - secondary osteons (towards the endosteum)

Tab. 6 – Histomorphological analysis of swine femoral diaphysis.

Animal	Medial	Lateral	Cranial	Caudal
1	- plexiform (subperiosteum) - rare secondary osteons (towards the endosteum)	- plexiform - area of isolated secondary osteons (towards the endosteum)	- plexiform (subperiosteum) - fibrolamellar with primary osteons (towards the endosteum)	- fibrolamellar with primary osteons (subperiosteum) - primary and secondary osteons (towards the endosteum)
2	- plexiform (subperiosteum) - primary osteons (towards the endosteum)	- plexiform (subperiosteum) - primary and isolated secondary osteons (towards the endosteum)	plexiform	- circumferential line of longitudinal vascular canals (subperiosteum) - plexiform with isolated osteons (towards the endosteum)
3	plexiform	- plexiform (subperiosteum) - primary osteons (towards the endosteum)	- plexiform (towards the periosteum and endosteum) - primary and isolated secondary osteons	plexiform
4	- plexiform (subperiosteum) - primary osteons (towards the endosteum)	- laminar (subperiosteum) - primary (and secondary) osteons (towards the endosteum)	plexiform	- osteon banding (subperiosteum) - plexiform with isolated secondary osteons (towards the endosteum)
5	- plexiform (subperiosteum) - fibrolamellar with longitudinal vascular canals (towards the endosteum)	fibrolamellar with primary osteons	plexiform	- plexiform (subperiosteum) - radial vascular canals (towards the endosteum)
6	- plexiform - primary and secondary osteons (towards the endosteum)	- plexiform - secondary osteons (towards the endosteum)	- plexiform - secondary osteons (towards the endosteum)	- plexiform - secondary osteons (towards the endosteum)
7	- fibrous with primary osteons (subperiosteum) - primary and secondary osteons (towards the endosteum)	- plexiform - primary and secondary osteons (towards the endosteum)	- plexiform - rare secondary osteons (towards the endosteum)	- plexiform - primary and secondary osteons (towards the endosteum)
8	- fibrous (periosteum) - secondary osteons	- plexiform (subperiosteum) - plexiform and secondary osteons (towards the endosteum)	- plexiform with osteon banding (subperiosteum) - secondary osteons	- laminar (subperiosteum) - laminar with secondary osteons
9	- plexiform - secondary osteons (towards the endosteum)	- plexiform (subperiosteum) - plexiform with secondary osteons (towards the endosteum)	- plexiform - secondary osteons (towards the endosteum)	- laminar (subperiosteum) - laminar with secondary osteons (towards the endosteum)
10	- fibrous with primary osteons (subperiosteum) - secondary osteons (towards the endosteum)	- plexiform - secondary osteons (towards the endosteum)	- plexiform - primary osteons (towards the endosteum)	- plexiform (subperiosteum) - plexiform with primary osteons (towards the endosteum)

Tab. 7 – Histomorphological analysis of swine tibial diaphysis.

Animal	Medial	Lateral	Cranial	Caudal
1	- laminar - area of dense secondary osteons (towards the endosteum)	- lamellar with longitudinal vascular canals (circumferential line - subperiosteum, subendosteum) - laminar (subperiosteum) - haversian with secondary dense osteons (towards the endosteum)	- fibrous (subperisoteum) - laminar	- lamellar in circumferential line (subperiosteum) - haversian with isolated secondary osteons
2	laminar	- laminar (subperiosteum) - primary and secondary osteons (towards the endosteum)	- fibrous with primary osteons (subperiosteum) - secondary osteons (towards the endosteum)	- laminar (subperiosteum) - fibrous with primary and secondary osteons (towards the endosteum)
3	- laminar (subperiosteum) - dense secondary osteons (towards the endosteum)	- laminar (subperiosteum) - isolated secondary osteons (towards the endosteum)	- laminar (subperiosteal) - laminar with primary and secondary osteons (towards the endosteum)	haversian with dense secondary osteons
4	- lamellar with longitudinal vascular canals (subperiosteum) - haversian with isolated secondary osteons (towards the endosteum)	- laminar (subperiosteum) - haversian with secondary osteons (towards the endosteum)	- laminar (subperiosteum) - secondary osteons (towards the endosteum)	- haversian with secondary osteons
5	- primary and rare, isolated secondary osteons	- fibrous with primary osteons (subperiosteum) - laminar - primary and secondary osteons (towards the endosteum)	- laminar - radial vascular canals (towards the endosteum)	haversian with isolated secondary osteons
6	fibrous with primary osteons	laminar	- lamellar (circumferential line – subperiosteum, subendosteum) - haversian with primary and secondary osteons	- lamellar (circumferential line – subperiosteum, subendosteum) - haversian with primary and secondary osteons - laminar (towards the endosteum)
7	- laminar (subperiosteum) - lamellar (circumferential line - subendosteum) - primary and secondary osteons	- laminar (subperiosteum) - haversian with secondary osteons - lamellar (circumferential line – subendosteum)	- fibrous with longitudinal vascular canals (subperiosteum) - lamellar (circumferential line – subendosteum) - laminar - rare isolated secondary osteons (towards the endosteum)	- fibrous (subperiosteum) - haversian with dense secondary osteons - lamellar (circumferential line – subendosteum)
8	- lamellar (circumferential line – subperiosteum) with longitudinal vascular canals - plexiform - haversian with dense secondary osteons (towards the endosteum)	- lamellar (circumferential line – subperiosteum) with longitudinal vascular canals - lamellar (circumferential line – subendosteum) with radial vascular canals - plexiform - haversian with dense secondary osteons (towards the endosteum)	- lamellar (circumferential line – subperiosteum) - laminar	- fibrous (subperiosteum) - haversian with dense secondary osteons - lamellar (circumferential line – subperiosteum) with longitudinal vascular canals
9	- lamellar with primary osteons and longitudinal vascular canals (subperiosteum) - laminar - haversian with isolated (towards the endosteum)	- lamellar (circumferential line – subperiosteum, subendosteum) - haversian with dense secondary osteons	- lamellar (circumferential line – subperiosteum, subendosteum) - haversian with dense secondary osteons	- lamellar (circumferential line – subperiosteum, subendosteum) with longitudinal vascular canals and primary osteons - haversian with dense secondary osteons (towards the endosteum)

Tab. 8 – Histomorphological analysis of ovine femoral diaphysis.

Animal	Medial	Lateral	Cranial	Caudal
1	- plexiform - area of isolated secondary osteons (towards the endosteum)	plexiform	plexiform	plexiform
2	- laminar - rare secondary osteons (towards the endosteum)	- laminar - rare secondary osteons (towards the endosteum)	- fibrous (subperiosteum) - lamellar (subendosteum) - haversian with dense secondary osteons	- lamellar (circumferential line – subperiosteum, subendosteum) - haversian with dense secondary osteons
3	- plexiform - lined secondary osteons (towards the periosteum)	plexiform	- haversian with dense secondary osteons - plexiform (towards the endosteum)	- lamellar (circumferential line subendosteum) - plexiform - rare secondary osteons (towards the endosteum)
4	- haversian with dense osteons (towards the periosteum) and isolated osteons (towards the endosteum) - reticular vascular canals	- haversian with isolated osteons - lamellar (towards the periosteum)	- laminar (towards the periosteum) - plexiform - secondary osteons (towards the endosteum)	- laminar (towards the periosteum) - plexiform
5	- plexiform - lamellar (circumferential line – subperiosteum, subendosteum)	- plexiform - lamellar (circumferential line – subperiosteum, subendosteum)	- lamellar (circumferential line – subperiosteum, subendosteum) - haversian with dense secondary osteons	- plexiform - lamellar (circumferential line – subperiosteum, subendosteum)
6	plexiform	- laminar (towards the endosteum) - plexiform - isolated secondary osteons (towards the endosteum)	- lamellar (circumferential line – subendosteum) - haversian with dense secondary osteons (towards the periosteum) - plexiform	- lamellar (circumferential line – subendosteum) - fibrous (towards the periosteum) - plexiform
7	plexiform	plexiform	- haversian, with dense secondary osteons	- plexiform - laminar (towards the periosteum)
8	- laminar with reticular vascular canals (towards the periosteum) - plexiform (towards the endosteum)	- laminar with osteon banding (towards the periosteum) - plexiform (towards the endosteum)	- haversian with dense secondary osteons (towards the endosteum) - plexiform (towards the endosteum)	- fibrous (subperiosteum) - lamellar (circumferential line – subendosteum) - plexiform - secondary osteons (towards the endosteum)
9	plexiform	plexiform	- fibrous (subperiosteum) - haversian with dense secondary osteons - lamellar (towards the endosteum)	- plexiform - isolated secondary osteons (towards the endosteum)

Tab. 9 – Histomorphological analysis of ovine tibial diaphysis.

Bone	Thickness	Region	mean±ES	min	max
Femur	Minimum	Medial	3,1±0,3	2,5	4,0
		Lateral	3,8±0,6	2,0	5,3
		Cranial	3,4±0,5	1,8	4,6
		Caudal	3,6±0,6	2,5	5,4
	Maximum	Medial	3,7±0,2	3,3	4,3
		Lateral	5,4±0,5	4,1	6,6
		Cranial	4,1±0,6	2,8	5,6
		Caudal	4,2±0,5	3,2	6,0
Tibia	Minimum	Medial	4,2±0,4	3,2	5,6
		Lateral	4,3±0,4	3,4	5,5
		Cranial	3,1±0,2	32,6	3,7
		Caudal	3,2±0,09	3,0	3,5
	Maximum	Medial	5,0±0,3	4,4	6,3
		Lateral	4,8±0,4	3,6	6,0
		Cranial	3,5±0,2	2,8	4,1
		Caudal	3,4±0,8	3,3	3,7

Tab. 10 – Cortical thickness of swine femur and tibia. Values are expressed in mm.

Bone	Thickness	Region	mean±ES	min	max
Femur	Minimum	Medial	2,7±0,1	2,2	3,3
		Lateral	2,8±0,2	1,8	3,4
		Cranial	2,9±0,2	2,0	3,7
		Caudal	2,8±0,2	1,9	3,7
	Maximum	Medial	2,9±0,1	2,3	3,7
		Lateral	2,9±0,2	2,1	3,6
		Cranial	3,5±0,4	2,3	6,3
		Caudal	3,2±0,1	2,7	3,9
Tibia	Minimum	Medial	4,0±0,3	2,5	5,4
		Lateral	3,6±0,2	2,6	4,7
		Cranial	4,2±0,3	3,2	5,9
		Caudal	3,6±0,2	2,6	4,4
	Maximum	Medial	4,5±0,3	3,1	5,6
		Lateral	4,1±0,2	2,9	5,0
		Cranial	4,7±0,3	3,7	6,3

| | | | Caudal | 3,3±0,2 | 3,0 | 5,2 |

Tab. 11 – Cortical thickness of ovine femur and tibia. Values are expressed in mm.

Bone	Parameter		Region	mean±ES	min	max
Femur	Osteon	Min. diameter	Medial			
			Lateral	186±10	118	270
			Cranial	147±23	111	189
			Caudal	184±10	126	260
		Max. diameter	Medial			
			Lateral	231±10	158	344
			Cranial	180±19	143	204
			Caudal	224±11	174	290
		Perimeter	Medial			
			Lateral	677±27	449	902
			Cranial	532±66	413	641
			Caudal	659±32	489	847
		Area	Medial			
			Lateral	35654±2922	15145	45928
			Cranial	22238±5440	12960	31800
			Caudal	33546±3276	17523	54846
	Havers. canal	Min. diameter	Medial			
			Lateral	32±2	24	49
			Cranial	26±3	20	29
			Caudal	31±2	21	42
		Max. diameter	Medial			
			Lateral	41±3	29	72
			Cranial	42±4	35	49
			Caudal	42±2	25	57
		Perimeter	Medial			
			Lateral	118±6	92	195
			Cranial	122±11	102	139
			Caudal	121±7	80	158
		Area	Medial			
			Lateral	1071±122	639	2777
			Cranial	1038±179	709	1323

			Caudal	1119±126	470	1754
Tibia	Osteon	Min. diameter	Medial	163±5	131	213
			Lateral	170±5	138	201
			Cranial	163±6	122	193
			Caudal	150±7	109	215
		Max. diameter	Medial	204±8	164	315
			Lateral	208±8	161	278
			Cranial	205±11	144	271
			Caudal	189±7	151	264
		Perimeter	Medial	591±19	493	801
			Lateral	612±17	496	767
			Cranial	590±29	417	733
			Caudal	546±20	440	774
		Area	Medial	26910±1754	18964	44776
			Lateral	28650±1580	18936	44084
			Cranial	26826±2327	13421	38613
			Caudal	22885±1851	14736	45650
	Havers. canal	Min. diameter	Medial	32±1	22	46
			Lateral	31±2	20	50
			Cranial	28±2	19	45
			Caudal	26±2	17	43
		Max. diameter	Medial	39±2	26	56
			Lateral	38±3	22	67
			Cranial	34±3	20	57
			Caudal	28±2	23	54
		Perimeter	Medial	115±5	86	159
			Lateral	113±7	73	187
			Cranial	97±8	61	157
			Caudal	95±6	68	155
		Area	Medial	1020±92	555	1905
			Lateral	1007±130	403	2559
			Cranial	766±133	278	1854
			Caudal	713±95	337	1812

Tab. 12 – Histomorphometric analysis of swine femoral and tibial diaphysis. Values are expresses in μm (diameters, perimeters) or μm²(area).

Bone	Parameter		Region	mean±ES	min	max
Femur	Osteon	Min. diameter	Medial	168±8	122	225
			Lateral	176±6	127	220
			Cranial	169±5	125	217
			Caudal	157±5	115	236
		Max. diameter	Medial	205±10	143	301
			Lateral	213±6	163	254
			Cranial	214±5	174	252
			Caudal	197±6	132	271
		Perimeter	Medial	582±25	428	797
			Lateral	612±18	466	727
			Cranial	605±15	489	722
			Caudal	560±16	415	795
		Area	Medial	26346±2266	14239	47681
			Lateral	29076±1632	16315	40710
			Cranial	28066±1362	17647	39462
			Caudal	24284±1399	13345	49122
	Havers. canal	Min. diameter	Medial	20±1	13	27
			Lateral	23±2	14	43
			Cranial	23±1	11	29
			Caudal	20±1	12	28
		Max. diameter	Medial	25±1	13	35
			Lateral	28±2	16	47
			Cranial	28±1	17	38
			Caudal	26±1	19	40
		Perimeter	Medial	73±4	42	98
			Lateral	80±6	49	141
			Cranial	79±3	46	102
			Caudal	73±3	51	108
		Area	Medial	412±40	133	712
			Lateral	532±85	164	1541
			Cranial	472±34	153	768
			Caudal	404±38	182	865
Tibia	Osteon	Min. diameter	Medial	163±7	133	190
			Lateral	162±10	133	179
			Cranial	162±4	108	229

			Caudal	157±4	127	209
		Max. diameter	Medial	208±12	156	274
			Lateral	207±14	167	225
			Cranial	196±6	125	311
			Caudal	192±6	157	276
		Perimeter	Medial	587±28	463	709
			Lateral	592±41	471	639
			Cranial	570±15	383	845
			Caudal	556±15	445	742
		Area	Medial	26465±2405	16587	37604
			Lateral	26413±3290	16546	29976
			Cranial	28785±3525	11246	199907
			Caudal	23806±1294	15092	6726
	Havers. canal	Min. diameter	Medial	30±2	20	45
			Lateral	26±3	18	30
			Cranial	22±1	14	41
			Caudal	24±1	18	34
		Max. diameter	Medial	39±3	25	56
			Lateral	35±5	22	44
			Cranial	27±1	17	51
			Caudal	28±1	19	45
		Perimeter	Medial	107±8	71	159
			Lateral	96±12	63	118
			Cranial	78±3	47	131
			Caudal	81±3	56	112
		Area	Medial	883±141	378	1904
			Lateral	696±156	288	1018
			Cranial	485±39	160	1277
			Caudal	505±35	229	881

Tab. 13 – Histomorphometric analysis of ovine femoral and tibial diaphysis. Values are expresses in µm (diameters, perimeters) or µm²(area).

		mean±ES	min	max	95%LIC	95%UIC
Tb.N	ETB	1,92±0,05	1,61	2,76	1,81	2,02
	MTB	2,90±0,11	1,89	3,87	1,81	2,02
Tb.Th	ETB	0,11±0,003	0,09	0,17	0,11	0,12
	MTB	0,11±0,002	0,09	0,13	0,10	0,11
Tb.Sp	ETB	0,50±0,01	0,34	0,60	0,47	0,52
	MTB	0,32±0,01	0,24	0,48	0,29	0,35
SMI	ETB	0,47±0,10	-0,45	1,39	0,26	0,68
	MTB	1,37±0,09	0,41	1,96	0,26	0,68
DA	ETB	1,64±0,02	1,44	1,92	1,59	1,69
	MTB	1,87±0,03	1,59	2,06	1,80	1,94
Conn.	ETB	16,67±1,24	7,77	35,29	14,10	19,23
	MTB	35,50±2,8	13,34	59,37	29,63	41,37

Tab. 14 - Micro-CT parameters for swine trabecular (tibia and femur). ETB=epiphyseal trabecular bone; MTB: metaphyseal trabecular bone. BV/TV=relative bone volume density; Tb.N= trabecular number (1/mm); Tb.Th=mean trabecular thickness (mm); Tb.Sp=mean trabecular separation (mm); SMI= structural model index; Conn=connectivity (1/mm); DA=degree of anisotropy.

			mean±ES	min	max	95%LIC	95%UIC
BV/TV	femur	medial	0,42±0,02	0,32	0,50	0,38	0,47
		lateral	0,28±0,01	0,23	0,31	0,26	0,31
	tibia	medial	0,32±0,02	0,23	0,41	0,27	0,37
		lateral	0,29±0,02	0,22	0,42	0,24	0,34
Tb.N	femur	medial	2,00±0,04	1,79	2,17	1,91	2,10
		lateral	1,66±0,03	1,53	1,82	1,58	1,74
	tibia	medial	1,53±0,07	1,26	1,76	1,37	1,69
		lateral	1,52±0,04	1,38	1,74	1,43	1,61
Tb.Th	femur	medial	0,20±0,01	0,16	0,25	0,17	0,22
		lateral	0,16±0,01	0,13	0,18	0,14	0,17
	tibia	medial	0,19±0,01	0,15	0,23	0,16	0,22
		lateral	0,18±0,01	0,14	0,26	0,15	0,21
Tb.Sp	femur	medial	0,42±0,01	0,39	0,49	0,40	0,45
		lateral	0,54±0,01	0,49	0,61	0,51	0,57
	tibia	medial	0,61±0,02	0,52	0,70	0,55	0,67
		lateral	0,61±0,02	0,52	0,69	0,56	0,65
SMI	femur	medial	-1,50±0,18	-2,43	-0,43	-1,93	-1,06
		lateral	-0,27±0,06	-0,59	-0,12	-0,41	-0,13

			mean±ES	min	max	95%LIC	95%UIC
	tibia	medial	-0,47±0,16	-1,18	0,1	-0,86	-0,07
		lateral	-0,32±0,20	-1,72	0,35	-0,77	0,15
DA	femur	medial	1,76±0,02	1,68	1,86	1,72	1,81
		lateral	1,80±0,07	1,53	2,08	1,63	1,96
	tibia	medial	1,70±0,09	1,31	2,06	1,71	1,74
		lateral	1,78±0,10	1,48	2,52	1.54	2,00
Conn	femur	medial	5,72±0,42	3,86	7,50	4,77	6,68
		lateral	6,02±0,27	5,13	7,13	5,39	6,66
	tibia	medial	4,45±0,53	2,28	5,97	3,15	5,75
		lateral	4,60±0,45	2,30	6,77	3,58	5,63

Tab. 15 - Micro-CT parameters for ovine trabecular bone at different locations. BV/TV=relative bone volume density; Tb.N= trabecular number (1/mm); Tb.Th=mean trabecular thickness (mm); Tb.Sp=mean trabecular separation (mm); SMI= structural model index; Conn=connectivity (1/mm); DA=degree of anisotropy.

Bone	Region		mean±ES	min	max	95%LIC	95%UIC
Femur	Diaphysis	Medial	20,14±4,66	6,99	55,70	9,59	30,68
		Lateral	14,24±1,82	6,90	18,99	9,56	18,92
		Cranial	20,07±3,45	9,06	41,04	11,92	28,22
		Caudal	15,07±1,91	9,05	29,08	10,75	19,40
Tibia	Diaphysis	Medial	22,80±4,52	11,52	44,79	12,12	33,48
		Lateral	19,92±3,02	12,66	35,04	12,78	27,06
		Cranial	17,65±2,31	8,63	32,55	12,43	22,86
		Caudal	20,73±3,27	11,90	40,89	13,19	28,27

Table 16 – E values (GPa) for swine cortical bone from femur and tibia at different locations.

	mean±ES	min	max	95%LIC	95%UIC
ETB	1,11±0,17	0,45	2,62	0,75	1,46
MTB	1,34±0,23	0,73	3,34	0,82	1,86

Table 17 – E values (GPa) for swine trabecular bone. ETB=epiphyseal trabecular bone; MTB: metaphyseal trabecular bone.

Bone	Region		mean±ES	min	max	95%LIC	95%UIC
Femur	Diaphysis	Medial	88,93±12,06	48,17	179,53	61,66	116,20
		Lateral	75,39±13,03	42,93	118,13	41,88	108,90
		Cranial	96,89±13,68	68,46	187,75	64,55	129,24
		Caudal	84,93±10,47	45,34	148,46	61,25	108,62
Tibia	Diaphysis	Medial	144,40±29,89	58,39	322,00	73,71	215,10
		Lateral	77,59±8,03	50,26	126,02	58,60	96,58
		Cranial	100,60±14,68	42,80	218,66	67,40	133,80
		Caudal	96,40±11,95	48,82	156,18	68,85	123,95

Table 18 – US values (MPa) for swine cortical bone from femur and tibia at different locations.

	mean±ES	min	max	95%LIC	95%UIC
ETB	9,22±0,78	4,99	15,32	7,56	10,88
MTB	12,54±1,12	4,77	18,05	10,04	15,05

Table 19 – US values (MPa) for swine trabecular bone. ETB=epiphyseal trabecular bone; MTB: metaphyseal trabecular bone.

Bone	Region		mean±ES	min	max	95%LIC	95%UIC
Femur	Diaphysis	Medial	57,71±5,37	36,30	77,03	44,50	70,42
		Lateral	48,39±6,64	31,00	95,16	33,08	63,69
		Cranial	42,49±4,04	26,36	57,67	32,48	51,60
		Caudal	54,39±6,07	30,53	76,08	40,40	68,38
	Condyles	Medial	0,57±0,08	0,21	0,90	0,29	0,76
		Lateral	0,55±0,09	0,24	0,95	0,35	0,75
Tibia	Diaphysis	Medial	67,95±8,37	31,07	104,83	48,66	87,25
		Lateral	63,17±4,84	37,58	77,32	51,99	74,34
		Cranial	56,80±6,14	35,82	83,75	42,29	71,30
		Caudal	59,80±9,06	36,05	123,38	38,91	80,69
	Condyles	Medial	0,42±0,08	0,14	0,91	0,23	0,62
		Lateral	0,43±0,06	0,11	0,60	0,29	0,56

Table 20 – E values (GPa) for ovine cortical and trabecular bone from femur and tibia at different locations.

Bone	Region		mean±ES	min	max	95%LIC	95%UIC
Femur	Diaphysis	Medial	109,37±8,71	70,01	150,37	89,28	108,27
		Lateral	113,40±13,68	70,00	205,91	81,86	144,94
		Cranial	108,82±7,85	74,87	147,50	90,72	126,93
		Caudal	128,95±7,61	91,31	164,22	111,39	146,50
	Condyles	Medial	21,62±2,33	10,80	32,40	16,25	26,99
		Lateral	13,12±1,23	5,70	18,10	19,30	15,95
Tibia	Diaphysis	Medial	146,02±15,67	88,60	229,62	108,89	182,15
		Lateral	167,62±27,33	82,66	364,29	104,60	230,65
		Cranial	210,09±15,78	146,61	289,60	173,69	246,48
		Caudal	169,76±23,76	105,90	342,97	114,96	224,56
	Condyles	Medial	19,21±3,89	5,90	44,50	10,23	28,19
		Laateral	13,12±2,26	2,70	25,40	7,92	18,34

Table 21 – US values (MPa) for ovine cortical and trabecular bone from femur and tibia at different locations.

Cartilage canals in newborn dogs: histochemical and immunohistochemical findings

A. Di Giancamillo,[1] M.E. Andreis,[1]
P. Taini,[1] M.C. Veronesi,[2]
M. Di Giancamillo,[2] S.C. Modina[1]

[1]Department of Health, Animal Science and Food Safety, University of Milan
[2]Department of Veterinary Medicine, University of Milan, Italy

Abstract

Cartilage canals (CCs) are microscopic structures involved in secondary ossification centers (SOCs) development. The features of CCs were investigated in the humeral and femoral proximal epiphyses of small-sized newborn dogs (from premature to 28 days after birth) with histochemical and immunohistochemical approaches. Masson's Trichrome revealed a ring-shaped area around CCs, which changes in colour from green (immature collagen) to red (mature collagen) as ossification progresses; perichondrium staining always matched the ring color. Safranin-O was always negative. Immunohistochemical analysis revealed immunopositivity for both collagen type I and V around the CCs; collagen type II was negative. CCs count showed a tendency to be higher in the humerus than in the femur. This work enlightened for the first time changes in composition of CCs surrounding matrix during SOCs development in dogs, paving the way to further investigations.

Introduction

Mammalian long bones develop *via* endochondral ossification, by formation of primary ossification centers and secondary ossification centers (SOCs). A crucial event preceding the formation of SOCs is the initial generation of cartilage canals (CCs). Cartilage canals have been described in the long bones of birds and mammals, as well as in human tarsal bones.[1] Their growth and development have been detailed mostly in mice[2,3] and chickens.[4,5] Cartilage canals are tube-shaped formations containing a central arteriole which branches out into an anastomosing network of capillaries; a single venule follows the course of the arteriole back to the perichondral plexus[6] from which the CCs derives as an invagination.[2] They also house lymphatics,[6] unmyelinated nerve fibers[6-8] and mesenchymal stem cells, embedded within a loose extracellular matrix (ECM).[1] The primary function of CCs is to supply nutrition to the growing cartilage and eliminate waste products. A wide variety of CCs size and shape was described in the humeral head of the dog, reflecting the metabolic needs of specific areas. Cartilage canals varied from short unbranched channels to channels coursing from one side of the epiphysis to the other,[6] and they were tightly associated with SOCs.[9] Other functions of CCs are still under discussion: some authors suggest they may contribute to the formation and maintenance of SOCs[2,3,5,10] and they may serve the cartilage growth itself, turning perivascular cells into matrix-producing chondrocytes as cartilage physiologically regresses.[11] Evidence demonstrated that defects of cartilage canal blood supply lead to disturbance of endochondral ossification, in human being as well as in animal species, including dogs.[12] The way in which these diseases is initiated is still debated. The aim of this work was to continue and to expand the researches on CCs behavior in the dog. Previous researches, in fact, although very extensive, only concern the first week of age and medium and large breeds.[6,9] Humerus and femur proximal epiphyses were investigated with morphological, histochemical and immunohistochemical analyses in prematurely born and up-to-28-days-aged. Expected result could provide anatomical basis for a better understanding of the onset of such endochondral disturbances, in the light of dog health, translational and/or comparative research.

Materials and Methods

Animals

Sixteen spontaneously dead puppies aged up to 28 days and belonging to breeds categorized as small-sized according to the standard breed adult body weight <7 kg[13] were examined (Supplementary Table 1) and stored at -20°C.

Puppies were full term and died as a consequence of hypoxia during birth and/or bacterial diseases in the first days of life. Their body weight was normal in relation to the breed and the age at the time of death. Two puppies were premature (49 days of gestation). A spontaneously dead skeletally mature small-sized dog (15-year-old) was enrolled as positive control of ossification. The presence of skeletal abnormalities was excluded by macroscopic examination and confirmed by radiographic investigation: the expected appearance of the ossification centers was confirmed and no sign of degenerative joint disease in the shoulder and in the hip joint was detected in the mature dog.

All cadavers were obtained from breeder prior their informed consent signature; the research was approved by the Ethic Committee of the University of Milan (OPBA, 58/2016).

Histology and histochemistry

Cadavers were thawed at room temperature. The proximal epiphyses of the left humerus and femur (total number of specimens = 32) were separated from the remaining bone and fixed in buffered 10% formalin (Bio-Optica, Milan, Italy) for 24 h as a whole. Samples were decalcified with 45% formic acid (Sigma Chemical Co., St. Louis, MO, USA), for 2-3 days and then with 15% 0.5 M EDTA solution (pH 8.0 - Sigma) for 7-10 days[14] and embedded in paraffin. Serial sections (4 μm thickness) were mounted on glass slides. Sections corresponding to the sagittal median plane of each proximal epiphysis were stained with standard Hematoxylin-Eosin (HE), Masson's Trichrome (MT) and Safranin-O (SO) (Bio-Optica) in order to follow ossification progression. Quantitative analysis of CCs was performed on both HE and MT stained sections, with the Olympus DP-software program at 20x magnification: the area corresponding to the sagittal median plane of each proximal epiphysis was measured, and the number of CCs in each of them contained calculated for each dog (total CCs: humerus *vs* femur; green (immature collagen fibers) or red (mature collagen fibers) CCs: humerus *vs* femur).

Immunohistochemistry

Collagen type I and II were localized with immunohistochemical analyses according to Di Giancamillo *et al.*[15] A mouse anti-collagen type V (ab-112551, Abcam, Cambridge, UK) antibody was used too, utilizing the same procedure previously described. Briefly, all the primary antisera were diluted 1:200 with a 0.05 M pH 7.4 Tris–HCl saline buffer (TBS: 0.05 M, pH 7.4, 0.55 M NaCl). Antigene-antibody complexes were detected with a ready-to-use secondary antibody (Dako REALTM EnVisionTM/ Horseradish Peroxidase, Rabbit/Mouse) and with 3,3'-diaminobenzidine (DAB, Dako Cytomation) as substrate.[15] Sections from the humerus of the adult dog were used as positive control; negative controls were performed replacing primary and secondary antibodies. Photomicrographs were captured with an Olympus BX51 microscope (Olympus, Milan, Italy) equipped with a digital camera.

Statistical analysis

Statistical analysis was performed with SAS statistical software (version 9.3, Cary Inc., NC). Data from the CCs counts were analyzed using 2-way ANOVA with bone (humerus/femur) and color (green/red) as main factors, and co-variated for the area corresponding to the sagittal median plane of each humeral and femoral proximal epiphysis. Values from each dog were considered as the experimental unit of all response variables. The data are presented as least-square means (SEM). Differences between means were considered significant at $P<0.05$.

Results

Histology and histochemistry

Analyses showed the appearance and the gradual development of the SOCs of the humeral and femoral proximal epiphyses, according with the age. Therefore, animals were categorized on the basis of the total number of the examined proximal epiphyses of both humerus and femur, as follows: No Ossification Center (NO, 43.75% humerus *vs* 37.50% femur; animals age: preterm up to 7 days); Early Ossification Center (EO, 18.75% humerus and 50% femur; animals age: 7-15 days) and Ossification Center (OC 37.50% humerus *vs* 12.50% femur; animals age: 15-28 days).

Hematoxylin-Eosin

In both humerus and femur, CCs were scattered in the chondroepiphysis in NO group (Figure 1a), scattered both in the mineralized ECM (Figure 1b) and surrounding resting cartilage in EO group, both scattered and entering
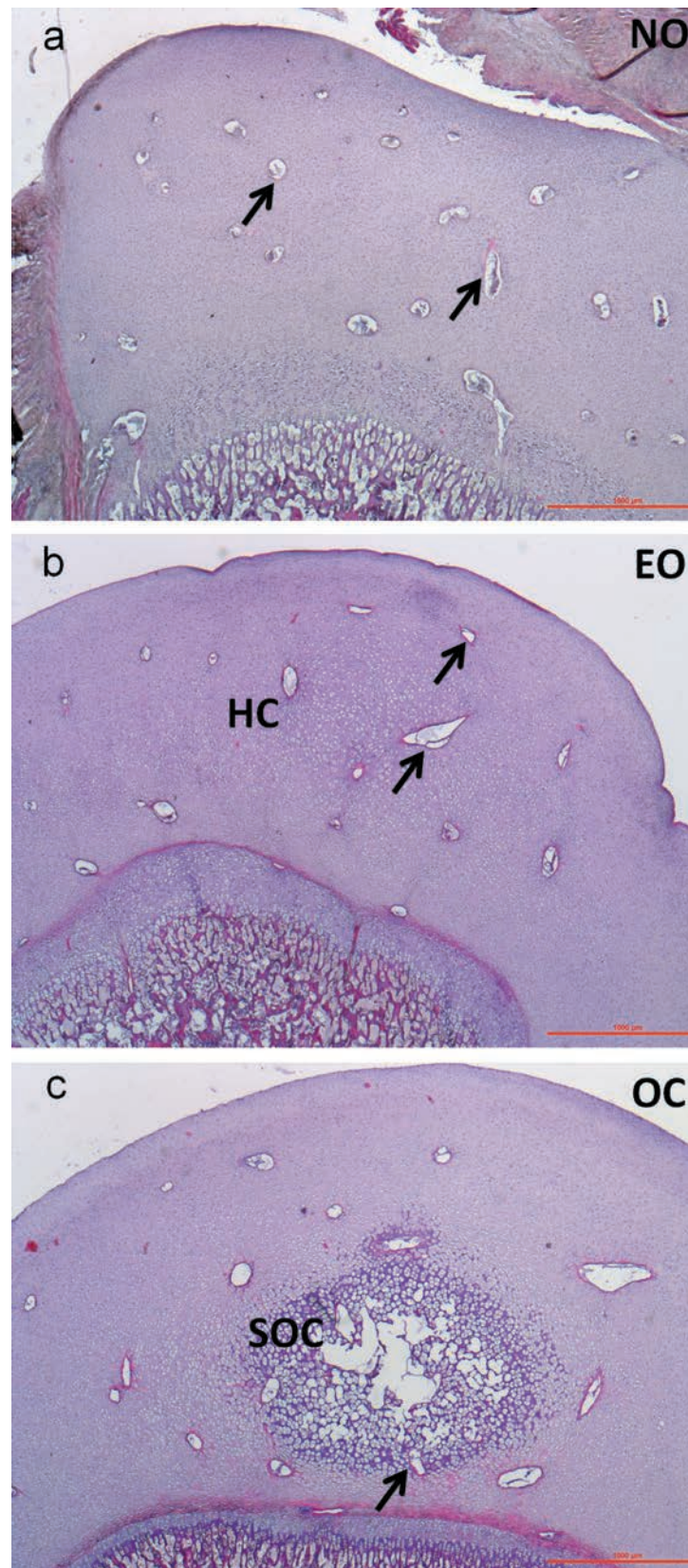
Figure 1. Representative image of the SOC formation in the left humerus of growing dogs - HE staining; a) at 0 days of age; b) at 7 days of age; c) at 21 days of age. NO, no ossification; EO, early ossification; OC, ossification center; arrow, cartilage canal; HC, hypertrophic chondrocytes; SOC, secondary ossification center. Scale bar: 1000 μm.

the SOC in the OC group (Figure 1c). Quantitative analysis revealed a tendency of the total CCs number in the humerus, which was higher than in femur (27.32±2.52 *vs* 22.15±2.27; P=0.078). As expected, the adult dog showed no CCs.

Masson's Trichrome

In NO group all CCs were surrounded by a light green matrix, and the same reactivity was always observed in the perichondrium indicating that these areas were 'immature' concerning the collagen fibers detected. Cartilage canals were surrounded by a basal membrane and hosted capillaries embedded by an amorphous matrix in the lumen. No sign of chondrification has been observed (Figure 2 a,i). In the EO group, 50% of the CCs appeared surrounded by green matrix, while the other 50% by red matrix (Figure 2 b,c, respectively). In the perichondrium the histochemical reactivity revealed both a green and red color indicating a gradual passage from an 'immature' to a 'mature' collagen composition in both localizations. In the OC group the presence of a well-structured SOC was accompanied by areas of matrix reactivity in red color, also when the CCs were incorporated within the SOC (Figure 2d).

Perichondrium appeared in its definitive histochemical red reactivity (Figure 2j). In the skeletally mature dog, articular cartilage stained light green, subchondral bone stained red (Supplementary Figure 1a). The quantitative analysis conducted on the three new born studied ages revealed that total green CCs number was significantly higher in the humerus compared to the red CCs of the humerus and to the green/red CCs of the femur (P<0.05 all comparisons, Figure 2).

Safranin-O

Staining around CCs was evident, and it was
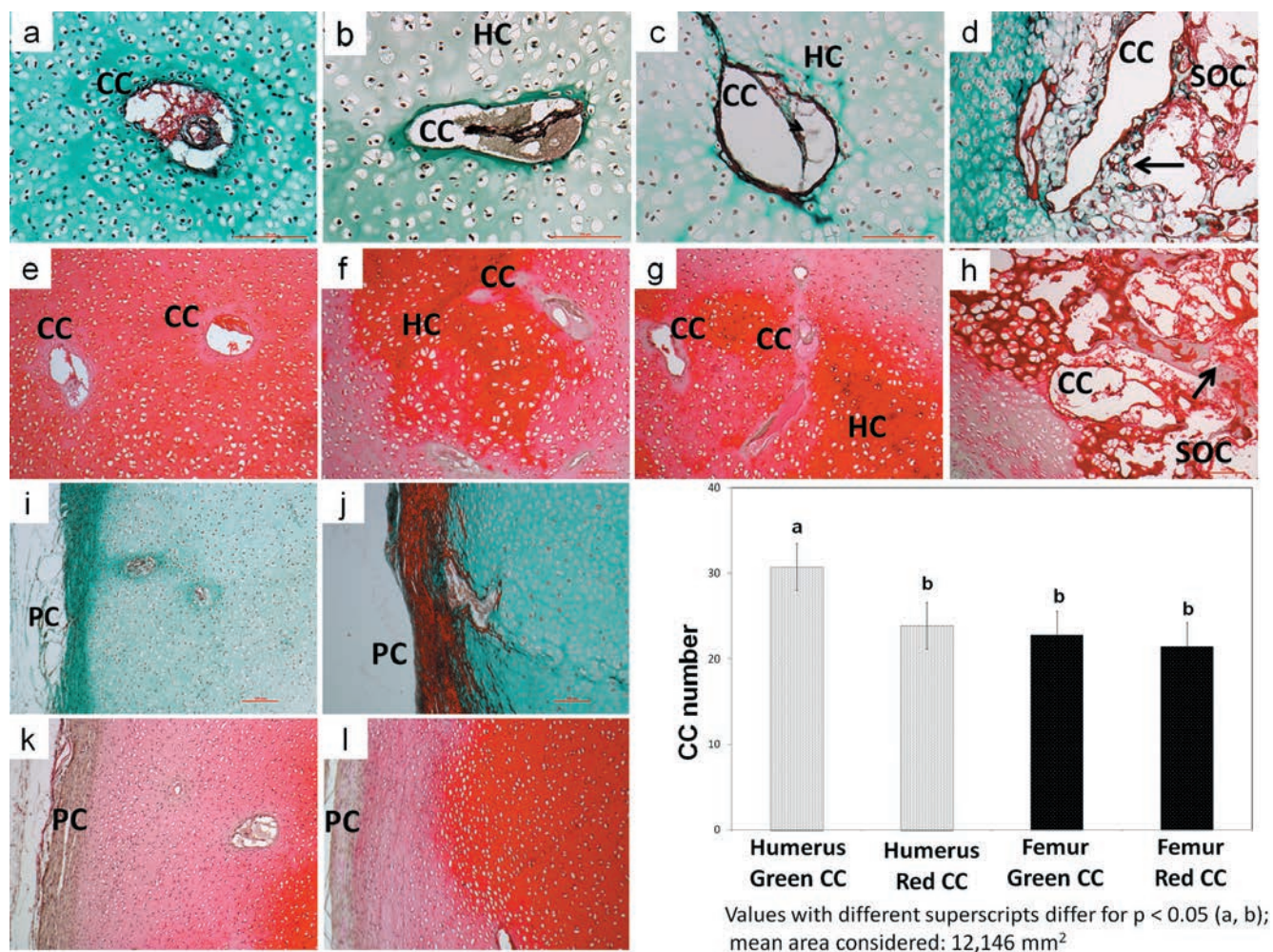
Figure 2. Images of CCs and perichondrium in NO, EO and OC groups - Masson's Trichrome and Safranin-O staining (left humerus). Masson's Trichrome staining: in NO group a homogeneously green ECM surrounds a CC (a); an amorphous matrix surrounds the capillaries hosted in its lumen (a); the perichondrium stains green (i); in EO group a subtle green ring of matrix surrounds 50% of the CC (b) and a red ring surrounds the other 50% (c); the number of CCs tends to decrease as the matrix ring changes in colour from green to red (b,c); perichondrium colour always reflects the ring color (i,j); in OC group a red ring matrix surrounds all CC (d); the content of SOC CCs is markedly decreased (d); the perichondrium stains red (j). Safranin-O staining: in all groups the staining of ECM around CCs is always paler than in the surrounded areas (e-h); the perichondrium is negative (k,l). Green ring CCs number was significantly higher in the humerus compared to the red rings CCs of the humerus and to the green/red rings CC of the femur (P<0.05 all comparisons). All described features are observed both in the humeral and femoral head. CC, cartilage canal; HC, hypertrophic chondrocytes; arrows, trabeculae; SOC, secondary ossification center; PC, perichondrium. Scale bar: 100 μm.

paler than the surrounding ECM in all groups, irrespective of the ossification stage (Figure 2 e-h); perichondrium was always negative (Figure 2 k,l). Very intense staining was evident in the deep layers of the articular cartilage, close to the tight mark line in the adult dog (Supplementary Figure 1b).

Immunohistochemistry

Collagen type I was localized in a thin ring surrounding the CCs in all groups (Figure 3 a-c); the perichondrium showed an immunopositive staining in all groups (Figure 3d).

Collagen type II showed a very pale signal in the ring around the CCs in all groups and a more intense reactivity in the ECM (Figure 3 e-g); the perichondrium revealed to be unreactive in all groups (Figure 3h).

Collagen type V was localized in a very subtle ring surrounding CCs, in all the structures inside them in all groups and in bone marrow (Figure 3 i-k); the perichondrium revealed a very slight immunopositivity in all groups (Figure 3l). A clear immunolocalisation of collagen type I in the subchondral bone, of colla-gen type II in the articular cartilage and collagen type V inside the bone marrow was observed in the adult dog (Supplementary Figure 2 a,c, respectively).

Discussion

To date, the timing of SOCs appearance in limb bones has only been described in medium and large breed dogs.[6,9,16] The present work indicates that this pattern is confirmed in small-sized dogs; it also suggests that SOC matures faster in the humerus than in the femur (OC humerus = 37.50% *vs* OC femur =12.50%). Since CCs proved to be involved in SOC development,[1] a more precise characterization of these structures was attempted. In rabbits,[17-19] mice,[3,17,20,21] rats[22] and pigs,[23] CCs appear long before the SOC formation; in medium and large breed dogs they have been identified at birth.[6,9] In this study their presence before birth was proved, as in humans[24] and rabbits.[18,25] Cartilage canals scattering in all humeral and femoral heads were observed, irrespective of the ossification stage. Age-matched CCs number analysis was not performed due to the small number of animals per group, however the CCs number tended to be higher in the humerus.

This value, identified at the level of the sagittal median plane of each proximal epiphysis, may be put in relation with a higher vascularization in the humerus than in the femur. Nonetheless, CCs number may also partially refer to the same canal, considering that canal itself becomes curved and branched thorough the humeral epiphyses as SOC develops, inducing the formation of several capillary glomeruli.[9] Authors opinion is that CCs numbers or CCs possible repeated counts, caused by branched canals, is always to be referred to a higher vascularization. So that the humerus receives a greater metabolic intake that in turn may explain the more rapid SOC maturation. This is also confirmed by another hypothesis: from birth to the age of about 4 weeks, the new-born puppy ability to stand and to walk increases, by the rudimentary crawling mainly
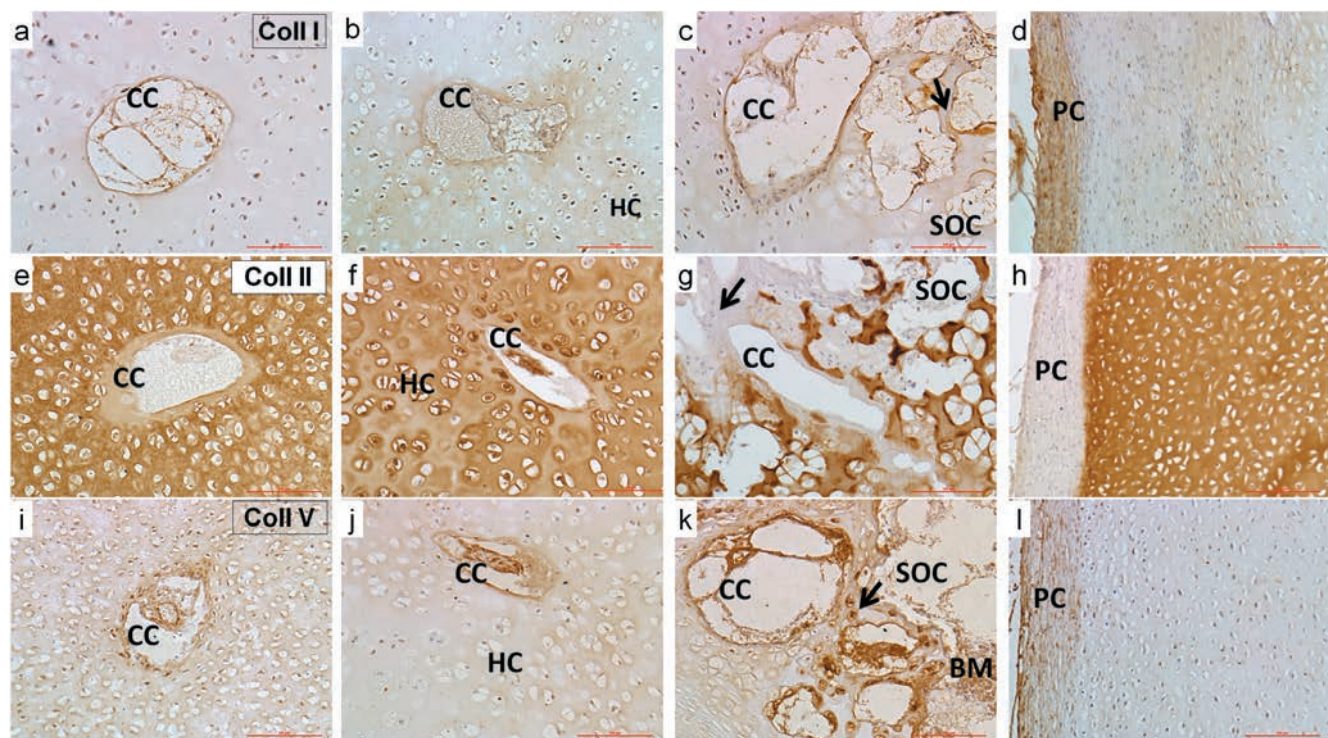

Figure 3. Images of CCs and perichondrium in NO (a,e,i), EO (b,f,j) and OC (c,g.k) groups - Collagen type I, II and V immunolocalization. A thin CC ring positive signal for collagen type I is evident in all groups (a-c) as well as in the perichondrium (d). The signal for collagen type II around the CC is very pale in all groups (e-g) and always negative in the perichondrium (h). The immunopositivity for collagen type V is evident in the inner side of the CC and in the structures inside them in all groups (i-k). The perichondrium is weakly immunopositive (l). A positive signal is also observed in the bone marrow, when present (k). A positive signal was observed in the trabeculae of OC group for all collagen types (c,g,k). All described features are observed both in the humeral and femoral head.CC, cartilage canal; arrows, trabeculae; HC, hypertrophic chondrocytes; SOC, secondary ossification center; PC, perichondrium; BM, bone marrow. Scale bar: 100 μm.

on its hind limbs to the well-coordinated walking on both hind and fore limb.[26] This implies that humeral epiphysis earlier undergoes to mechanical stimuli compared to the femur. This could stimulate CCs formation and expansion and the release of hypertrophic factors[27] and in turn a earliest SOC formation. Masson's Trichrome staining showed that the subtle area surrounding CCs changed in color from green to red as age increased, indicating that SOC formation is accompanied by a maturation of collagen fibers surrounding CCs. The same color change accordingly occurred in the perichondrium.

Moreover, the number of humerus green CCs was significantly higher than the number of red CCs, and also higher than the number of red CCs in both humerus and femur. In order to find a functional meaning for such changes in histochemical reactivity, the expression of collagen type I and II have been immunoistochemically investigated, together with presence of collagen type V. Collagen type V is a minor, but important component of connective tissues that are rich in collagen type I.[28] In mice, a strong expression of pro-a I (V) has been observed concomitantly with the appearance of the ossification centers, both in long bones and vertebrae.[29] Little is known about the role of collagen V in developing bones: it might play a role in the brittleness of the bone by interfering with the process of mineralization[30] and/or be involved in osteogenesis.[29,31,32] It has been hypothesized that fibrillar components of the collagen matrix contribute to the formation of a firm shell around the CCs, in order to protect the structures located in their lumen from the density of the cartilage matrix.[33] A positive label for collagen type I and V in CCs was found, while the ring around each CC was devoid of collagen type II. This was in agreement with the pale Safranin-O staining. These results suggest that CCs mesenchymal cells are involved in bone ECM production rather than cartilage ECM production, according to Blumer *et al.*[4] This happens in dogs even before the SOC formation, as previously demonstrated in pre-[5] and post hatching chickens.[3] The perichondrium collagen type I and V staining confirmed that mesenchymal cells could directly derive from the perichondrium.[2] Collagen V was also localized in the bone marrow:[28,32] it is therefore possible to speculate that bone marrow cells could be involved in type V collagen production as well as type I.[34] This is the first time that collagen type V is described near CCs. Further studies are needed to better characterize the histochemical changes. Unfortunately, our results did not prove any differences related to the color changes that we observed. Future studies will be performed in order to investigate collagen structural organization and detect other collagen types. These data, although preliminary, lay the basis for more extensive studies on the delicate mechanisms that modulate endochondral bone development also in the context of the growth disorders affecting the proximal femoral epiphysis of small-sized breeds dogs.[35] Moreover, it could be useful to study the role of CCs in the pathogenesis of the joint disorders affecting growing large sized dogs, such as the humeral osteochondritis[12] as well as the fracture of the medial coronoid process.[36,37]

This study finally suggests that cadaver may be considered a useful tool, not only in gross anatomy research,[38] but also a convincing alternative for histochemical and immunohistochemical investigation to the *in vivo* animal models.

References

1. Blumer MJ, Longato S, Fritsch H. Structure, formation and role of cartilage canals in the developing bone. Ann Anat 2008;190:305-15.
2. Blumer MJ, Longato S, Richter E, Perez MT, Konakci KZ, Fritsch H. The role of cartilage canals in endochondral and perichondral bone formation: are there similarities between these two processes? J Anat 2005;206:359-72.
3. Blumer MJ, Longato S, Schwarzer C, Fritsch H. Bone development in the femoral epiphysis of mice: the role of cartilage canals and the fate of resting chondrocytes. Dev Dyn 2007;236:2077-88.
4. Blumer MJ, Fritsch H, Pfaller K, Brenner E. Cartilage canals in the chicken embryo: ultrastructure and function. Anat Embryol (Berl) 2004;207(6):453-62.
5. Blumer MJ, Schwarzer C, Perez MT, Konakci KZ, Fritsch H. Identification and location of bone-forming cells within cartilage canals on their course into the secondary ossification centre. J Anat 2006;208: 695-707.
6. Wilsman NJ, Van Sickle DC. Cartilage canals, their morphology and distribution. Anat Rec 1972;173:79-93.
7. Stockwell RA. The ultrastructure of cartilage canals and the surrounding cartilage in the sheep fetus. J Anat 1971;109:397-410.
8. Hedberg A, Messner K, Persliden J, Hildebrand C. Transient local presence of nerve fibers at onset of secondary ossification in the rat knee joint. Anat Embryol (Berl) 1995;192:247-55.
9. Wilsman NJ, Van Sickle DC. The relationship of cartilage canals to the initial osteogenesis of secondary centers of ossification. Anat Rec 1970;168:381-91.
10. Alvarez J, Costales L, Lopez-Muniz A, Lopez JM. Chondrocytes are released as viable cells during cartilage resorption associated with the formation of intrachondral canals in the rat tibial epiphysis. Cell Tissue Res 2005;320:501-7.
11. Olstad K, Ytrehus B, Ekman S, Carlson CS, Dolvik NI. Early lesions of osteochondrosis in the distal tibia of foals. J Orthop Res 2007;25:1094-105.
12. Ytrehus B, Carlson CS, Ekman S. Etiology and pathogenesis of osteochondrosis. Vet Pathol 2007;44:429-48.
13. Brianza SZ, D'Amelio P, Pugno N, Delise M, Bignardi C, Isaia G. Allometric scaling and biomechanical behavior of the bone tissue: an experimental intraspecific investigation. Bone 2007;40:1635-42.
14. Ozaki S, Toida K, Suzuki M, Nakamura Y, Ohno N, Ohashi T, et al. Impaired olfactory function in mice with allergic rhinitis. Auris Nasus Larynx 2010;37575-83.
15. Di Giancamillo A, Deponti D, Addis A, Domeneghini C, Peretti GM. Meniscus maturation in the swine model: changes occurring along with anterior to posterior and medial to lateral aspect during growth. J Cell Mol Med 2014;18:1964-74.
16. Hare WC. The ages at which the centers of ossification appear roentgenographically in the limb bones of the dog. Am J Vet Res 1961;22:825-35.
17. Cole AA, Wezeman FH. Morphometric analysis of cartilage canals in the developing mouse epiphysis. Acta Anat 987;128:93-7.
18. Rivas R, Shapiro F. Structural stages in the development of the long bones and epiphyses: a study in the New Zealand white rabbit. J Bone Joint Surg Am 2002;84-A:85-100.
19. Shapiro F. Epiphyseal and physeal cartilage vascularization: a light microscopic and tritiated thymidine autoradiographic study of cartilage canals in newborn and young postnatal rabbit bone. Anat Rec 1998;252:140-8.
20. Kugler JH, Tomlinson A, Wagstaff A, Ward SM. The role of cartilage canals in the formation of secondary centres of ossification. J Anat 1979;129):493-506.
21. Blumer MJ, Longato S, Fritsch H. Localization of tartrate-resistant acid phosphatase (TRAP), membrane type-1 matrix metalloproteinases (MT1-MMP) and macrophages during early endochondral bone formation. J Anat 2008;213:431-41.
22. Delgado-Baeza E, Gimenez-Ribotta M, Miralles-Flores C, Nieto-Chaguaceda A, Santos-Alvarez I. Morphogenesis of cartilage canals: experimental approach in the rat tibia. Acta Anat 1991;142:132-7.
23. Visco DM, Hill MA, Van Sickle DC, Kincaid SA. Cartilage canals and lesions typical of

osteochondrosis in growth cartilages from the distal part of the humerus of newborn pigs. Vet Rec 1991;128:221-8.

24. Burkus JK, Ganey TM, Ogden JA. Development of the cartilage canals and the secondary center of ossification in the distal chondroepiphysis of the prenatal human femur. Yale J Biol Med 1993;66:193-202.

25. Doschak MR, Cooper DM, Huculak CN, Matyas JR, Hart DA, Hallgrimsson B, et al. Angiogenesis in the distal femoral chondroepiphysis of the rabbit during development of the secondary centre of ossification. J Anat 2003;203:223-33.

26. Peterson ME, Kutzler MA. Small animal pediatrics: the first 12 months of life. Elsevier-Saunders, St. Louis, MO, USA; 2011.

27. Peinado Cortes LM, Vanegas Acosta JC, Garzon Alvarado DA. A mechanobiological model of epiphysis structures formation. J Theor Biol 2011;287:13-25.

28. Gelse K, Poschl E, Aigner T. Collagens - structure, function, and biosynthesis. Adv Drug Deliv Rev 2003;55:1531-46.

29. Roulet M, Ruggiero F, Karsenty G, LeGuellec D. A comprehensive study of the spatial and temporal expression of the col5a1 gene in mouse embryos: a clue for understanding collagen V function in developing connective tissues. Cell Tissue Res 2007;327:323-32.

30. Bonaventure J, Zylberberg L, Cohen-Solal L, Allain JC, Lasselin C, Maroteaux P. A new lethal brittle bone syndrome with increased amount of type V collagen in a patient. Am J Med Genet 1989;33:299-310.

31. Kahai S, Vary CP, Gao Y, Seth A. Collagen, type V, alpha1 (COL5A1) is regulated by TGF-beta in osteoblasts. Matrix Biol 2004;23:445-55.

32. Yamaguchi K, Matsuo N, Sumiyoshi H, Fujimoto N, Iyama KI, Yanagisawa S, et al. Pro-alpha3(V) collagen chain is expressed in bone and its basic N-terminal peptide adheres to osteosarcoma cells. Matrix Biol 2005;24:283-94.

33. Le Guellec D, Mallein-Gerin F, Treilleux I, Bonaventure J, Peysson P, Herbage D. Localization of the expression of type I, II and III collagen genes in human normal and hypochondrogenesis cartilage canals. Histochem J 1994;26:695-704.

34. Waterhouse EJ, Quesenberry PJ, Balian G. Collagen synthesis by murine bone marrow cell culture. J Cell Physiol 1986;127:397-402.

35. Scherzer C, Windhagen H, Nellesen J, Crostack HA, Rohn K, Witte F, et al. Comparative structural analysis of the canine femoral head in Legg-Calve-Perthes disease. Vete Radiol Ultrasound 2009;50:404-11.

36. Wolschrijn CF, Gruys E, van der Wiel CW, Weijs WA. Cartilage canals in the medial coronoid process of young Golden Retrievers. Vet J 2008;176:333-7.

37. Lau SF, Hazewinkel HA, Grinwis GC, Wolschrijn CF, Siebelt M, Vernooij JC, et al. Delayed endochondral ossification in early medial coronoid disease (MCD): a morphological and immunohistochemical evaluation in growing Labrador retrievers. Vet J 2013;197:731-8.

38. Longo M, Modina SC, Bellotti A, Di Giancamillo M. Advances in the anatomic study of the interscapular region of the cat. BMC Vet Res 2015;11:249.

# Novel contributions in canine craniometry: Anatomic and radiographic measurements in newborn puppies

Maria Elena Andreis[1☯], **Umberto Polito**[1☯], **Maria Cristina Veronesi**[2], **Massimo Faustini**[2], **Mauro Di Giancamillo**[2]*, **Silvia C. Modina**[1]

1 Department of Health, Animal Science and Food Safety, Università degli Studi di Milano, Milano, Italy,
2 Department of Veterinary Medicine, Università degli Studi di Milano, Milano, Italy

☯ These authors contributed equally to this work.
* mauro.digiancamillo@unimi.it
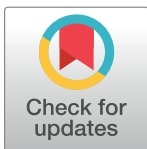
Abstract

The largest differences in intraspecific head shape among the *Carnivora* order are to be found in dogs. Based on their skull morphotypes, dog breeds are currently classified as dolichocephalic, mesaticephalic and brachycephalic. Due to the fact that some breeds have not been yet defined, this classification is incomplete; moreover, multi-breed studies on the skull morphology of puppies have never been performed. The aim of this work was to verify (i) whether differences in the skull conformation of purebred puppies are already present within the first week of age; (ii) whether radiographic and anatomic measures could be considered interchangeable, and (iii) to possibly classify puppies from non-categorized breeds thanks to their radiographic cranial measurements using neural nets. One hundred and thirty-seven dead puppies aged 0–7 days were examined considering their anatomic and radiographic measures. All linear measures and anatomic indices significantly differed among brachycephalic and non-brachycephalic puppies. Radiographic indices, with the exception of CI, identified the three skull morphotypes ($p<0.05$, for all comparisons). Radiographic and anatomic measures proved to be non-interchangeable in newborn puppies. Finally, nineteen puppies belonging to 5 non-categorized breeds could be classified thanks to neural nets in the three skull morphotypes with different probability (P between 0,66 and 0,95).

Introduction

The phenotypic differences existing within the canine species can be well-represented by their skull shape. Although some heterogeneity in skull shape and size is found within the *Carnivora* order [1, 2], *Canis lupus familiaris* exhibits the largest intraspecific differences [3, 4], mainly due to human selection. In fact, particularly during the last two centuries, dogs have been selected according to the shape of their skull on account of attitudinal traits, personal taste or common trends, to exceed the significant number of 200 breeds [http://www.thekennelclub.org.uk/]. Currently, dog breeds are classified as dolichocephalic, mesaticephalic and brachycephalic based on morphological ratios that consider the neurocranium and/or the

splanchnocranium [5–16]. As a general rule, dolichocephalic dogs show a greater development of the skull longitudinal axis; brachycephalic dogs have a shorter and larger skull, and mesaticephalic dogs exhibit intermediate skull features. This traditional craniometry-based classification is still used despite the outcomes of several recent studies based on genetics performed also to investigate the canine skull pattern derived from the wolf [1, 17, 18, 19, 20].

A better characterization of all the different phenotypes was gained after several morphometric and allometric studies together with reference values obtained from anatomic and radiographic linear measures and derived indices. In literature, most linear measures are anatomical and performed on the skull deprived of the soft tissues [1, 2, 12, 21–23]. Other data are based on the observation of living subjects [24, 25] or on measures from pictures [26–28]. Moreover, imaging studies on living animals by radiography [15, 29] or Computed Tomography [14] have been performed. Nevertheless, not all dog breeds have been classified unanimously on the basis of their skull morphology. In fact, while some breeds fall within defined categories, some others are still unclassified. The different techniques employed for skull measurements (anatomical, photographic or radiographic) may account for this heterogeneity and the variation of breed standards along time, depending on human selection, may as well have influenced the results. Moreover, some authors do not agree with the imposition of strict categories and propose a continuous spectrum of skull shapes ranging from extreme brachycephaly (e.g. Chihuahua) to extreme dolichocephaly (e.g. Borzoi) based on the cephalic index [26–28, 30–34].

Noticeably, most veterinarian craniometric studies have been performed on adult animals, so no detailed information is currently available on growing dogs. To the authors' knowledge, the only exception is represented by two studies on German Shepherd puppies [22, 23]. However, it has been postulated that in brachycephalic breeds the skull shape is generated before birth and continues its development after birth [35]. Recently, an allometric study was performed on newborn puppies belonging to small-sized breeds. The study included craniometric measures, but skull morphotype was not considered [36]. Since literature lacks study design standardization, the present investigation aimed to evaluate skull morphometry in newborn dogs and to classify puppies belonging to previously non-categorized canine breeds. In particular, it was conducted to find out any possible (i) difference in craniometric measures between newborn puppies belonging to dolichocephalic, mesaticephalic and brachycephalic breeds; (ii) interchange of craniometric anatomical measures performed on newborn puppies with radiological measures, and (iii) classification as dolichocephalic, mesaticephalic or brachycephalic for newborn puppies belonging to non-categorized breeds.

Materials and methods

Animals

Puppies under examination were obtained from breeders signing a prior informed consent, and the research was approved by the Animal Welfare Body of the University of Milan (AWB/OPBA, 58/2016). They all aged 0–7 days and were clinically evaluated by one of the authors, a Diplomate at the European College of Animal Reproduction (MCV). They were born full term, after normal pregnancies and parturitions by healthy bitches, regularly vaccinated and dewormed before mating. During the second half of gestation, all bitches had been fed a pregnancy-specific commercial diet. The study was strictly conducted on normal puppies only, i.e. considered as conforming with their specific breed. All enrolled puppies showed normal development and weight, no malformations or physical defects, and their death had occurred suddenly without any disease interference on their weight gain and growth. To be eligible for the study they had to satisfy the following criteria: stillborn puppies, dying because of intra-partum

asphyxia, born alive but dying within 1 hour after birth; puppies dying within their first week of age because of sudden death (i.e. at an interval between first symptoms and death shorter than 24 hours), caused by sudden septicemia, as evidenced by post mortem examination. From the time of their death, puppies were stored at 4˚C for less than 12 hours and refrigerated during their transfer to the laboratory unit at Università degli Studi di Milano. Breed, gender, age and body weight were recorded before their storage at– 20˚C.

Measures

Anatomic measures and indices. Consistent with literature [16], the following linear measures were obtained for each dog by a calliper: Cranial Length (CL), Cranial Width (CW), Skull Length (SL), Skull Width (SW) and Facial Length (FL). Every measure was blindly repeated three times on the whole head, accurately palpating its landmarks (Fig 1). The following indices were also calculated: Cranial Index (CI) and Skull Index (SI) [16] (Tables 1 and 2).

Radiographic measures and indices. Radiographic exams were performed by a CR system (FCR Fuji Capsula X®) assembled with a radiological unit (ARCOM–Simply), using a 0.6 mm focal spot. The focal spot-film distance was 100 cm and no grid was employed. Latero-lateral (LL) and dorso-ventral (DV) views of the skull were obtained for each puppy. The images were stored in an Apple database and post-processing measures were performed by Osirix PRO®. Facial Length (FL-DV) and Cranial Length (CL-DV) were obtained on DV view [15]. Additional linear measures, extrapolated from the corresponding anatomic measures, were evaluated [16]. Some of them, Cranial Width (CW), Skull Width (SW) and Skull Length on LL view (SL-LL), were transferred unaltered. Others were modified, i.e. Cranial Length on LL view (CL-LL) was measured from *Inion* to the most caudal part of the fronto-nasal suture and Facial Length on LL projection (FL-LL) was measured from *Prosthion* to the most caudal part of the fronto-nasal suture (Fig 2). Every measure was blindly repeated three times. The S-index (S-I) was calculated according to literature [16]. Additional indices were extrapolated from the corresponding anatomic ones: Cranial Index (CI), Facial Index (FI) and Skull Index (SI) [16] (Tables 1 and 2).
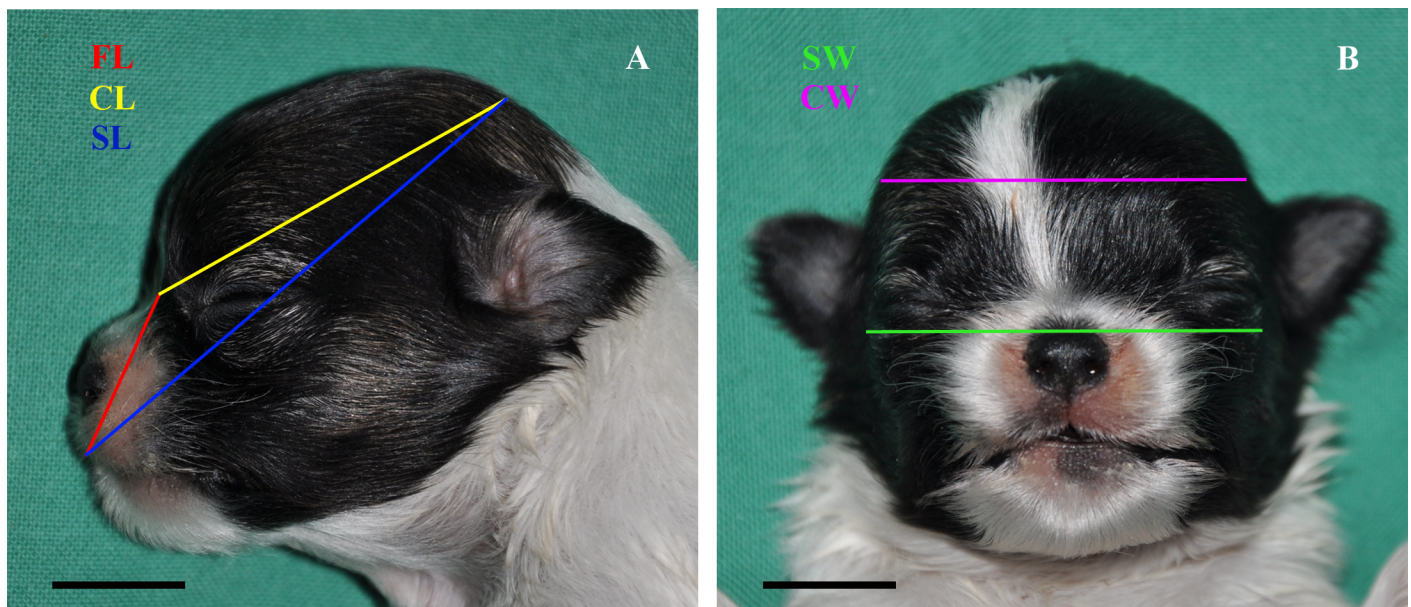

Fig 1. Anatomic linear measures. A: Facial Length (FL); Cranial Length (CL); Skull Length (SL); B: Skull Width (SW); Cranial Width (CW); Bar = 1 cm.

Table 1. Linear measures.

Linear measures	Landmarks
Skull Length (SL)[a]	from *Prosthion* to *Inion*
Cranial Length (CL)[a]	from *Inion* to *Nasion*
Cranial Length on LL view (CL-LL)[a*]	from *Inion* to the caudal edge of the fronto-nasal suture
Facial Length (FL)[a]	from *Nasion* to *Prosthion*
Facial Length on LL view (FL-LL)[a*]	from *Prosthion* to the caudal edge of the fronto-nasal suture
Cranial Width (CW)[a]	the most lateral points of the neurocranium
Skull Width (SW)[a]	the most lateral points of the zygomatic arch
Facial Length DV (FL-DV)[b]	from *Prosthion* to *Nasion*
Cranial Length DV (CL-DV)[b]	from *Nasion* to the caudal edge of the occipital condyle

[a]Evans and de Lahunta, 2013 [16]
[b]Koch et al., 2012 [15]
*modified measure (S1 Table).

https://doi.org/10.1371/journal.pone.0196959.t001

The adopted terminology was chosen in accordance to the *Nomina Anatomica Veterinaria* (2012) and to the textbook "Miller's anatomy of the dog" [16].

Statistical analysis

Repeatability of each measure taken in triple was evaluated by Friedman's test and the mean value for each measurement was considered for further statistical analysis. Analysis of variance was performed on puppy groups according to the traditional craniometric categories (brachycephalic, mesaticephalic, dolichocephalic) to detect differences among the groups. Agreement between anatomical and radiographic linear measurements was evaluated by the graphical method of Bland-Altman plots and also bias between tests was calculated. Results are graphically reported indicating the average *versus* the difference between the couples of variables. Two confidence bands (generally 95%) delimit the cloud of points to evaluate the number of points falling into the bands space, thus indicating goodness of concordance between the two methods. Neural nets were used in the attempt to classify puppies belonging to unclassified breeds within the categories of brachycephalic, mesaticephalic or dolichocephalic. Standardized radiographic parameters were classified by cluster analysis after processing in an artificial neural network. The neural network was the unsupervised perceptron network, with a holdback value of 0.6 and three hidden nodes. Through the training set, the neural network can classify new cases based on the experience acquired. Analysis of variance was further performed after the new classification obtained by neural nets, as internal control. Statistical analysis was performed by the program JMP7.0 (SAS Inst., Inc., NC, USA) and the software XLstat for Windows platform.

Table 2. Indices.

Index	Formula
Cranial index (CI) [a]	(CW x 100)/CL
Skull index (SI) [a]	(SW x 100)/SL
S-index (S-I) [b]	FL-DV/CL-DV
Facial index (FI) [a]	(SW x 100)/FL

[a]Evans and de Lahunta, 2013 [16]
[b]Koch et al., 2012 [15].

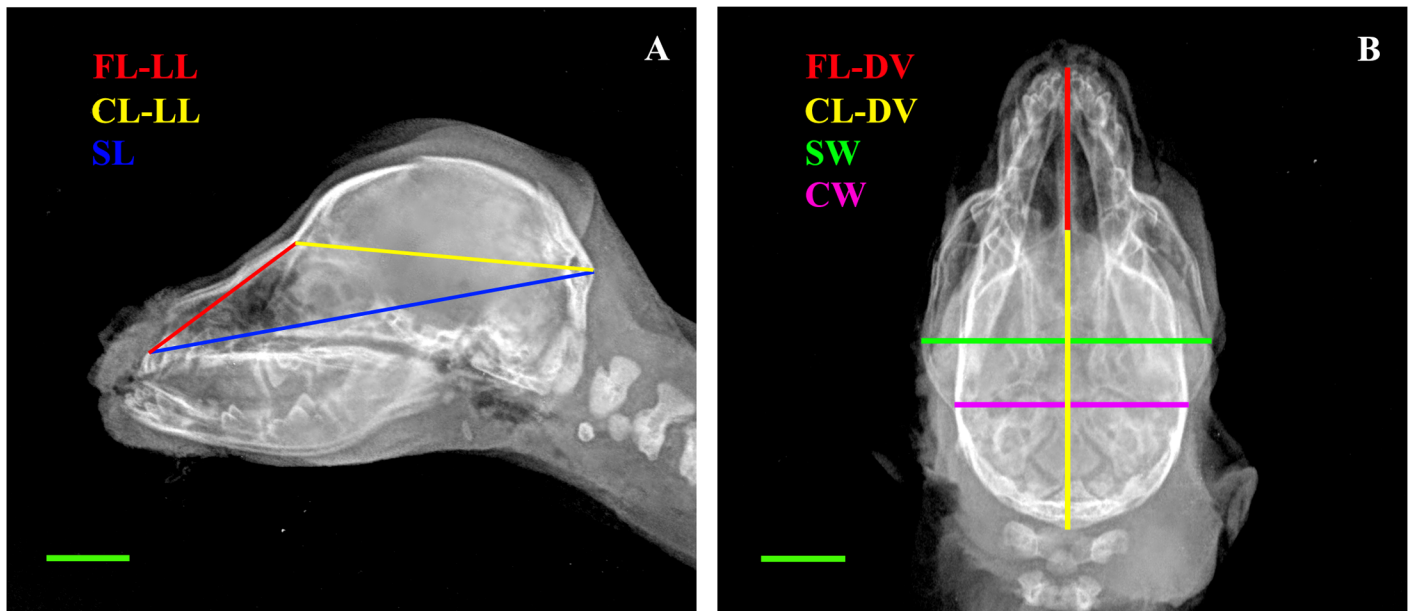https://doi.org/10.1371/journal.pone.0196959.t002

Fig 2. Radiographic linear measures. A: Latero-lateral view (LL): Facial Length (FL-LL); Cranial Length (CL-LL); Skull Length (SL); B: Dorso-ventral view (DV): Facial Length (FL-DV); Cranial Length (CL-DV); Skull Width (SW); Cranial Width (CW); Bar = 1 cm.

Results

One hundred thirty-seven puppies (0–7 days) belonging to 33 different breeds met the inclusion criteria and were categorized according to literature. In case of discrepancies in the results derived from different studies, the cephalic index, when available from literature [26, 27, 33, 37] was employed to define the category for each breed, together with the results of previous studies [5–16]. Few breeds had never been included in any craniometric study and were considered unclassified: a) Dolichocephalic (n = 24): Afghan Hound (n = 5), Schnauzer (giant) (n = 5), English Setter (n = 4), German Shepherd (n = 3), Springer Spaniel (n = 3), Whippet (n = 1), Dachshund (n = 1), Hovawart (n = 1), Saint Bernard (n = 1); b) Mesaticephalic (n = 29): Labrador Retriever (n = 7), Leonberger (n = 5), Jack Russel Terrier (n = 5), Shar Pei (n = 3), Beagle (n = 2), American Cocker Spaniel (n = 2), Pinscher (n = 2), Alaskan Malamute (n = 1), Golden Retriever (n = 1), Border Collie (n = 1); c) Brachycephalic (n = 64): Chihuahua (n = 25), Bullmastiff (n = 13), English Bulldog (n = 9), Rottweiler (n = 8), Maltese (n = 4), Shih Tzu (n = 2), Boxer (n = 1), American Staffordshire Terrier (n = 1), Epagneul Breton (n = 1); d) Unclassified (n = 20): Poodle (toy) (n = 8), Maremma Sheepdog (n = 6), Jagd Terrier (n = 4), Bull Terrier (miniature) (n = 1), Belgian Shepherd (n = 1). Results of anatomic and radiographic linear measures are provided as supporting information (S3 Table and S4 Table, respectively). Results of the ANOVA performed on puppies classified as dolichocephalic, mesaticephalic and brachycephalic according to literature are shown in (Fig 3A and 3B) and Table 3.

All linear measures and anatomic indices significantly differed among brachycephalic and non-brachycephalic puppies. Only the radiographic CW identified dolichocephalic puppies as intermediate between brachycephalic and mesaticephalic ones. On the other hand, radiographic indices (with the exception of the CI) discriminate among the three categories (Fig 4).

Bland-Altman plots for anatomic and radiographic linear measures indicate that a limited though unacceptable number of outliers is present for all measures. Graphs depict the bias, the
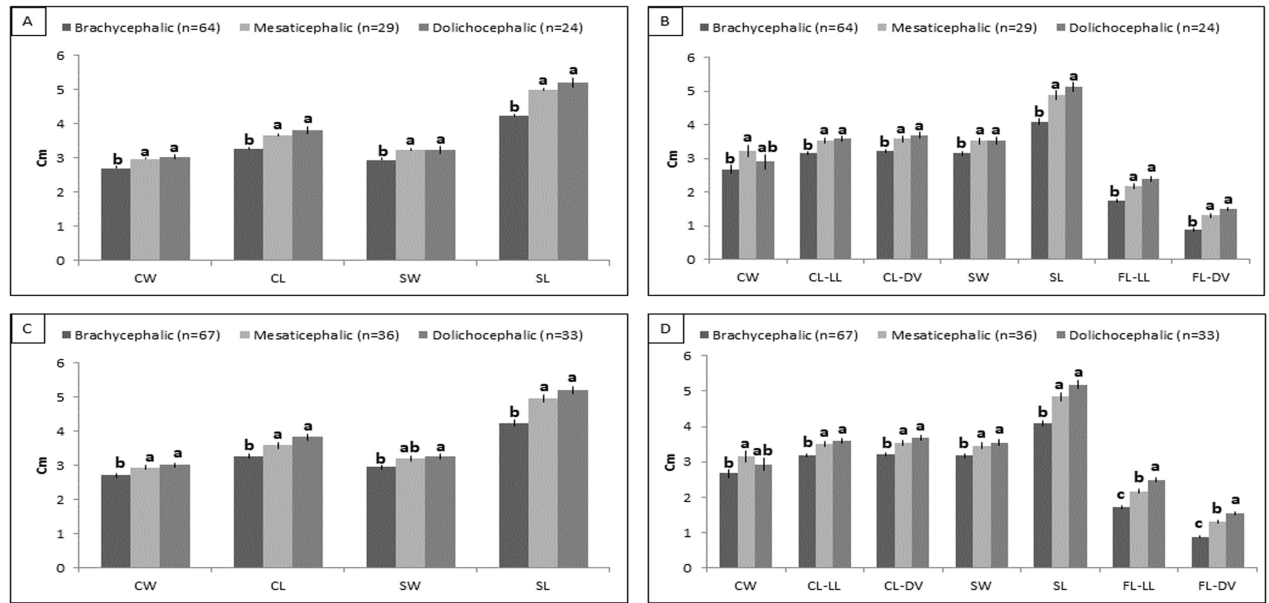
Fig 3. ANOVA for anatomic and radiographic linear measures pre- and post-neural net. Anatomic linear measures pre- (A) and post- (C) neural nets; Radiologic linear measures pre- (B) and post- (D) neural nets. Values (means±SEM) are expressed as cm. [a-c] Means with different letters within rows are significantly different (*p*<0,05). Cranial Width (CW); Cranial Length (CL); Skull Width (SW); Skull Length, (SL); Cranial Length LL (CL-LL); Cranial Length DV (CL-DV); Facial Length LL (FL-LL); Facial Length DV (FL-DV).

https://doi.org/10.1371/journal.pone.0196959.g003

bias 95% confidence interval and the 95% confidence interval for the data: CW -0.043±0.189; CL -0.067±0.246; SW 0.272±0.239; SL 0.265±0.309 (Fig 5).

Results from the new classification of puppies with neural nets indicate that 19/19 (100%) puppies belonging to 5 previously unclassified breeds were categorized as dolichocephalic (n = 9), mesaticephalic (n = 7) and brachycephalic (n = 3) with different probabilities (P

Table 3. ANOVA for anatomic and radiographic indices pre- and post-neural nets (mean±SEM).

Pre-Neural Nets	Indices	Brachycephalic (n = 64)	Mesaticephalic (n = 29)	Dolichocephalic (n = 24)	*p*
Anatomy	SI	69.67 ±0.54[a]	64.36±0.69[b]	62.53±0.75[b]	***
	CI	84.26±2.05[a]	81.245±0.69[b]	80.56±0.76[b]	***
Radiology	SI	70.89±0.38[a]	66.33±0.52[b]	64.29±0.56[c]	***
	CI	84.26±2.05	89.56±2.77	81.24±2.99	
	FI	182.99±3.17	161.61±2.37[b]	146.04±2.55[c]	***
	S-I	0.26±0.01[c]	0.36±0.01[b]	0.41±0.01[a]	***
Post-Neural Nets	Indices	Brachycephalic (n = 67)	Mesaticephalic (n = 36)	Dolichocephalic (n = 33)	*p*
Anatomy	SI	69.50±0.54[a]	64.30±0.71[b]	62.90±0.73[b]	***
	CI	83.34±0.50[a]	82.02±0.73[b]	79.12±0.75[b]	***
Radiology	SI	71.12±0.35[a]	66.20±0.49[b]	63.88±0.50[c]	***
	CI	84.38±2.09	89.84±2.93	82.04±2.97	
	FI	186.31±1.61[a]	159.42±2.26[b]	143.96±2.30[c]	***
	S-I	0.27±0.01[c]	0.37±0.01[b]	0.42±0.01[a]	***

Values are expressed as means±SEM.

[a-c] Means with different letters within rows are significantly different (*p*<0,05). Asterisks evidence the ANOVA significance (***p*<0.01).

Skull index (SI); Cranial Index (CI); Facial Index (FI); S-Index (S-I).

https://doi.org/10.1371/journal.pone.0196959.t003

Fig 4. Radiographic exams depicting differences in skull shape among dolichocephalic, mesaticephalic and brachycephalic newborn puppies. Representative images of a dolichocephalic puppy (Afghan Hound A, B), a mesaticephalic puppy (Labrador Retriever C, D) and a brachycephalic puppy (Chihuahua E, F). A, C, E: Latero-lateral views; B, D, F: Dorso-ventral views. Bar = 1 cm.
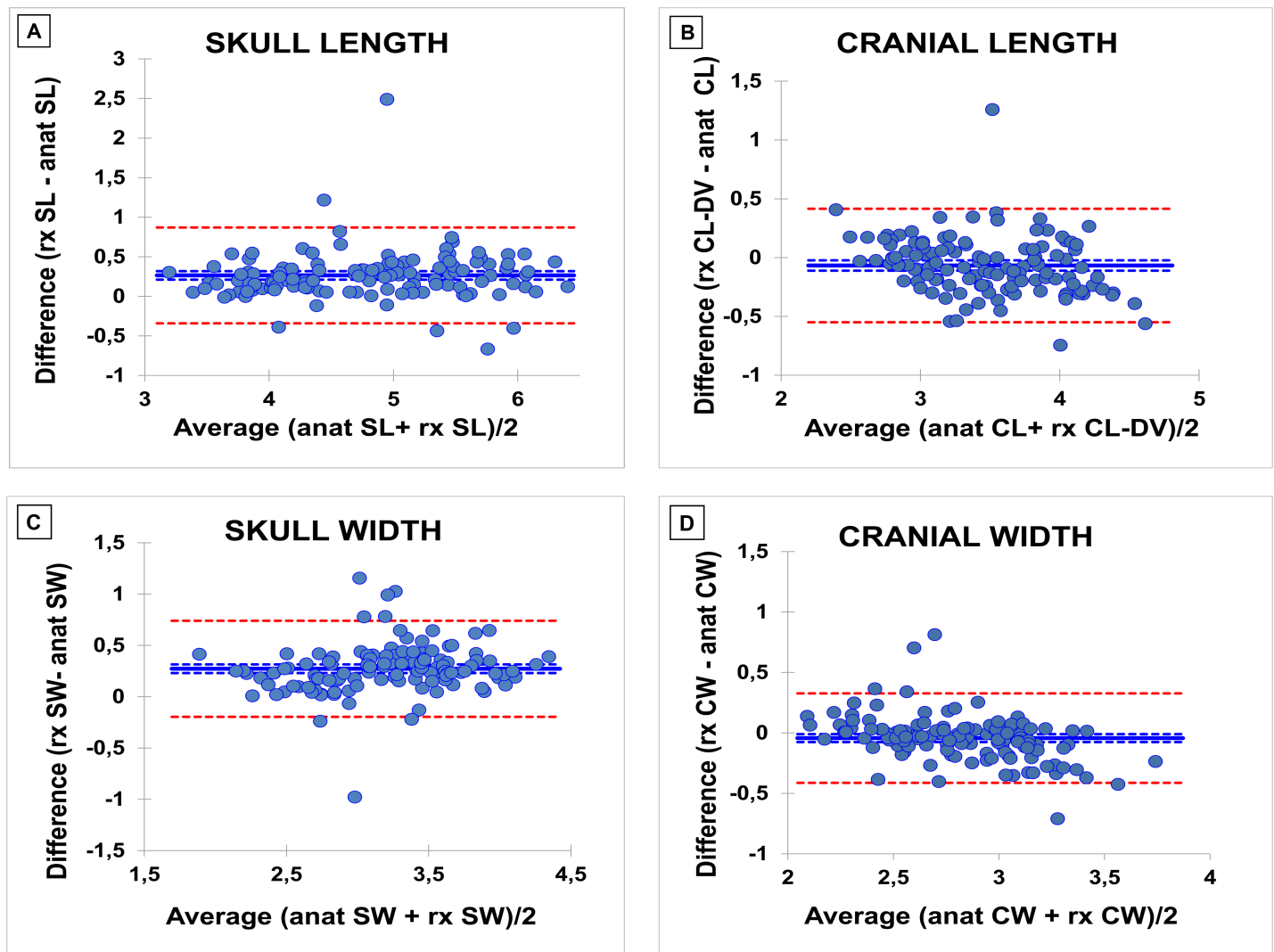
https://doi.org/10.1371/journal.pone.0196959.g004

Fig 5. Bland–Altman difference plots to compare radiographic and anatomic measures. Differences between 2 values are plotted against the mean of the 2 values. The blue solid line represents the bias (mean difference) and the red dotted lines represent the 95% limits of agreement. A: Skull Length (SL); B: Cranial Length (CL); C: Skull Width (SW); D: Cranial Width (CW).

between 0.66 and 0.95) (S2 Table). One puppy (Poodle toy) was excluded from the neural nets analysis due to missing radiographic data.

Results of the ANOVA performed including puppies newly classified with neural nets are shown in (Fig 3C and 3D) and Table 3: they confirm the results of the previous ANOVA for almost all parameters ($p < 0.05$).

Discussion

To the authors' knowledge, this is the first multi-breed craniometric study on newborn puppies based on linear measures and indices. In fact, the present investigation provides new insights on the craniometry of newborn puppies aged 0–7 days belonging to 33 different breeds. The first aim of this work was to verify whether the craniometric differences that are typical of adult dogs (brachycephalic, mesaticephalic, dolichocephalic) are already present in newborn purebred puppies during the first week of age. Grouping puppies into these three

categories allowed highlighting significant differences among them. Linear measures almost constantly identified two groups: brachycephalic *vs* non-brachycephalic morphotype (Fig 3), as previously described by Starck [35]. Anatomy and radiography provided contrasting results about the indices. While anatomic indices highlighted differences in skull conformation without a clear identification of three separate categories, almost all radiographic indices constantly distinguished among the three categories. The radiographic CI is the only index that displayed no differences among puppies (Table 3): this could be due to a quite uniform cranial shape among puppies, as supported by the anatomical corresponding index, which only isolates the brachycephalic morphotype. However, it should also be taken into account that radiographic landmarks (e.g. frontonasal suture) may be challenging to identify in newborns, as shown by their higher SEM. These results were not surprising: in fact, our study suggests that anatomic and radiographic methods cannot be used interchangeably when measuring puppies' skulls. Being radiographic measures considered as invasive, we tried to provide a non-invasive method: despite a low bias, the differences in Bland-Altman plots (sometimes even higher than 1 cm) were considered unacceptably high for the purpose (Fig 5). This negative though expected result may be likely due to the presence of soft tissues that make radiographic and anatomic landmarks markedly different.

The last aim of this work was to classify as dolichocephalic, mesaticephalic or brachycephalic puppies belonging to previously uncategorized breeds using neural nets. Neural nets provided useful craniometric information, assigning 19/19 puppies (100%) to the three categories with different probability. Some of the skulls were classified with relatively low probability (e.g a Jagd Terrier was classified as dolichocephalic with P = 0,66, S2 Table): this could be due to a limited over-fitting effect of the neural network procedure and/or to the inner multivariate variability of each sample. Multivariate samples hide an intimate structure that a "classical" examination (as for the historical classification) cannot put on the surface. Moreover, it must be taken into account that growing animals are submitted to dramatic morpho-functional allometric changes [23], that in some animals can evolve more or less rapidly compared to others. After the new classification, an ANOVA test was repeated as internal control, including the newly classified puppies in their respective groups. The results largely confirmed the previously performed ANOVA: this was considered as a proof of the results of the neural nets, which were used for the first time in this study in attempt to craniometrically classify newborn puppies. Neural nets are bio-inspired computational models created to simulate the human brain data processing, consisting of networks of highly interconnected virtual neurons that can autonomously output decisions based on previously provided input information. Thus, neural nets are able to learn from past experience through a specific training process and provide outcome on new data based on such experience [38–40]. This learning ability makes them perfectly suitable for the solution of classification issues. As a basis, the large amount of radiographic data obtained from puppies belonging to classified breeds was used for the set-up in this study. However, growing animals cannot perfectly fit the static nature of neural nets: since the skull does not grow in all directions at the same time, the classification determined during the first week of age could be contradicted by what determined during other periods of their skull growth. For this reason, this method can represent a useful but not definitive tool to define puppies' morphotype, that in our opinion could be more helpful in the categorization of adult dogs.

A few flaws are present in this study. A very small sample size available for some breeds (e.g. Belgian Shepherd, Saint Bernard and Hovawart) could have influenced its results, especially the ones obtained by the neural nets, which may not be fully representative for a larger population (breed). Unfortunately, uneven sampling is often intrinsic in cadaveric studies and hardly ever avoidable. However, the main purpose of the study, excluding the definition of breed standards for the puppies, was in favour of the choice to enrol all available puppies,

irrespective of their number per breed. Increasing sample size and homogeneity could allow a better definition of breed-specific craniometry and establish breed standard references to evaluate skull development in newborn puppies. It could also help to define cut-off values to early recognise skull-shape measures linked to pathologies' predisposition such as Chiari-like malformation [14, 41–43] and brachycephalic obstructive airways syndrome (BOAS) [44]. For this reason, more studies on puppies belonging to predisposed breeds could provide new clinical insights in dogs as well as in humans. A recent study of dog DNA revealed a genetic mutation linked to two brachycephalic breeds, suggesting that the craniofacial diversity of dogs could be useful to discover candidate genes involved in canine as well as human craniofacial anomalies [45]. Future perspectives also include the evaluation of adult dogs belonging to unclassified breeds, aiming to apply neural nets in a "craniometrically stable" sample.

Conclusion

This study ascertained for the first time the skull morphometric differences among dolichocephalic, mesaticephalic and brachycephalic purebred puppies in their early neonatal period. Such differences were observed after both anatomic and radiologic evaluation, constantly isolating brachycephalic from non-brachycephalic puppies. Anatomic and radiologic measures, however, were not interchangeable. The investigation made it also possible to reliably classify 19 puppies belonging to 5 previously uncategorized breeds using the neural nets. Moreover, it suggested that canine cadavers can represent a valid alternative to *in vivo* animal models in the study of skeleton development, as previously demonstrated [36, 46].

Supporting information

S1 Table. Landmarks description [16].
(DOCX)

S2 Table. Results of the neural nets. The second, third and fourth columns show the probability for each uncategorized puppy to be classified in the corresponding craniometric group. Results are indicated as the probability between 0–1. The highest probability is bold-typed.
(DOCX)

S3 Table. Anatomic linear measures. Mean values, expressed in cm.
S = stillborn. M = male; F = female. In red, brachycephalic breeds; in blue, mesaticephalic breeds; in green, dolicocephalic breeds; in black, unclassified breeds. CW = Cranial Width, CL = Cranial Length, SW = Skull Width, SL = Skull Length, SI = Skull Index, CI = Cranial Index, MD = Missing Data.
(DOCX)

S4 Table. Radiographic linear measures. Mean values, expressed in cm.
S = stillborn. M = male; F = female. In red, brachycephalic breeds; in blue, mesaticephalic breeds; in green, dolicocephalic breeds; in black, unclassified breeds. CL = Cranial Length, FL = Facial Length, FLDV = Facial Length on DV projection, CLDV = Cranial Length on DV projection, SL = Skull Length, CBL = Condylobasal length, SW = Skull Width, CW = Cranial Width, MD = Missing Data.
(DOCX)

Acknowledgments

Author Contributions

Conceptualization: Mauro Di Giancamillo, Silvia C. Modina.

Data curation: Maria Elena Andreis, Umberto Polito, Maria Cristina Veronesi, Massimo Faustini.

Formal analysis: Massimo Faustini.

Funding acquisition: Maria Cristina Veronesi, Mauro Di Giancamillo, Silvia C. Modina.

Investigation: Maria Elena Andreis, Umberto Polito, Maria Cristina Veronesi.

Methodology: Massimo Faustini.

Project administration: Mauro Di Giancamillo, Silvia C. Modina.

Resources: Maria Cristina Veronesi.

Software: Massimo Faustini.

Supervision: Maria Cristina Veronesi, Mauro Di Giancamillo, Silvia C. Modina.

Validation: Massimo Faustini.

Visualization: Maria Elena Andreis, Umberto Polito.

Writing – original draft: Maria Elena Andreis, Umberto Polito, Mauro Di Giancamillo, Silvia C. Modina.

Writing – review & editing: Maria Elena Andreis, Umberto Polito, Maria Cristina Veronesi, Massimo Faustini, Mauro Di Giancamillo, Silvia C. Modina.

References

1. Drake AG, Klingenberg CP. Large-scale diversification of skull shape in domestic dogs: disparity and modularity. Am Nat. 2010; 175(3):289–301. https://doi.org/10.1086/650372 PMID: 20095825

2. Saber AS, Gummow B. Skull morphometry of the lion (Panthera leo), dog (Canis lupus familiaris) and cat (Felis catus). Journal of Veterinary Anatomy. 2015; 8(1):13–30.

3. Getty R. Sisson and Grossman 's The Anatomy of the Domestic Animals. Fifth Edition ed. Sisson S, Grossman JD, Getty R, editors. Philadelphia: W.B. Saunders Company; 1975. 2480 p.

4. Dyce KM, Sack WO, Wensing CJG. Textbook of Veterinary Anatomy. 4th Revised Edition ed. St Louis-Missouri: Sunders/Elsevier; 2010. 864 p.

5. Ellenberger W, Baum H. Handbuch der vergleichenden Anatomie der Haustiere. Berlin: Hirschwald, A.; 1932. 1156 p.

6. Stockard CR. The genetic and endocrinic basis for differences in form and behavior. American Anatomy Memoir. 19. Philadelphia: Wistar Institute of Anatomy and Biology; 1941.

7. Bourdelle E, Bressou C. Anatomie regionale des animaux domestiques. Paris1953.

8. Seiferle E. [On the topography of the brain on long and short skulls in dog breeds]. Acta anatomica. 1966; 63(3):346–62. PMID: 5918444

9. Brehm H, Loeffler K, Komeyli H. [Skull forms in dogs]. Anatomia, histologia, embryologia. 1985; 14 (4):324–31. PMID: 2936276

10. Lignereux Y, Regodon S, Pavaux C. Cephalic typology in dogs Typologie cephalique canine. Revue de Medecine Veterinaire. 1991; 142(6):469–80.

11. Onar V, Ozcan S, Pazvant G. Skull typology of adult male Kangal dogs. Anatomia, histologia, embryologia. 2001; 30(1):41–8. PMID: 11284162

12. Alpak H, Mutus R, Onar V. Correlation analysis of the skull and long bone measurements of the dog. Annals of anatomy = Anatomischer Anzeiger: official organ of the Anatomische Gesellschaft. 2004; 186 (4):323–30.

13. Gacsi M, McGreevy P, Kara E, Miklosi A. Effects of selection for cooperation and attention in dogs. Behav Brain Funct. 2009; 5:31. https://doi.org/10.1186/1744-9081-5-31 PMID: 19630939

14. Schmidt MJ, Neumann AC, Amort KH, Failing K, Kramer M. Cephalometric measurements and determination of general skull type of Cavalier King Charles Spaniels. Veterinary radiology & ultrasound: the official journal of the American College of Veterinary Radiology and the International Veterinary Radiology Association. 2011; 52(4):436–40.

15. Koch DA, Wiestner T, Balli A, Montavon PM, Michel E, Scharf G, et al. Proposal for a new radiological index to determine skull conformation in the dog. SAT, Schweizer Archiv fur Tierheilkunde. 2012; 154 (5):217–20. https://doi.org/10.1024/0036-7281/a000331 PMID: 22547337

16. Evans HE, De Lahunta A. Miller's Anatomy of the Dog. Fourth edition ed. St Louis (MO) USA: Saunders/Elsevir; 2013. 872 p.

17. Bannasch D, Young A, Myers J, Truve K, Dickinson P, Gregg J, et al. Localization of canine brachycephaly using an across breed mapping approach. PloS one. 2010; 5(3):e9632. https://doi.org/10.1371/journal.pone.0009632 PMID: 20224736

18. Boyko AR, Quignon P, Li L, Schoenebeck JJ, Degenhardt JD, Lohmueller KE, et al. A simple genetic architecture underlies morphological variation in dogs. PLoS Biol. 2010; 8(8):e1000451. https://doi.org/10.1371/journal.pbio.1000451 PMID: 20711490

19. Shearin AL, Ostrander EA. Canine morphology: hunting for genes and tracking mutations. PLoS Biol. 2010; 8(3):e1000310. https://doi.org/10.1371/journal.pbio.1000310 PMID: 20209140

20. Schoenebeck JJ, Ostrander EA. The genetics of canine skull shape variation. Genetics. 2013; 193 (2):317–25. https://doi.org/10.1534/genetics.112.145284 PMID: 23396475

21. Trouth CO, Winter S, Gupta KC, Millis RM, Holloway JA. Analysis of the sexual dimorphism in the basioccipital portion of the dog's skull. Acta anatomica. 1977; 98(4):469–73. PMID: 883490

22. Onar V. A morphometric study on the skull of the German shepherd dog (Alsatian). Anatomia Histologia Embryologia-Journal of Veterinary Medicine Series C-Zentralblatt Fur Veterinarmedizin Reihe C. 1999; 28(4):253–6.

23. Onar V, Gunes H. On the variability of skull shape in German shepherd (Alsatian) puppies. Anatomical Record Part a-Discoveries in Molecular Cellular and Evolutionary Biology. 2003; 272A(1):460–6.

24. Trangerud C, Grondalen J, Indrebo A, Tverdal A, Ropstad E, Moe L. A longitudinal study on growth and growth variables in dogs of four large breeds raised in domestic environments. Journal of Animal Science. 2007; 85(1):76–83. https://doi.org/10.2527/jas.2006-354 PMID: 17179542

25. Sutter NB, Mosher DS, Gray MM, Ostrander EA. Morphometrics within dog breeds are highly reproducible and dispute Rensch's rule. Mammalian Genome. 2008; 19(10/12):713–23.

26. McGreevy PD, Georgevsky D, Carrasco J, Valenzuela M, Duffy DL, Serpell JA. Dog behavior co-varies with height, bodyweight and skull shape. PloS one. 2013; 8(12):e80529. https://doi.org/10.1371/journal.pone.0080529 PMID: 24358107

27. Carrasco JJ, Georgevsky D, Valenzuela M, McGreevy PD. A pilot study of sexual dimorphism in the head morphology of domestic dogs. Journal of Veterinary Behavior: Clinical Applications and Research. 2014; 9(1):43–6.

28. Georgevsky D, Carrasco JJ, Valenzuela M, McGreevy PD. Domestic dog skull diversity across breeds, breed groupings, and genetic clusters. Journal of Veterinary Behavior: Clinical Applications and Research. 2014; 9(5):228–34.

29. Regodon S, Vivo JM, Franco A, Guillen MT, Robina A. Craniofacial angle in dolicho-, meso- and brachycephalic dogs: radiological determination and application. Annals of anatomy = Anatomischer Anzeiger: official organ of the Anatomische Gesellschaft. 1993; 175(4):361–3.

30. McGreevy P, Grassi TD, Harman AM. A strong correlation exists between the distribution of retinal ganglion cells and nose length in the dog. Brain Behav Evol. 2004; 63(1):13–22. https://doi.org/10.1159/000073756 PMID: 14673195

31. Helton WS. Cephalic index and perceived dog trainability. Behav Processes. 2009; 82(3):355–8. https://doi.org/10.1016/j.beproc.2009.08.004 PMID: 19683035

32. Stone HR, McGreevy PD, Starling MJ, Forkman B. Associations between Domestic-Dog Morphology and Behaviour Scores in the Dog Mentality Assessment. PloS one. 2016; 11(2):e0149403. https://doi.org/10.1371/journal.pone.0149403 PMID: 26919495

33. Teng KT, McGreevy PD, Toribio JA, Dhand NK. Trends in popularity of some morphological traits of purebred dogs in Australia. Canine Genet Epidemiol. 2016; 3:2. https://doi.org/10.1186/s40575-016-0032-2 PMID: 27051522

34. Pilegaard AM, Berendt M, Holst P, Moller A, McEvoy FJ. Effect of Skull Type on the Relative Size of Cerebral Cortex and Lateral Ventricles in Dogs. Front Vet Sci. 2017; 4:30. https://doi.org/10.3389/fvets.2017.00030 PMID: 28361057

35. Starck D. Der Heutige Stand de fetalisationsproblems J Anim Breed Genet. 1962; 77:129–55.

36. Modina SC, Veronesi MC, Moioli M, Meloni T, Lodi G, Bronzo V, et al. Small-sized newborn dogs skeletal development: radiologic, morphometric, and histological findings obtained from spontaneously dead animals. BMC veterinary research. 2017; 13(1):175. https://doi.org/10.1186/s12917-017-1092-6 PMID: 28615055

37. Roberts T, McGreevy PD. Selection for breed-specific long-bodied phenotypes is associated with increased expression of canine hip dysplasia. Vet J. 2010; 183(3):266–72. https://doi.org/10.1016/j.tvjl.2009.11.005 PMID: 19959383

38. Fogel GB. Computational intelligence approaches for pattern discovery in biological systems. Brief Bioinform. 2008; 9(4):307–16. https://doi.org/10.1093/bib/bbn021 PMID: 18460474

39. Contri A, Zambelli D, Faustini M, Cunto M, Gloria A, Carluccio A. Artificial neural networks for the definition of kinetic subpopulations in electroejaculated and epididymal spermatozoa in the domestic cat. Reproduction. 2012; 144(3):339–47. https://doi.org/10.1530/REP-12-0125 PMID: 22753767

40. Pouliakis A, Karakitsou E, Margari N, Bountris P, Haritou M, Panayiotides J, et al. Artificial Neural Networks as Decision Support Tools in Cytopathology: Past, Present, and Future. Biomed Eng Comput Biol. 2016; 7:1–18.

41. Schmidt MJ, Amort KH, Failing K, Klingler M, Kramer M, Ondreka N. Comparison of the endocranial-and brain volumes in brachycephalic dogs, mesaticephalic dogs and Cavalier King Charles spaniels in relation to their body weight. Acta veterinaria Scandinavica. 2014; 56(30):13 May 2014.

42. Knowler SP, v/d Berg H, McFadyen A, La Ragione RM, Rusbridge C. Inheritance of Chiari-Like Malformation: Can a Mixed Breeding Reduce the Risk of Syringomyelia? PloS one. 2016; 11(3):e0151280. https://doi.org/10.1371/journal.pone.0151280 PMID: 27008271

43. Cross CL, McFadyen AK, Jovanovik J, Tauro A, Driver CJ, Fitzpatrick N, et al. Forebrain conformation changes in Chiari-like malformation. BSAVA Congress 2016 Proceedings, 7–10 April 2016, Birmingham, UK. 2016:542–3.

44. Meola SD. Brachycephalic airway syndrome. Topics in Companion Animal Medicine. 2013; 28(3):91–6. https://doi.org/10.1053/j.tcam.2013.06.004 PMID: 24182996

45. Marchant TW, Johnson EJ, McTeir L, Johnson CI, Gow A, Liuti T, et al. Canine Brachycephaly Is Associated with a Retrotransposon-Mediated Missplicing of SMOC2. Curr Biol. 2017; 27(11):1573–84 e6. https://doi.org/10.1016/j.cub.2017.04.057 PMID: 28552356

46. Di Giancamillo A, Andreis ME, Taini P, Veronesi MC, Di Giancamillo M, Modina SC. Cartilage canals in newborn dogs: histochemical and immunohistochemical findings. Eur J Histochem. 2016; 60(3):2701. https://doi.org/10.4081/ejh.2016.2701 PMID: 27734993

6. QUADRICEPS CONTRACTURE INDUCES HIND LIMB OSSIFICATION CENTRES HYPOPLASIA AND DEFORMATION: RADIOGRAPHIC AND COMPUTED TOMOGRAPHIC STUDY IN 13 LITTERMATES WITH SUSPECTED INJECTION-INDUCED CONTRACTURE

M. E. Andreis[1], S. C. Modina[1], L. M. Carnevale[2], U. Polito[1], M. C. Veronesi[2], A. Di Giancamillo[1], P. Roccabianca[2], M. Di Giancamillo[2]

[1]Department of Health, Animal Science and Food Safety, Università degli Studi di Milano, Milano, Italy

[2]Department of Veterinary Medicine, Università degli Studi di Milano, Milano, Italy

Introduction

Quadriceps contracture is an uncommon condition in dogs, mainly reported in immature animals (Bardet and Hohn, 1983). It is generally due to trauma, especially distal femoral fractures that are left untreated or are mistreated with extension devices and prolonged immobilization (Braund et al., 1980; Leighton, 1981; Bardet eand Hohn, 1984; Bardet, 1987). It has also been reported as a congenital anomaly (Stead et al., 1977; Leighton, 1981) or following parasitic infections by *Neospora caninum* (Dubey et al., 2007; Jacobson and Jardine, 1993) or *Toxoplasma gondii* (Holliday et al., 1963; Drake and Hime, 1967). The disease has also been reported in humans, but it is very rare; it is classified into three types according to the part of the muscle which is affected (*rectus femori, vastus* and mixed type) (Hagen, 1968; Williams, 1968; Sano and Kokubun, 1985). It is most frequently described in children exposed to repeated intramuscular antibiotic administration into the thighs (Milcan et al., 2004; Hagen, 1968), but congenital cases have also been described (Tercier et al., 2012; Özdemir et al., 2006; Nozawa et al., 2004). In dogs, withdrawal of mechanical loading due to immobilization and lack of weight bearing result in rapid, yet reversible osteoporosis, which is more evident at the limb extremities (Bardet and Hohn, 1983). Muscular atrophy affecting all heads of the quadriceps occurs in few weeks as well, and it is also reversible (Bardet and Hohn, 1983). Irreversible changes occur at the level of the joints, most extensively described in the stifle (Bardet and Hohn, 1983). Two weeks after immobilization a *pannus* appears, progressively replaced by fibrous tissue that reduces the joint space and eventually obliterates the joint cavity after 6-8 weeks. The synovia actively proliferates, the ligaments become weak and the joint capsule thickens. Due to the lack of intraarticular adhesion, prevention of joint motion is attempted through stiff implementation of periarticular structures. The increased intraarticular pressure causes the articular cartilage to undergo fibrillation and deep erosion, finally leading to "pressure necrosis" (Bardet and Hohn, 1983). Quadriceps contracture is diagnosed at clinical examination. Affected dogs typically present with severe hind limb lameness. The affected limb is held in marked rigid extension and is not used during ambulation. At rest, it is carried cranially with respect to the unaffected limb. Both the stifle and the hock cannot be flexed, and the stifle might be bent backward in *genu recurvatum*. The patella is

usually dislocated proximo-medially and marked muscular atrophy is evident. The affected limb may appear shorter due to hip subluxation (Bardet and Hohn, 1983). In human beings, MRI examination of congenitally affected limbs shows muscle volume reduction, fatty atrophy and fibrosis on transverse T1-weighted spin echo and T2-weighted images (Özdemir et al., 2006; Nozawa wt al., 2004). Due to its severe and rapidly developing consequences, early diagnosis and complete evaluation are essential. Treatment options for quadriceps contracture in dogs depend on whether a realistic chance of limb's return to function exists (Moores and Sutton, 2009). When severe and irreversible joint changes are evident, amputation cannot be avoided (Moores and Sutton, 2009). If some remaining joint function is prospected, Z-plasty of the quadriceps has been described (Bardet and Hohn, 1983; Leighton, 1981), without high prognostic expectations. Static (Moores and Sutton, 2009) and dynamic (Wilkens et al., 1993) apparatuses have been proposed, coupled with physical therapy, hydrotherapy, heat therapy and neuromuscular electrical stimulation (Moores and Sutton, 2009). Finally, Hinged Ilizarov external fixation has been successfully used for the correction of post-traumatic quadriceps contracture in one dog and one cat (Carnevale and Jacchetti, 2004).

To the Authors' knowledge, changes occurring to hind limb ossification centres in puppies affected by quadriceps contracture have never been reported. The skeletal system is extremely plastic in young animals and likely to be dramatically affected by muscular contracture. Skeletal maturation, in fact, is a very delicate process and a non-physiological distribution of forces can contribute to the development of skeletal deformities. The aim of this study was to describe the changes caused by quadriceps contracture to the hind limb ossification centres in 13 affected Dobermann littermates, evaluated by Radiography and Computed Tomography. Some degree of shape abnormality was expected. Since compression is known to inhibit bone growth (Hueter-Volkmann law (Villemure and Stokes, 2009)), we also hypothesized a smaller size of the ossification centres exposed to compressive forces generated by quadriceps contracture in the affected limbs.

Methods

Thirteen dead Dobermann puppies affected by quadriceps contracture were examined. All puppies belonged to a single litter; 11 were male and 2 were female. Twelve puppies (11 males and 1 female) were affected by unilateral right-sided contracture (Fig. 1) and were 57 days old at the time of euthanasia; 1 puppy (female) had bilateral contracture and was 55 days old at the time of euthanasia. They were symptomatic since the age of one month and had no history of skeletal trauma. The owner had repeatedly injected all puppies intramuscularly in the same thigh with a non-prescription hydro-soluble drug (Stimulfos, 1ml/10 kg SID for 10 days) due to their poor condition, as suggested by the referring Veterinarian in a similar circumstance for a previous litter. Puppies were referred to the Veterinary Teaching Hospital of the University of Milan for post-mortem examination. The owner authorized in writing the use of the cadavers for research purpose. All puppies underwent a complete radiographic examination of both hind limbs. Radiographic images were acquired with a CR25 ADC AGFA (S.p.A.) assembled with a radiological unit (Simply - Arcom S.r.l. - Italy) using a 0.6 mm focal spot. The focal spot-film distance was 100 cm. For each puppy, ossification centres

were evaluated on orthogonal views (medio-lateral and cranio-caudal/caudo-cranial); the hip was evaluated in ventro-dorsal view. Attention was focused on potential shape abnormalities. All puppies also underwent a CT examination that included the whole hind limbs from the pelvis to the digits. They were positioned in ventral recumbence, with the forelimbs extended cranially and the hind limbs extended caudally, as symmetrically as the muscular contracture allowed. Images were acquired with a 16-slices CT scanner (Ge Brightspeed®, GE Healthcare Milano – Italy), using a bone algorithm. Scanning parameters were set as follows: kV=120, mA=210, slice thickness=1.25 mm, pitch=0.9375. For a better evaluation of the small ossification centres of the feet, the hind paws were also acquired with slice thickness=0.625 mm and pitch=0.5625. All images were reconstructed using smoothing and edge enhancement algorithms, reformatted into 1,25 mm slices in transverse, dorsal and sagittal image planes and viewed in soft tissue and bone windowing, transferred to the picture archiving and communication system (MyPACS – MD Saronno - Italy) and processed with a certified medical software (OsirixPRO 64 Bit; Aycan Medical Systems). Images were reviewed through a 64-bit medical image viewer (Osirix MD™) by a single operator. Hind limb ossification centres were evaluated for both limbs in relation to their presence (present/absent), shape (normal/abnormal, with a brief description of abnormalities) and volume. For volume computation, an appropriate Region Of Interest (ROI) was manually selected on each transverse slice for each ossification centre, to maximally reduce the measurement errors due to automatic segmentation. Volume was then calculated through the "Compute volume" function, selecting all pertinent ROIs for each centre. The distal quadriceps tendon (including the patella and tibial tuberosity) was sampled immediately after euthanasia in 8 dogs for histological/biomechanical evaluation not related to this study; so these centres were only measured in 5 dogs. For the study of hind paws' sesamoid bones, each sesamoid bone was subjectively evaluated in relation to its dimension and attenuation with hard and soft tissues windowing and comprehensively scored 0-3 (0=not visible; 1=barely visible; 2=well visible; 3=completely formed) (Fig. 2). The mean volume of each ossification centre (except for the tibial tuberosity and the patella) and the visibility of hind paws' sesamoids in the affected and unaffected limbs were compared with paired t test or a corresponding non-parametric test, depending on data distribution. A p value <0.05 was considered to be statistically significant. The difference in sesamoids' visibility was first compared considering all digits together, then considering each digit separately. Statistical analyses were performed with a dedicated software (SPSS Statistics 24.0, IBM).

Bone and muscle samples from 3 affected and unaffected puppies were macroscopically evaluated and submitted for histopathologic analysis. Cross-sectional bone specimens were obtained from the femur, at the level of the new bone formation observed at CT examination. Muscle specimens were obtained throughout the whole quadriceps. Bone specimens were fixed in 10% neutral buffered formalin for 48 hours and decalcified in acid solution (1,85% hydrochloric acid and 4% formic acid) for 8 days; muscle specimens were frozen at -20°C, then routinely processed. All samples were paraffin-embedded; 3-μm sections were stained with hematoxylin and eosin (HE) and microscopically evaluated.

Fig. 1 – Clinical presentation of quadriceps contracture (unilateral right-sided contracture in a puppy cadaver). The affected limb is rigidly hyperextended; the stifle and the hock cannot be flexed; the stifle is bent backward in *genu recurvatum*.
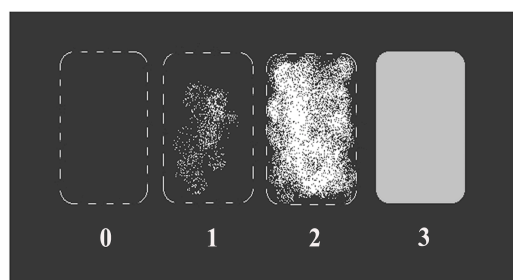

Fig. 2 - Representative images of sesamoid bones' subjective scoring. 0=not visible (the area where the sesamoid should be cannot be distinguished from the adjacent soft tissues); 1=barely visible (small and faint areas of mineralization are recognizable); 2=well visible (the sesamoid bone is clearly but not entirely mineralized, and its margins cannot be identified); 3=completely formed (the sesamoid is completely mineralized, and its margins are well defined).

Results

The affected limbs appeared shorter than the unaffected ones and hyperextended (Fig. 3). The femoral head tended to be subluxated (Fig. 3, Fig. 4) and the stifle was back-turned (Figure3). The patella was subluxated proximo-medially (Figure 3, 3). Time of appearance of all examined ossification centres matched the time reported in literature (Newton and Nunamaker, 1985), in both affected and unaffected limbs.

Few ossification centres exhibited shape abnormalities in all affected limbs, most of which were already evident at the radiographic examination: the femoral head was evidently flattened (Figure 4); the femoral distal epiphysis was slightly flattened and extra-rotated of almost 45° (Figure 5, 6); the tibial plateau was flattened, wedged into the growth plate and slightly tilted caudodorsally-cranioventrally (Figure 5); the proximal tibial epiphysis was slightly bent cranially and the calcaneal tuberosity was slightly misshaped. No other shape abnormalities were evident at the extremities.

The mean volume of each evaluated ossification centre is showed in Appendix 1; differences among the affected and unaffected limbs are depicted in Fig. 7. The ischiatic tuberosity, femoral lesser trochanter and metatarsal I were considered too small to be reliably evaluated.

Among the hind paws' sesamoid bones, only the plantar sesamoids were partially visible. The score assigned to each of them is reported in Appendix 4. Overall, the sesamoids of the affected limbs were less visible than the ones of the unaffected limbs ($p<0.05$). This was due to differences in the II and III digit ($p<0.05$), but not in the IV and V digit (Table 1).

All affected limbs had a solid, slightly irregularly marginated endosteal and periosteal new bone formation along the proximomedial/proximo-caudal surface of the femoral diaphysis (Fig. 3), which corresponded to asymmetric deposition of trabecular bone in the medullary cavity (Fig. 8); the quadriceps muscle was severely hypotrophic. Histopathological examination of affected muscles revealed replacement of the normal muscular architecture by severe interstitial fibrosis (Fig. 9). Muscle fibers were diffusely atrophied and

severely and diffusely dissected by thickened perimiseal septa and by mature collagen deposition (fibrosis). On transverse sections, myocites were severely reduced in size, angulated (severe atrophy) with prominent variation of sizes (diameters). In longitudinal sections, irregular distribution (frequent) or loss of cross striations were variably severe. In lesional skeletal muscleonly occasional nuclear internalization was observed while nuclear rowing was absent (lack of regeneration). Evaluation of the newly formed bone of affected femurs revealed massive endosteal proliferation of non-pathologic and slightly immature trabecular bone, asymmetrically occupying part of the medullary cavity.

Fig. 3 - General features of unilateral quadriceps contracture (radiography). A, affected limb, medio-lateral view; B, both limbs, ventro-dorsal view; C, unaffected limb, medio-lateral view. Due to marked hyperextension, *genu recurvatum* and impossibility to flex the stifle and the hock, the affected limb cannot be positioned properly; the femur is extra-rotated, and the hip is subluxated. A solid, slightly irregularly marginated periosteal new bone formation is visible along the proximomedial surface of the femoral diaphysis (arrow). Bar=1 cm.

Fig. 4 - Hip alterations induced by unilateral quadriceps contracture (computed tomography, Multi Planar Reconstruction). A, affected limb; B, unaffected limb. In the affected limb, the femoral head is smaller, hypodense and flattened (white arrow); the acetabular cavity is also flattened (asterisk) and the hip is subluxated. Bar=1 cm.
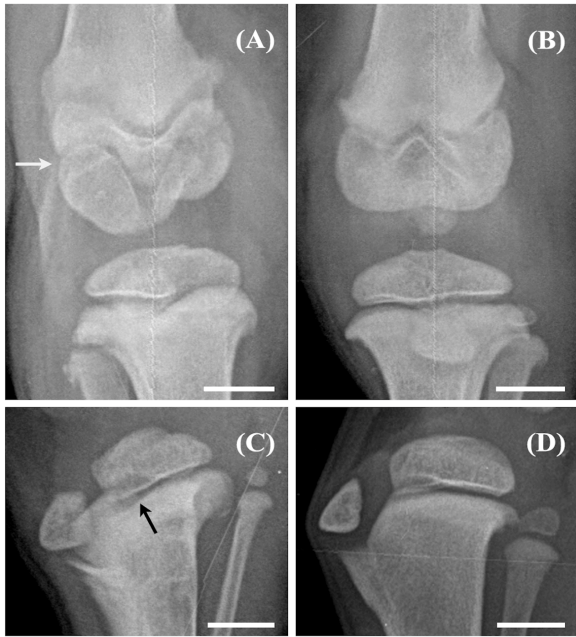
Fig. 5 - Stifle and proximal tibial alterations induced by unilateral quadriceps contracture (radiography). A, affected limb, stifle, caudo-cranial view; B, unaffected limb, stifle, caudo-cranial view. C, proximal tibia, affected limb, medio-lateral view; D, proximal tibia, unaffected limb, medio-lateral view. In the affected limb, the femur is extra-rotated, and the epiphyseal ossification centre appears misshaped (white arrow). The patella cannot be easily identified, and the joint space appears narrowed. The tibial plateau is abnormally shaped and wedged into the growth plate (black arrow).
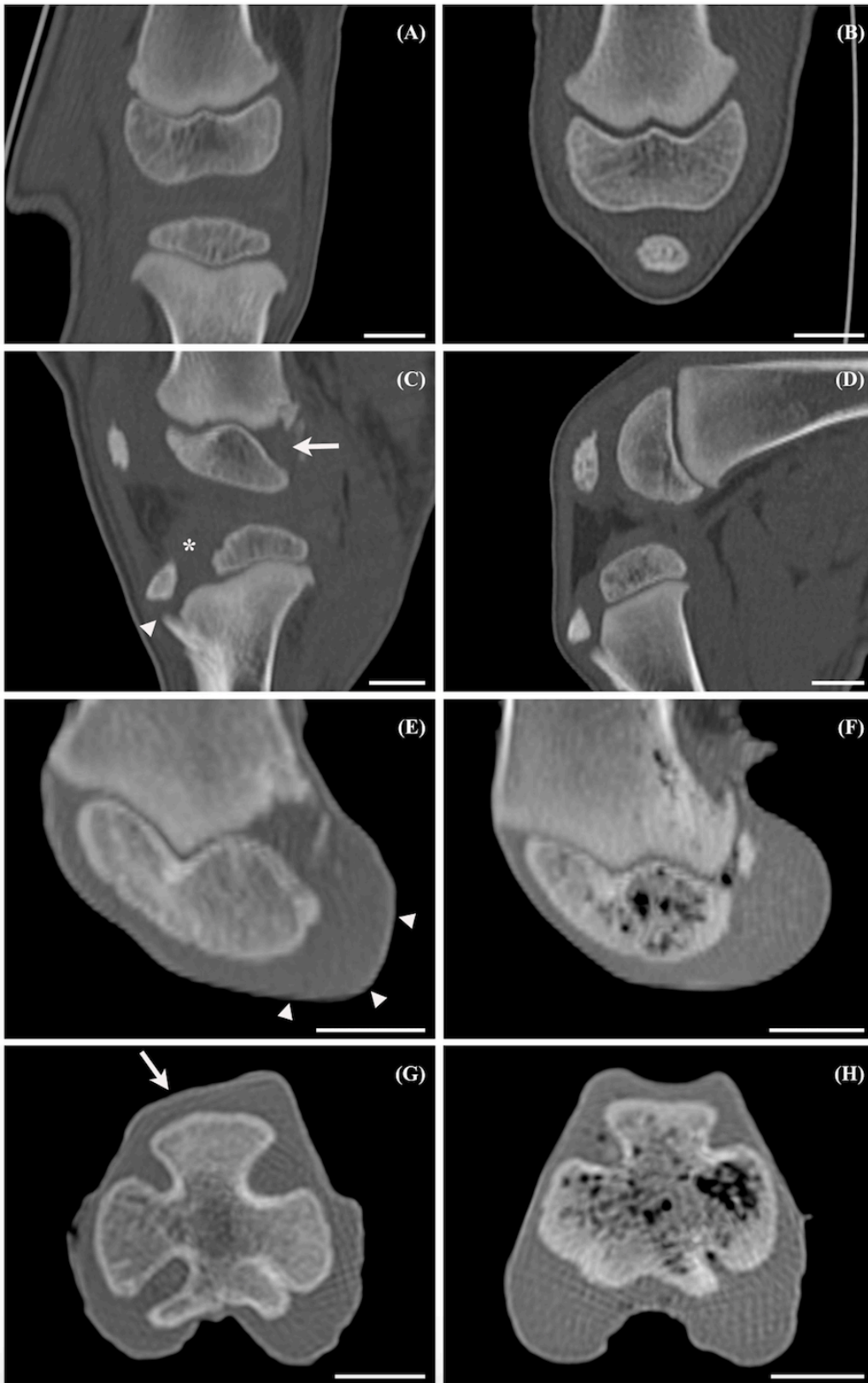
Fig. 6 - Stifle and femoral distal epiphysis' alterations induced by unilateral quadriceps contracture (computed tomography, Multi Planar Reconstruction). A, C, E, G, affected limb; B, D, F, H, unaffected limb. E, F, G, H, isolated bone. A, B, coronal plane. C, D, sagittal plane. E, F, oblique plane passing through the lateral condyle. G, H, transverse plane. Despite its abnormal radiographic appearance, the affected distal epiphysis has a normal general shape, being only flattened proximo-distally, but the distal femur is extra-rotated (C, white arrow); the stifle cannot be flexed and intra-articular soft tissues appear thickened (asterisk). Note the marked flattening of the articular cartilage (E, arrow heads) and femoral trochlea (G, white arrow), which has an oblique slope.
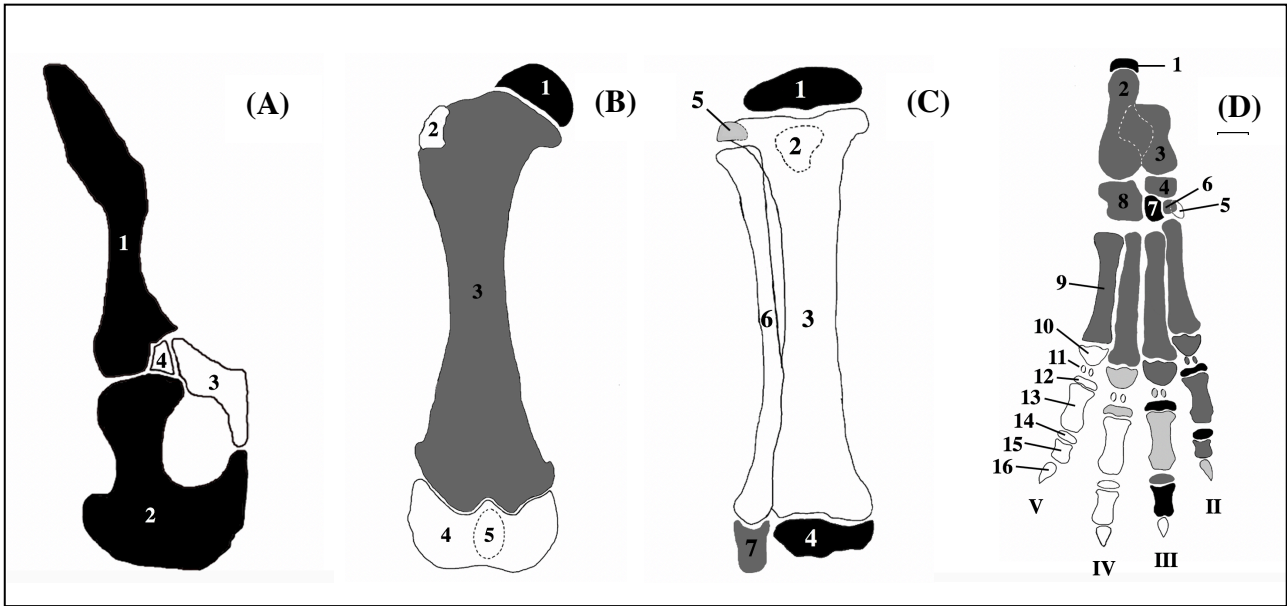
Fig. 7 – Graphical representation of the comparison of the volume of each hindlimb ossification centre among affected and unaffected limb. A=pelvis; B=thigh; C=leg; D=foot. A1=iliac body; A2: ischiatic body; A3: pubis; A4: acetabular bone. B1: femoral head; B2: greater trochanter of the femur; B3: femoral diaphysis; B4: femoral distal epiphysis; B5: patella. C1: tibial plateau; C2: tibial tuberosity; C3: tibial diaphysis; C4: distal epiphysis; C5, C6, C7: fibula; C5: proximal epiphysis; C6: diaphysis; C7: distal epiphysis. D1: calcaneal tuberosity: D2: calcaneal body; D3: talus; D4: central tarsal bone; D5: tarsal bone I; D6: tarsal bone II; D7; tarsal bone III; D8: tarsal bone IV; D9: proximal epiphysis and diaphysis of the metatarsus; D10: distal epiphysis of the metatarsus; D11: plantar sesamoids; D12: proximal epiphysis of the proximal phalanx; D13: distal epiphysis and diaphysis of the proximal phalanx; D14: proximal epiphysis of the middle phalanx; D15: diaphysis and distal epiphysis of the middle phalanx; D16: distal phalanx.
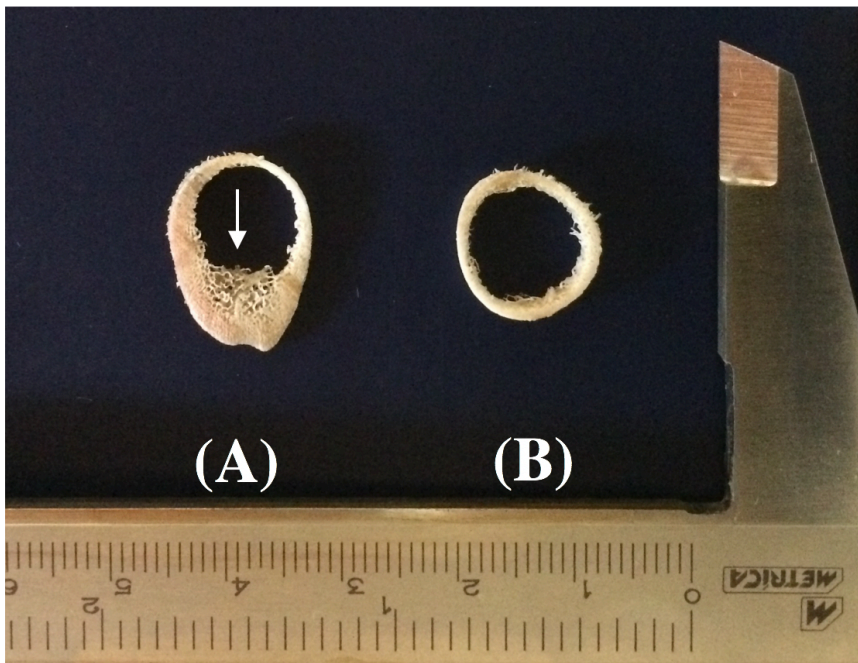

Fig. 8 – Macroscopic features of the new bone formation in the medullary cavity of the femur. A: affected limb; B: unaffected limb. The shape of the diaphysis is slightly irregular; the cortex of the femur of the affected limb shows uneven thickness and there is asymmetric trabecular new bone apposition in the medullary cavity (white arrow). Transverse section of the femoral diaphysis, after the removal of the soft tissues.
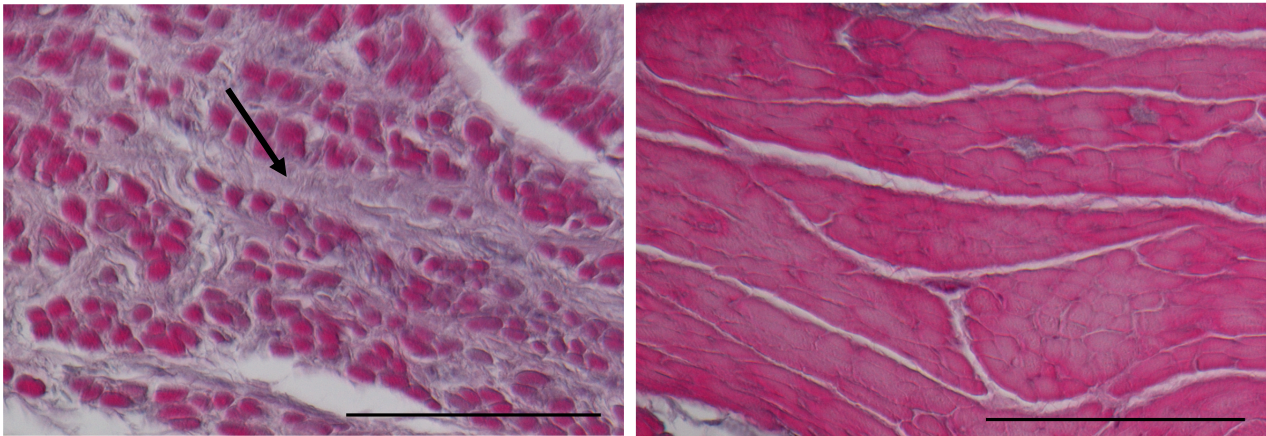
Fig. 9 – Microscopic features of the quadriceps muscle. A: affected; B: unaffected. Normal muscle architecture is replaced by severe interstitial fibrosis in the affected limb. Muscle fibres are atrophied and dissected by thickened perimiseal septa and mature collagen deposition. Myocites are severely reduced in size, angulated, with prominent variation of sizes. Transverse section of the quadricepmuscle, hematoxylin and eosin staini.g; bar: 100 μm.

	Unaffected			Affected			
	median	min	max	median	min	max	*p*
All sesamoids	0	0	2	0	0	2	***
II digit	0	0	2	0	0	1	**
III digit	0	0	2	0	0	2	*
IV digit	0	0	2	0	0	1	NS
V digit	0	0	2	0	0	1	NS

Table 1. Differences in the visibility of plantar sesamoids

Median, minimum and maximum values are reported. *p<0,05; **p<0,01; ***p<0,001; NS=not significant.

Discussion

To the Authors' knowledge, this study describes for the first time the ossification centres' abnormalities induced by quadriceps contracture in the hind limbs of dog puppies.

Radiographic and CT examination confirmed the skeletal deformities previously described in affected dogs (Bardet and Hohn, 1983 and 1984; Bardet, 1987).

The presence of quadriceps contracture did not seem to influence the time of appearance of hind limb ossification centres, since every centre that was supposed to be present at the age of 55-57 days (Newton and Nunamaker, 1985) was constantly recognised.

All the centres of the hip were smaller in the affected limbs, but the difference was significant only for the ischiatic body. The dorsolateral aspect of the acetabular cavity is the area that is believed to receive the highest mechanical stress in normal conditions (Weigel and Wasserman, 1992), so it is likely to be the most affected by loading withdrawal in a non-load bearing limb. In the developing skeleton, this area is mainly occupied by the centre of the ischiatic body. The other centres that contribute to the formation of the acetabular cavity (iliac body, acetabular bone and pubis), have a more medial location: the lack of

mechanical stimulation may have influenced these centres as well (especially the iliac body), but to a lesser extent. The constant compression produced by the *rectus femuri*, which inserts on the ilium, may have caused the flattening and reduced size observed in the femoral head of the affected limbs, as well as flattening of the acetabulum and hip subluxation (Fig. 3, Fig. 4). The abnormal action of this muscular head may be also responsible for the overall hip asymmetry noted in most unilaterally affected puppies. The femoral diaphysis was smaller in the affected limb; on the other hand, although expected, no significant difference in volume was noted for the femoral distal epiphysis, which only appeared moderately flattened. The spaciousness of the stifle joint, together with the possibility of extra-rotation of the distal femur (unable to develop distally), were thought as a possible explanation.

Quadriceps contracture was thought to be responsible for the tibial plateau flattening and wedging into the growth plate (Fig. 5), due to the constant traction produced by the muscle through its distal insertion on the tibial tuberosity. The condition probably caused constant compression on the tibial plateau and progressively complete inability to flex the stifle, finally leading to *genu recurvatum*. The tibial tuberosity was only measured in 5 animals, due to the necessity of sampling part of it together with the patella and the distal quadriceps tendon for reasons unrelated to the present study. No statistical analysis was performed due to the small sample size, but the results of the mean volume evaluation do not suggest a possible difference. While compression is known to inhibit bone growth (Hueter-Volkmann law (Villemure and Stokes, 2009), very little information is available about the effects of traction on physeal growth (Akbas et al., 1995). As well as for the tibial tuberosity, the patella was examined in 5 dogs only: the results of volume evaluation showed a smaller patella in the affected limbs. The patella has a very short timeframe of ossification (Newton and Nunamaker, 1985), that could be responsible for the volume reduction in affected limbs; however, due to the small sample size, this difference was not statistically evaluated. It is worth noticing that the patella showed high degree of mineralization and regular margins in all evaluated limbs: this finding seems to suggest an early development compared to the timeframe reported in literature(Newton and Nunamaker, 1985).

The tibial distal epiphysis was smaller in the affected limbs. Again, the compressive forces produced by the disto-proximal traction from the hyperextended hock were thought to be responsible. The proximal and distal epiphyses of the fibula were also smaller in the affected limbs, probably undergoing the same mechanical stimuli produced on the tibia. The diaphyses of the tibia and fibula were smaller in the affected limbs, but this difference was not significant. The small size and shape of the epiphyseal ossification centres may have made them easier to compress when compared to the diaphyseal centres. On the other hand, the lower size of the femoral diaphysis in the affected limb was thought to be due to the direct and stronger action of the quadriceps on the femur when compared to the tibia/fibula. Although not very evident at the radiographic examination, almost all the centres of the tarsus and metatarsus were smaller in the affected limb. Since the quadriceps has no direct action on the distal part of the limb, the differences observed in this region may be more likely to be produced by the lack of weight bearing. In fact, quadriceps contracture induces a progressive inability to flex the stifle and the hock, to the point that the affected limb at rest is carried cranially, held in rigid extension, and is not used during ambulation (Bardet and Hohn, 1983; Bardet, 1987).

The absence of difference in volume for the I tarsal bone may be caused by its medial location, articulating distally only with the I metatarsal, so that no strong mechanical stimulus acts on it while standing or ambulation.

The differences in volume of the ossification centres of the digits were hypothesized to follow a pathologic load-dependant distribution (Fig. 7). In the affected limbs, all centres of the II and III digit were smaller, except for the diaphysis of the proximal phalanx and the distal phalanx of the III digit; only the epiphysis of the proximal phalanx of the IV digit was smaller; and no differences were noted in the volume of any of the centres of the V digit. Quadriceps contracture induces progressive hyperextension and extra-rotation of the limb, that might be coupled with a gradual withdrawal of loading on the medial aspect of the paw. This may induce a precocious absence of weight bearing on the II and III digits, while the IV and V digits become unloaded later: such progression in asymmetrical loading may explain why differences were observed only in the medial part of the foot. According to literature, only the plantar sesamoids were partially recognisable. Their appearance, in fact, is reported to be between 6 and 15 weeks after birth (Newton and Nunamaker, 1985). Overall, they were less visible in the affected limbs, confirming the hypothesis of a global lack of load-bearing. When evaluated for each digit separately, they followed the trend of the other centres of the digits, being less visible in the II and III digit of the affected paw, but not in the IV and V (Figure 5). These results seem to confirm the hypothesis of uneven loading due to limb extra-rotation.

It is worth noticing that the dramatic alterations described in the ossification centres were evident in puppies that started to show symptoms only one month before this study was performed, when they started to walk around the age of 4 weeks. The extreme plasticity of the skeleton in puppies, in fact, makes them very susceptible to the effects of abnormal forces distribution. The joint degenerative changes induced by quadriceps contracture (especially at the level of the stifle) are described to be even more precocious than the skeletal ones, already appearing 2 weeks after immobilization and rapidly progressing to become irreversible within 6-8 weeks (Bardet and Hohn, 1983). An early diagnosis and a thorough evaluation are therefore mandatory when presented with puppies affected by the disease.

The solid, slightly irregularly marginated periosteal new bone formation noted along the proximo-medial surface of the femoral diaphysis of every affected limb is not reported as a consequence of quadriceps contracture. Since no pathologic features were noted, the newly formed bone was considered to be a biomechanical consequence of the abnormal load distribution in the affected leg, which may have led to asymmetrical deposition and resorption of bone in the medullary cavity of the femur. The cause of the disease could not be definitely elucidated. The presence of almost exclusively unilateral right-sided disease makes a parasitic infection unlikely; moreover, the puppies were tested for *Neospora caninum* and *Toxoplasma gondii* with negative results. The features and location of the periosteal abnormality, together with the history of repeated injections in the same thigh, makes the hypothesis of a iatrogenic disease most likely, as previously demonstrated in children (Hagen, 1968; Milcan et al., 2004). Anyway, although less likely based on history, a congenital form cannot be excluded.

This study has some limitations. CT volume evaluation was performed by a single operator and the measures were not repeated. Together with the difficulties in manual segmentation (especially for the abnormally-shaped and the small-sized centres), this may have influenced the obtained results. The overall visibility of plantar sesamoid bones was evaluated taking subjectively into account their dimension and HU attenuation, and this may have influenced the obtained scores. However, the concordance between the results obtained for the digits' ossification centres and the sesamoid bones seems to suggest reliability of the method. Finally, even if the cause of the disease was not confirmed, it seems unlikely that different causes of quadriceps contracture could produce different effects.

Conclusion

This study describes the abnormalities induced by quadriceps contracture on the hind limb ossification centres of 2-months-old littermate puppies with suspected injection-induced pathology, mainly consisting of volume reduction and abnormal shape of several centres. Together with the degenerative joint changes induced by the disease, previously reported in literature, such alterations should be carefully considered when evaluating puppies affected by the disease to plan a therapy.

References

1. Akbas A, Unsaldi T, Körüklü, Göze F. The effect of physeal traction applied to the triradiate cartilage on acetabular growth. *Int Orthop* 1995;19(2):122-126.
2. Bardet JF and Hohn RB. Subluxation of the hip joint and bone hypoplasia associated with quadriceps contracture in young dogs. *JAAHA* 1984 May/Jun;20(3):421-428.
3. Bardet JF, Hohn RB. Quadriceps contracture in dogs. *JAVMA* 1983 Sep;183(6):680-685.
4. Bardet JF. Quadriceps contracture and fracture disease. *Vet Clin North Am Small Anim Pract* 1987 Jul;17(4):957-973.
5. Braund KG, Shires PK, Mikeal RL. Type I fiber atrophy in the vastus lateralis in dogs with femoral fractures treated by hyperextension. *Vet Pathol* 1980;17:166-177.
6. Carnevale LM, Jacchetti A. Hinged Ilizarov external fixation for correction of post- traumatic quadriceps contracture in one dog and in one cat. Proceedings 12° ESVOT Congress, Münich, 10th-12th September 2004
7. Drake JC, Hime JM. Two Syndromes in Young Dogs Caused by *Toxoplasma Gondii*. *JSAP 1967 Nov;11(8):621-626.*
8. Dubey JB, Vianna MCB, Kwok OCH, Hill DE, Miska KB, Tuo V, Velmurugan GV, Conors M, Jenkins MC. Neosporosis in Beagle dogs: Clinical signs, diagnosis, treatment, isolation and genetic characterization of Neospora caninum. *Vet Parasitol* 2007;149:158–166.
9. Hagen R. Contracture of the quadriceps muscle in children: a report of 12 cases. *Acta Orthop Scand* 1968;39(4):564-578.
10. Holliday TA, Olander HJ, Wind AP. Skeletal muscle atrophy associated with canine toxoplasmosis. A case report. *Cornell Vet* 1963 Apr;53(Apr):288-300.
11. Jacobson LS, Jardine JE. Neospora caninum infection in three Labrador littermates. *J S Afr Vet Assoc* 1993 Mar;64(1):47-51.
12. Leighton RL. Muscle contractures in the limbs of dogs and cats. *Vet Surg* 1981;10(3):132-135.
13. Leighton RL. Quadriceps contracture (ischemic contracture of the quadriceps), in Bojrab M (ed): Pathophysiology in Small Animal Surgery. Philadelphia, Lea and Febiger, 1981, pp550-552.
14. Milcan A, Eskandari MM, Öztuna V, Çolak M, Kuyurtar F. Injection-induced contracture of the quadriceps femoris muscle in children. *Orthopedics* 2004 Jan;27(1):65-66.
15. Moores AP, Sutton A. Management of quadriceps contracture in a dog using a static flexion apparatus and physiotherapy. J Small Anim Pract 2009 May;50(5):251-254.
16. Newton CD, Nunamaker DM Textbook of small animal orthopedics. Philadelphia JB Lippincott Company, 1985; pp1108-1112.
17. Nozawa S, Tanaka C, Shikata J, Yamamuro T. Congenital contracture of the quadriceps muscle: a case report with magnetic resonance imaging. *Arch Orthop Trauma Surg* 2004 May;124(4)272-274.
18. Özdemir O, Atalay A, Çeliker R, Kerimoğlu Ü, Özdemir Ö. Congenital contracture of the quadriceps muscle: confirming the diagnosis with magnetic resonance imaging. Joint Bone Spine 2006 Oct;73(5):554-556.
19. Sano S, Kokubun S. Report of the diagnosis and treatment of muscular contracture – the Ad Hoc Committee of the Japanese Orthopaedic Association of Muscular Contracture. *J Jpn Orthop Ass* 1985;59:223-253.
20. Stead AC, Camburn MA, Gunn HM, Kirk EJ. Congenital hindlimb rigidity in a dog. *J Small Anim Pract* 1977;18:39-46.
21. Tercier S, Shah H, Joseph B Quadriceplasty for congenital dislocation of the knee and congenital quadriceps contracture. *J Child Orthop* 2012 Oct;6(5):397-410.
22. Villemure I, Stokes IA. Growth plate mechanics and mechanobiology. A survey of present understanding. *J Biomech* 2009;42:1793-1803.
23. Weigel JP, Wasserman JF. Biomechanics of the normal and abnormal hip joint. *Vet Clin North Am Small Anim Pract* 1992 May;22(3):513-528.
24. Wilkens BE, McDonald DE, Hulse DA. Utilization of a dynamic stifle flexion apparatus in preventing recurrence of quadriceps contracture: a clinical report. *VCOT* 1993;4:44-48.
25. Williams PF. Quadriceps contracture. *J Bone Joint Surg* 1968 May;50(2):278-284.

BONE	OSSIFICATION CENTRE	Unaffected (n=12)	Affected (n=14)	Significance
Pelvis	Iliac body	6,99 (6,22-7,16)	7,61 (6,44-8,15)	***
	ischiatic body	4,82 (4,31-5,19)	4,10 (3,45-4,31)	***
	acetabular bone	0,14 (0,11-0,20)	0,13 (0,09-0,19)	NS
	pubis	0,68 (0,56-0,78)	0,67 (0,50-0,88)	NS
	ischiatic tuberosity	Not evaluable		
Femur	head	1,22 (1,06-1,46)	0,84 (0,64-1,25)	***
	greater trochanter	0,16 (0,11-0,20)	0,15 (0,07-0,18)	NS
	lesser trochanter	Not evaluable		
	diaphysis	15,25 (13,03-17,32)	14,21 (12,67-15,72)	**
	distal epiphysis (fused)	3,74 (2,82-4,46)	3,84 (2,21-4,96)	NS
Stifle sesamoids	patella (n=5 per group)	0,41 (0,22-0,46)	0,26 (0,24-0,31)	Not evaluated
Tibia	plateau	2,13 (1,79-2,63)	1,72 (1,89-2,26)	***
	tuberosity (n=5 per group)	0,28 (0,21-0,33)	0,27 (0,14-0,35)	Not evaluated
	diaphysis	11,63 (11,01-13,28)	11,58 (9,55-13,46)	NS
	distal epiphysis	1,67 (1,38-1,84)	1,20 (1,00-1,51)	***
Fibula	proximal epiphysis	0,06 (0,03-0,10)	0,03 (0,02-0,10)	*
	diaphysis	1,49 (1,32-1,76)	1,34 (1,16-1,95)	NS
	distal epiphysis	0,44 (0,35-0,51)	0,36 (0,27-0,47)	**
Tarsus	calcaneal tuberosity	0,29 (0,21-0,43)	0,24 (0,15-0,31)	***
	calcaneal body	3,90 (3,58-4,28)	3,04 (2,40-3,71)	**
	talus	1,94 (1,69-2,23)	1,46 (1,12-1,93)	**
	central tarsal bone	0,58 (0,48-0,68)	0,41 (0,25-0,59)	***
	tarsal bone I	0,06 (0,04-0,08)	0,07 (0,05-0,09)	NS
	tarsal bone II	0,07(0,06-0,09)	0,05 (0,03-0,06)	**
	tarsal bone III	0,43 (0,36-0,49)	0,32 (0,20-0,40)	**
	tarsal bone IV	1,35 (1,21-1,49)	1,04 (0,79-1,28)	**
Metatarsus I		Not evaluable		
Metatarsus II	diaphysis and proximal epiphysis	1,23 (1,15-1,45)	1,10 (0,79-1,32)	**
	distal epiphysis	0,28 (0,23-0,31)	0,24 (0,17-0,26)	**
Metatarsus III	diaphysis and proximal epiphysis	1,66 (1,56-1,81)	1,49 (1,14-1,74)	**
	distal epiphysis	0,47 (0,37-0,50)	0,40 (0,26-0,47)	**
Metatarsus IV	diaphysis and proximal epiphysis	1,65 (1,44-1,75)	1,46 (1,12-1,57)	**
	distal epiphysis	0,43 (0,34-0,48)	0,39 (0,27-0,46)	*
Metatarsus V	diaphysis and proximal epiphysis	1,29 (1,10-1,47)	1,16 (0,91-1,34)	**
	distal epiphysis	0,27 (0,23-0,32)	0,25 (0,21-0,29)	
Proximal phalanx II	proximal epiphysis	0,09 (0,08-0,10)	0,07 (0,05-0,08)	***
	diaphysis and distal	0,34 (0,32-0,41)	0,32 (0,24-0,36)	**

	epiphysis			
Proximal phalanx III	proximal epiphysis	0,13 (0,10-0,15)	0,10 (0,07-0,13)	***
	diaphysis and distal epiphysis	0,47 (0,44-0,55)	0,46 (0,34-0,49)	*
Proximal phalanx IV	proximal epiphysis	0,12 (0,08-0,14)	0,11 (0,07-0,13)	*
	diaphysis and distal epiphysis	0,45 (0,42-0,50)	0,45 (0,36-0,50)	NS
Proximal phalanx V	proximal epiphysis	0,09 (0,06-0,10)	0,08 (0,06-0,10)	NS
	diaphysis and distal epiphysis	0,31 (0,28-0,35)	0,31 (0,27-0,35)	NS
Middle phalanx II	proximal epiphysis	0,05 (0,04-0,05)	0,04 (0,03-0,05)	***
	diaphysis and distal epiphysis	0,12 (0,11-0,14)	0,12 (0,09-0,13)	**
Middle phalanx III	proximal epiphysis	0,08 (0,07-0,10)	0,07 (0,04-0,09)	**
	diaphysis and distal epiphysis	0,18 (0,15-0,20)	0,16 (0,13-0,18)	***
Middle phalanx IV	proximal epiphysis	0,07 (0,06-0,09)	0,07 (0,04-0,08)	NS
z	diaphysis and distal epiphysis	0,17 (0,16-0,20)	0,17 (0,13-0,20)	NS
Middle phalanx V	proximal epiphysis	0,05 (0,04-0,05)	0,04 (0,03-0,05)	NS
	diaphysis and distal epiphysis	0,12 (0,11-0,13)	0,11 (0,10-0,14)	NS
Distal phalanx II		0,09 (0,06-0,10)	0,08 (0,06-0,09)	*
Distal phalanx III		0,09 (0,07-0,11)	0,08 (0,06-0,10)	NS
Distal phalanx IV		0,09 (0,06-0,10)	0,08 (0,07-0,09)	NS
Distal phalanx V		0,07 (0,05-0,08)	0,07 (0,06-0,09)	NS

Appendix 1 - Results of the evaluation of hindlimb ossification centres. The volume (cm³) is provided as median value (min-max) for each centre. *p<0,05; **p<0,01; ***p<0,001; NS=not significant.

7. GENERAL DISCUSSION

With this project literature gaps about the normal features of bone in experimental animals, specific decalcification protocols in different species and skeletal development in dogs were filled. For these studies, cadavers were recycled, embracing the 3Rs principle.

The bone is a highly specialized connective tissue, specifically designed for structural, mechanical and metabolic functions. Due to the peculiar composition of its matrix, characterised by high mineral content in a densely packed network of collagenous and non-collagenous components, preparation of bone samples is a laborious process, especially when decalcification is approached (Liu et al., 2017). In particular, preserving both good morphology and antigenicity after decalcification is very challenging. The comparison of three different acid solutions (strong acid, weak acids, strong and weak acids combined) allowed to define basic guidelines for the decalcification of trabecular bone specimens from 5 different animals species. To our knowledge, no previous studies were performed which compared decalcification time and results in different species. Canine bone was decalcified significantly more slowly when compared to other species. Because of the signs of skeletal immaturity found in rodents' and pigs' samples, age-related differences were hypothesized: "young" bone, in fact, may be more sensitive to the action of decalcification solutions. However, although skeletally mature, sheep samples were decalcified in a significantly slower time when compared to dogs. While the reason for this result is not known, low bone BMD could be responsible for the difference: in fact, BMD changes in sheep based on the season (Arens et al., 2006), and the sheep used for this experiment were euthanized at the end of the winter, when BMD is lower (Arens et al., 2006). Overall, it was only possible to define approximate time protocols, because of the high standard error obtained with all solutions in all species. This could be due to interindividual variability, intraindividual regional variability (e.g. the bone/the part of bone considered), or to an internal bias in subjectively determining when the sample was ready to be processed. Even if different options exist for such evaluation (Mattuella et al., 2007; Verdenius and Alma, 1958; Guibas et al., 2014), in fact, it was chosen to base the decision on visual inspection and cutting with blade, a costless and easily repeatable method in everyday laboratory practice. The study confirmed that hydrochloric acid alone, although significantly faster than weak acids solutions, is not recommended for decalcification when good tissue morphology is needed. In fact, rapid deterioration of bone was noted with 10% hydrochloric acid. However, it must be underlined that excellent morphology was occasionally achieved in mice: this solution might therefore represent a valid alternative in this species, but very strict monitoring would be required. On the other hand, hydrochloric acid led to excellent results when combined with formic acid, as previously described for teeth (Silva et al., 2012): this combination allowed to obtain excellent morphology in mice, rats and pigs. Weak acids alone allowed to obtain good/excellent morphology in all species, at the expense of decalcification time: this should be carefully considered during experimental planning, as it could take several weeks and multiple renewals for these solutions to be effective. When testing the effect of the combination of decalcification solution and time on tissue morphology, high scores were obtained in mice and rats with 1,85% hydrochloric acid and 4% formic acid in

relatively short time (0-4 days in mice, 0-8 days in rats); similar results were obtained in mice also with 10% hydrochloric for 0-4 days. However, a very fast decline in score was noted with time progression, confirming its difficult handling. Excellent morphology, on the other hand, could never be achieved with 10% hydrochloric acid in mammalian specimens at any time. Immunolocalization of Collagen I allowed to test the preservation of tissue antigenicity: preliminary results agreed with the morphologic score; further experiments, however, need to be performed to confirm these results.

The peculiar composition of bone, which makes it so difficult to process, is responsible for its fundamental properties (such as density and mechanical behaviour), together with its microscopical tri-dimensional organisation. A multidisciplinary approach was proposed for the study of basic bone features in sheep and pigs, selected because of their common use as models in orthopaedic research. When approaching the design of bone substitutes or the evaluation of their efficacy, safety and biocompatibility in preclinical trials, in fact, none of basic bone features can be left behind without the risk of precluding results reliability. The bone is a very complex and metabolically active tissue, and each of its properties and functions, which have specific influence on its final performance as a whole, can be optimally tested with a specific method. In particular, microscopic organisation of cortical and trabecular bone can be evaluated with histomorphometry (Kang et al., 1998; Dalle Carbonare et al., 2005) and microCT (Faulkner et al., 1991; Odgaard, 1997; Müller et al., 1998; Hildebrand, et al., 1999; Chappard et al., 2005; Parr et al., 2012; Depalle et al., 2012), respectively; the amount of mineral inorganic components, represented by Bone Mineral Density, can be accurately evaluated with Dual-energy X-Rays Absorptiometry (Grier et al., 1996; Turner et al. 1995; Pouilles et al., 1999; Wu et al., 2014; den Boer et al., 1999; Floerkemeier et al., 2010; Heiss et al., 2017); and its biomechanical quality can be assessed with several different biomechanical tests, such as flexion and compression tests (Turner and Burr, 1993; Goodyear and Aspden, 2012). Basic parameters for each of these features were provided for both pigs and sheep; although based on a small sample, they could represent a baseline for future studies on these species. Interestingly, due to their skeletal immaturity, two different types of trabecular bone were found at each side of swine growth plates, which showed slight differences in spatial organisation (e.g. different porosity), reflected also in their BMD and mechanical behaviour. These results highlight the crucial importance of the choice of animal models for preclinical studies based on their body weight: in fact, pigs weighting 70-80 kg (often used as orthopaedic models) are far from being skeletally mature, and this can have important implications on results interpretation. Advantages and limitations of each employed technique were analysed, highlighting the importance of a consistent and combined approach to such a problematic tissue.

As demonstrated in the studies on the bone tissue in sheep and pigs and decalcification, although imaging techniques allow to study the bone precisely describing its tri-dimensional organisation, histology is fundamental for the evaluation of tissue microscopic morphology and composition. However, histologic analysis requires invasive sampling procedures, which make it unsuitable for *in vivo* studies. Once again, the use of cadavers for this type of studies proved to be a valid alternative, allowing to better understand limb

and skull development in dogs. With this research, results from a previous study on endochondral ossification in small-sized dogs performed in our laboratory (Modina et al., 2017) were confirmed. Bone growth starts during the fetal stage and continues after birth until complete skeletal maturity is reached. In the histogenesis of bone, an immature type of bone (woven bone) is initially formed, which is then replaced by secondary bone through intramembranous (e.g. flat bones of the skull) or endochondral (e.g. long bones) ossification (Webster, 1988). Perichondrium-derived tube-shaped formations called cartilage canals are involved in epiphyseal growth, supplying nutrients to the growing cartilage and eliminating waste products elimination (Wilsman and Van Sickle, 1970; Wilsman and Van Sickle, 1972; Blumer et al., 2005; Alvarez et al., 2005; Blumer et al., 2007; Blumer et al., 2006;; Olstad, 2007). Differently from what has been described in other species (Kulger et al., 1979; Cole and Wezeman, 1987; Shapiro, 1998; Rivas and Shapiro, 2002; Blumer et al., 2007; Blumer et al., 2008)), we confirmed that cartilage canals appear in canine humerus and femur before birth, as previously reported (Wilsman and Van Sickle, 1970; Wilsman and Van Sickle, 1972). Moreover, cartilage canals' number tended to be higher in the humerus, suggestinga a greater metabolic intake that, in turn, may induce a more rapid maturation of the secondary ossification centre observed in the humerus and femur. From birth to the age of about one month, newborns' ability to stand and walk increases in a cranio-caudal way, starting from the thoracic limbs (Peterson and Kutzler, 2011), so the humerus undergoes mechanical stimulation earlier as compared to the femur. This could turn in a earliest formation of the secondary ossificationc centre (Peinado Cortes et al., 2011). Histochemical studies showed that cartilage canals were surrounded by a connective tissue ring which changed in color from green to red as age increased, indicating collagen fibers maturation. A positive label for collagen type I was also found in cartilage canals, while no collagen II was found in the ring around the cartilage canals: these findings were in agreement with the rersults of Safranin-O staining, and suggest that the mesenchymal cells are involved in the production of bone extracellular matrix (Blumer et al., 2007); however, it does not explain the color changes found in collagen fibres, suggesting that other molecules may be involved in the development of secondary ossification centres. Collagen V, is a minor component of connective tissues that are rich in collagen type I, was also localized for the first time in this study near the cartilage canals Little is known about the role of collagen V in developing bones: it might play a role in bone brittleness interfering with mineralization (Bonaventure et al., 1989) and/or be involved in osteogenesis (Roulet et al., 2007; Kahai et al., 2004; Yamaguchi et al., 2005). These data, although preliminary, lay the basis for more extensive studies on the delicate mechanisms that modulate endochondral bone development also in the context of the growth disorders affecting the proximal femoral epiphysis of small-sized breeds dogs (Scherzer et al., 2009).

Not only long bones development, but also skull development is very complex in dogs, as the bones of the skull have different origines (intramembranous ossification for the face and flat calvarial bones; endochondarl ossification for the bones of the floor and ventral portion of the cranial vault) (Evans, 1993; Hyttel, 2010). To our knowledge, it is not known whether the shape of the skull of adult dogs is already recognisable at birth or whether it develops later in life. With the aim to enlight skull development patterns, differences in skull shape in newborn dogs belonging to brachycephalic, mesaticephalic and dolichocephalic

breeds (Evans, 1993) were investigated with anatomic and radiographic approach (linear cranial measures and cranial indices) in a large sample (137 animals). Linear measures almost constantly identified two major morphologic groups (brachycephalic vs non-brachycephalic morphotype), while contrasting results about the indices were obtained with anatomic and radiographic methods: in fact, while anatomic indices highlighted differences in skull conformation without clear identification of separate categories, almost all radiographic indices constantly distinguished among three categories (brachycephalic, mesaticephalic and dolichocephalic). Moreover, since radiographic examination is an invasive procedure (especially in newborns and puppies), an attempt to find a close correlation between anatomic and radiographic skull measures was made. However, results indicate that anatomic and radiographic methods cannot be used interchangeably, likely due to the presence of soft tissues that make radiographic and anatomic landmarks markedly different. Finally, neural nets were employed in attempt to classify 19 puppies belonging to previously unclassified breeds, providing a categorization with high probability for most of them. Although growing animals cannot perfectly fit the static nature of the method (the skull does not grow in all directions at the same time, so the classification determined at birth could be contradicted by what determined during other periods of skull growth), neural nets could represent a useful define both puppies' and adults' morphotypes.

Finally, the effects of pathology on skeletal development were studied in a litter of 2-months-old Dobermann Pinscher affected by quadriceps contracture. Since skeletal maturation is a very delicate and plastic process and a non-physiological distribution of forces can substantially contribute to the development of skeletal deformities, it may be dramatically affected by muscular contracture. To evaluate this hypothesis, the effects of quadriceps contracture on the time of appearence, shape and volume of hindlimb ossification centres were decsribed. The presence of quadriceps contracture did not seem to influence the time of appearance of the ssification centres of the pelvic limb, but several centres were smaller and/or misshaped in affected legs: the constant compression produced by the contracture of the different portions of the quadriceps muscle was thought to be responsible for these changes. In general, epiphyseal centres were more affected than diaphyseal ones, probably due to their small size, shape and location, which may have made them easier to compress when compared to the diaphyseal ones. Rectus femori contracture was thought to be responsible for femoral head/acetabulum flattening and hip subluxation, as well as for the overall hip asymmetry noted in the puppies. The constant traction produced by quadriceps distal insertion on the tibial tuberosity was thought to be responsible for the observed tibial plateau flattening, also causing progressively complete inability to flex the stifle (genu recurvatum). The compressive forces produced by the disto-proximal traction from the hyperextended hock were thought to be responsible for the abnormalities noted in the distal tibia. A different pathogenetic pattern (lack of weight-baring) was hypothesized to be responsible for the abnormalities noted in the distal part of the limb. In fact, quadriceps contracture induces a progressive inability to flex the stifle and the hock, to the point that the affected limb at rest is carried cranially, held in rigid extension, and is not used during ambulation. The differences in volume of the ossification centres of the digits were thought to follow a pathologic load-dependant distribution: hyperextension and extra-rotation

of the limb, in fact, might be coupled with a gradual withdrawal of loading on the medial aspect of the paw, which may induce a precocious absence of weight bearing on the medial digits (which were found to be smaller), while lateral digits become unloaded later. It is worth noticing that the severe alterations described in the ossification centres were evident in puppies that started to show symptoms only one month before this study was performed. Importantly, joint degenerative changes induced by quadriceps contracture have been described to be even more precocious than the skeletal ones, becoming irreversible within 6-8 weeks (Bardet and Hohn,1983). An early diagnosis and a thorough evaluation are therefore mandatory.

References

1. Arens D, Sigrist I, Alini M, Schawalder P, Schneider E, Egermann M. Seasonal changes in bone metabolism in sheep. Vet J. 2007 Nov;174(3):585-91. Epub 2006 Dec 1.
2. Bardet JF and Hohn RB. Subluxation of the hip joint and bone hypoplasia associated with quadriceps contracture in young dogs. JAAHA 1984 May/Jun;20(3):421-428.
3. Blumer MJ, Fritsch H, Pfaller K, Brenner E. Cartilage canals in the chicken embryo: ultrastructure and function. Anat Embryol (Berl) 2004;207(6):453-62.
4. Blumer MJ, Longato S, Fritsch H. Localization of tartrate-resistant acid phos- phatase (TRAP), membrane type-1 matrix metalloproteinases (MT1-MMP) and macrophages during early endochondral bone formation. J Anat 2008;213:431-41.
5. Blumer MJ, Longato S, Richter E, Perez MT, Konakci KZ, Fritsch H. The role of car- tilage canals in endochondral and peri- chondral bone formation: are there simi- larities between these two processes? J Anat 2005;206:359-72.
6. Blumer MJ, Longato S, Schwarzer C, Fritsch H. Bone development in the femoral epiphysis of mice: the role of car- tilage canals and the fate of resting chon- drocytes. Dev Dyn 2007;236:2077-88
7. Blumer MJ, Longato S, Schwarzer C, Fritsch H. Bone development in the femoral epiphysis of mice: the role of car- tilage canals and the fate of resting chon- drocytes. Dev Dyn 2007;236:2077-88.
8. Blumer MJ, Schwarzer C, Perez MT, Konakci KZ, Fritsch H. Identification and location of bone-forming cells within carti- lage canals on their course into the sec- ondary ossification centre. J Anat 2006;208: 695-707.
9. Bonaventure J, Zylberberg L, Cohen-Solal L, Allain JC, Lasselin C, Maroteaux P. A new lethal brittle bone syndrome with increased amount of type V collagen in a patient. Am J Med Genet 1989;33:299-310.
10. Chappard D, Retailleau-Gaborit N, Legrand E, Baslé MF, Audran M. Comparison insight bone measurements by histomorphometry and microCT. J Bone Miner Res. 2005 Jul;20(7):1177-84. Epub 2005 Feb 14.
11. Cole AA, Wezeman FH. Morphometric analysis of cartilage canals in the develop- ing mouse epiphysis. Acta Anat 987;128:93-7.
12. Dalle Carbonare L, Valenti MT, Bertoldo F, Zanatta M, Zenari S, Realdi G, Lo Cascio V, Giannini S. Bone microarchitecture evaluated by histomorphometry.Micron. 2005;36(7-8):609-16. Epub 2005 Sep 6.
13. den Boer FC, Patka P, Bakker FC, Wippermann BW, van Lingen A, Vink GQ, Boshuizen K, Haarman HJ. New segmental long bone defect model in sheep: quantitative analysis of healing with dual energy x-ray absorptiometry. J Orthop Res. 1999 Sep;17(5):654-60.
14. Depalle B, Chapurlat R, Walter-Le-Berre H, Bou-Saïd B, Follet H. Finite element analysis dependence of stress evaluation for human trabecular bone. J Mech Behav Biomed Mater. 2013 Feb;18:200-12. doi: 10.1016/j.jmbbm.2012.08.012. Epub 2012 Nov 21.
15. Evans H, editor: The Skeleton. Miller's Anatomy of the Dog, ed 3, Philadelphia, 1993, Saunders.
16. Evans HE, De Lahunta A. Miller's Anatomy of the Dog. Fourth edition ed. St Louis (MO) USA: Saunders/Elsevir; 2013.
17. Faulkner KG, Cann CE, Hasegawa BH. Effect of bone distribution on vertebral strength: assessment with patient-specific nonlinear finite element analysis. Radiology. 1991 Jun;179(3):669-74.
18. Floerkemeier T, Wellmann M, Thorey F, Hurschler C, Witte F, Windhagen H. Comparison of bone mineral parameter measurements by dual-energy x-ray absorptiometry with bone stiffness measurements as indicators of the load-bearing capacity of regenerating bone. J Orthop Trauma. 2010 Mar;24(3):181-7. doi: 10.1097/BOT.0b013e3181bae887.
19. Gelse K, Poschl E, Aigner T. Collagens - structure, function, and biosynthesis. Adv Drug Deliv Rev 2003;55:1531-46.
20. Goodyear SR, Aspden RM. Mechanical properties of bone ex vivo. Methods Mol Biol. 2012;816:555-71. doi: 10.1007/978-1-61779-415-5_35.
21. Grier SJ¹, Turner AS, Alvis MR. The use of dual-energy x-ray absorptiometry in animals. Invest Radiol. 1996 Jan;31(1):50-62.
22. Grier SJ¹, Turner AS, Alvis MR. The use of dual-energy x-ray absorptiometry in animals. Invest Radiol. 1996 Jan;31(1):50-62.

23. Guibas GV, Lakis S, Gkimpas C, Manda M, Kapoukranidou D, Spandou E. Efficiency of different decalcification protocols for nasal osseous structures in a rat experimental model of allergic rhinitis, and their effects on epithelial histology: an attempt at standardization. Exp Toxicol Pathol. 2014 Dec;66(9-10):469-75. doi: 10.1016/j.etp.2014.09.001. Epub 2014 Sep 18.

24. Heiss C, Kern S, Malhan D, Böcker W, Engelhardt M, Daghma DES, Stoetzel S, Schmitt J, Ivo M, Kauschke V, Lips KS, Tushtev K, Rezwan K, El Khassawna T. A New Clinically Relevant T-Score Standard to Interpret Bone Status in a Sheep Model. Med Sci Monit Basic Res. 2017 Oct 2;23:326-335.

25. Hildebrand T, Laib A, Müller R, Dequeker J, Rüegsegger P. Direct three-dimensional morphometric analysis of human cancellous bone: microstructural data from spine, femur, iliac crest, and calcaneus. J Bone Miner Res. 1999 Jul;14(7):1167-74.

26. Hyttel, P., Sinowatz, F., Vejlsted, M., 2010. Essentials of Domestic Animal Embryology.

27. Kahai S, Vary CP, Gao Y, Seth A. Collagen, type V, alpha1 (COL5A1) is regulated by TGF-beta in osteoblasts. Matrix Biol 2004;23:445-55.

28. Kang Q, An YH, Butehorn HF, et al: Morphological and mechanical study of the effects of experimentally induced inflammatory knee arthritis on rabbit long bones. J Mater Sci Mater Med 9:463–473, 1998.

29. Kugler JH, Tomlinson A, Wagstaff A, Ward SM. The role of cartilage canals in the for- mation of secondary centres of ossifica- tion. J Anat 1979;129):493-506.

30. Liu H, Zhu R, Liu C, Ma R, Wang L, Chen B, Li L, Niu J, Zhao D, Mo F, Fu M, Brömme D, Zhang D, Gao S. Evaluation of Decalcification Techniques for Rat Femurs Using HE and Immunohistochemical Staining. Biomed Res Int. 2017;2017:9050754. doi: 10.1155/2017/9050754. Epub 2017 Jan 26.

31. Mattuella LG, Bento LW, Vier-Pelisser FV, Araujo FB, Fossati ACM. Revista Odonto Ciência – Fac. Odonto/PUCRS, v. 22, n. 56, abr./jun. 2007 Verdenius HH; Alma L. A quantitative study of decalcification methods in histology. J Clin Pathol. 1958 May;11(3):229-36.

32. Müller R, Van Campenhout H, Van Damme B, Van Der Perre G, Dequeker J, Hildebrand T, Rüegsegger P. Morphometric analysis of human bone biopsies: a quantitative structural comparison of histological sections and micro-computed tomography. Bone. 1998 Jul;23(1):59-66.

33. Odgaard A. Three-dimensional methods for quantification of cancellous bonearchitecture. Bone. 1997 Apr;20(4):315-28.

34. Olstad K, Ytrehus B, Ekman S, Carlson CS, Dolvik NI. Early lesions of osteochondrosis in the distal tibia of foals. J Orthop Res 2007;25:1094-105.

35. Parr WC, Chamoli U, Jones A, Walsh WR, Wroe S. Finite element micro-modelling of a human ankle bone reveals the importance of the trabecular network to mechanical performance: new methods for the generation and comparison of 3D models. J Biomech. 2013 Jan 4;46(1):200-5. doi: 10.1016/j.jbiomech.2012.11.011. Epub 2012 Dec 4.

36. Peinado Cortes LM, Vanegas Acosta JC, Garzon Alvarado DA. A mechanobiological model of epiphysis structures formation. J Theor Biol 2011;287:13-25.

37. Peterson ME, Kutzler MA. Small animal pediatrics: the first 12 months of life. Elsevier-Saunders, St. Louis, MO, USA; 2011.

38. Pouilles JM¹, Collard P, Tremollieres F, Frayssinet P, Railhac JJ, Cahuzac JP, Autefage A, Ribot C. Accuracy and precision of *in vivo* bone mineral measurements in sheep using dual-energy X-ray absorptiometry. Calcif Tissue Int. 2000 Jan;66(1):70-3.

39. Rivas R, Shapiro F. Structural stages in the development of the long bones and epiphy- ses: a study in the New Zealand white rab- bit. J Bone Joint Surg Am 2002;84-A:85-100.

40. Roulet M, Ruggiero F, Karsenty G, LeGuellec D. A comprehensive study of the spatial and temporal expression of the col5a1 gene in mouse embryos: a clue for understanding collagen V function in developing connective tissues. Cell Tissue Res 2007;327:323-32.

41. Scherzer C, Windhagen H, Nellesen J, Crostack HA, Rohn K, Witte F, et al. Comparative structural analysis of the canine femoral head in Legg-Calve- Perthes disease. Vete Radiol Ultrasound 2009;50:404-11.

42. Shapiro F. Epiphyseal and physeal carti- lage vascularization: a light microscopic and tritiated thymidine autoradiographic study of cartilage canals in newborn and young postnatal rabbit bone. Anat Rec 1998;252:140-8.

43. Silva A, Rici REG, Neto AA: Techniques used for morphological and ultrastructural description from teeth white-tufted.ear-marmosets (Callithrix jacchus), 2012.

44. Turner CH[1], Burr DB. Basic biomechanical measurements of bone: a tutorial. Bone. 1993 Jul-Aug;14(4):595-608.

45. Webster S. S. J. The skeletal tissue; in Cell and tissue biology. Leon Weiss Editor, 1988, sixth edition, Urban and Schwarzenberg, Germany

46. Wilsman NJ, Van Sickle DC. Cartilage canals, their morphology and distribution. Anat Rec 1972;173:79-93.

47. Wilsman NJ, Van Sickle DC. Cartilage canals, their morphology and distribution. Anat Rec 1972;173:79-93.

48. Wilsman NJ, Van Sickle DC. The relation- ship of cartilage canals to the initial osteo- genesis of secondary centers of ossifica- tion. Anat Rec 1970;168:381-91.

49. Wu S, Liu X, Yeung K, Liu C, Yang X. Biomimetic porous scaffolds for bone tissue engineering. Materials Science and Engineering, 2014: R: Reports. 80. 1–36. 10.1016/j.mser.2014.04.001.

50. Yamaguchi K, Matsuo N, Sumiyoshi H, Fujimoto N, Iyama KI, Yanagisawa S, et al. Pro-alpha3(V) collagen chain is expressed in bone and its basic N-terminal peptide adheres to osteosarcoma cells. Matrix Biol 2005;24:283-94.

8. GENERAL CONCLUSION

This project grounds on the idea of cadaver recycle for research purposes. In fact, the use of cadavers allows to spare experimental animals and embraces the 3Rs principle (Replace, Reduct, Refine). All the bone specimens for these studies were collected from slaughterhouses, from laboratories after euthanasia for unrelated experiments or donated by private owners prior their informed consent. The bone, in fact, is very easy to study in cadavers since it suffers the early consequences of post-mortal decay to a lesser extent compared to other tissues. The bone is a highly specialized connective tissue, specifically designed for structural, mechanical and metabolic functions. Therefore, its structural, densitometric, compositional and biomechanical features depend on animal species, size and age, as well as on the specific bone that is considered. Moreover, literature gaps in specific patterns of skeletal development in dogs (e.g. limb and skull development) and the possible effect of pathological conditions on skeletal growth still exist.

With this project we confirmed that cadavers are an invaluable source of research material, providing a valid alternative to *in vivo* experiments and contributing to the reduction of the use of experimental animals. This was proved both for the study of skeletal development in dogs and the basic features of the bone tissue in experimental animals.

A multidisciplinary approach to the study of the bone in pigs and sheep was developed, evaluating several different parameters with different techniques on the same samples. This approach is crucial because it allows to elucidate all the fundamental features of the bone at once, in order to avoid omissions in preclinical study design. Moreover, reference parameters for normal swine and ovine bone features were provided. At the same time, basic protocols for bone decalcification in different species with different solutions were provided. Future perspectives include refining of the proposed decalcification protocols and testing new techniques for antigen unmasking and retrieval. Moreover, it would be desirable to optimize the provided multidisciplinary approach for swine and ovine bone, potentially extending it to other species.

New insights on cartilage canals in small-sized dogs were provided, which confirmed that cartilage canals mesenchymal cells are involved in bone extracellular matrix production in dogs, as they are in other species, laying the basis for more extensive studies on the delicate mechanism of endochondral ossification regulation. Future perspectives include the evaluation of cartilage canals in canine pathological conditions (e.g. osteocondrosis, femoral head avascular necrosis), potentially considering all the molecules wich are involved in the dewvelopment of cartilage canals and ossification centres. In fact, normal skeletal development can be dramatically influenced by orthopaedic conditions, as demonstrated by the description of the abnormalities induced by quadriceps contracture on hind limb skeletal development in a litter. Such abnormalities mainly consisted of volume reduction and abnormal shape of several centres, alteration that should be carefully considered to evaluate therapeutical approaches. Finally, novel contribution in canine craniometry and skull development were provided, documenting morphometric differences among

dolichocephalic, mesaticephalic and brachycephalic purebred puppies in the early neonatal period through a radiographic and anatomic study. Future perspectives include the study of abnormal skull development in canine pathological conditions (e.g. Chiari-like malformation, hydrocephalus) and the application of the neural nets to classified unclassified breeds, to better define breed standards.